Precambrian Research 365 (2021) 106406

Contents lists available at ScienceDirect

Precambrian Research

journal homepage: www.elsevier.com/locate/precamres

Paleomagnetic studies of rapakivi complexes in the Fennoscandian shield – Implications to the origin of Proterozoic massif-type anorthosite magmatism

Johanna Salminen [a,c,*], Sten-Åke Elming [b], Satu Mertanen [a], Chong Wang [c,d], Bjarne Almqvist [e], Mohsen Oveisy Moakhar [f]

[a] Geological Survey of Finland, P.O. Box 96, FI-02151 Espoo, Finland
[b] Department of Civil, Environmental and Natural Resources Engineering, Luleå University of Technology, 97187 Luleå, Sweden
[c] Department of Geosciences and Geography, University of Helsinki, P.O. Box 64, 00014, Finland
[d] State Key Laboratory of Lithospheric Evolution, Institute of Geology and Geophysics, Chinese Academy of Sciences, Beijing 100029, China
[e] Department of Earths Sciences, Uppsala University, 75236 Uppsala, Sweden
[f] Science Faculty, Physics Group, Razi University, Kermanshah, Iran

ARTICLE INFO

Keywords:
Paleomagnetism
Massif anorthosites
Rapakivi
Proterozoic, Baltica, Nuna supercontinent

ABSTRACT

Paleomagnetic studies have been performed on five rapakivi related complexes in Sweden and Finland. Poles of varying quality have been defined and the majority of the ~1640–1497 Ma poles are clustering on low latitudinal positions. By combining data from ~1500 Ma intrusions a new high-quality pole (Plat: 13°N; Plon: 190°E; A_{95}: 11°, K: 14) for Baltica has been defined. Tectonic reconstructions, on the basis of the new data and previously published high-quality data, indicate that Baltica experienced stable low latitude to equatorial positions during 1640–1470 Ma, temporally coinciding with globally pronounced rapakivi-anorthosite magmatism. Our study argues against single hotspot source for ~1640–1620 Ma, ~1590–1520 Ma, and 1470–1410 Ma rapakivi-anorthosites, but supports a model of large-scale superswell under a stationary low-latitude position of supercontinent Nuna for the origin of rapakivi-anorthosite magmatism. However, a possibility for convergent tectonism as the origin cannot be ruled out.

1. Introduction

The type locality of the Proterozoic rapakivi granites, the Wiborg batholith, extends from the southeastern Finland to Russia comprising a varied series of granitic rocks (e.g. Haapala et al., 1990; Rämö, 1991; Rämö et al., 2014). As the Wiborg batholith, also the global occurrences of these A-type granites (e.g. Rämö, 1991; Bonin, 2007; Dall'Agnol et al., 2012) are associated with coeval gabbroic rocks of the massif-type anorthosite clan (e.g. Ashwal, 1993; Alviola et al., 1999) and they often include both silicic and basic dykes (e.g. Haapala et al., 1990; Haapala and Rämö, 1992; Rämö and Haapala, 1995). Massif-type Proterozoic anorthosites occur as small plutons (1–10 km^2) to large composite batholiths (up to 18000 km^2). Composition, textures, variable contamination with continental crust, and continental crust setting of Proterozoic anorthosites distinguish them from the Archean anorthosites (Ashwal, 2010). Globally a majority of the Proterozoic massif-type anorthosites were emplaced in a time range ~1800–1000 Ma (e.g. Emslie, 1978; Ashwal and Bybee, 2017) implying a temporal link with the Paleo- to Mesoproterozoic supercontinent Nuna (e.g. Elming et al., 2021). In Baltica and Laurentia most of these magmatic rocks are found as rapakivi complexes and a majority in the age range ~1640–1400 Ma (e.g. Emslie, 1978; Windley, 1993; Åhäll and Connelly, 1998; Karlstrom et al., 2001; Ashwal and Bybee, 2017). Various theories have been put forward to explain this Proterozoic magmatism. In one set of models the common bimodal occurrence of the Proterozoic massif-type anorthosite batholiths and related crustal magmatic rocks (anorthosites-mangereite-charnockite-granitoids, AMCG complex; Emslie, 1978) are described as typical of "anorogenic" magmatism (e.g. Anderson, 1983) and linked with extensional environments like rifts or plumes (e.g. Emslie, 1978; Sharkov, 2010). Hoffman (1989) suggests

* Corresponding author at: Geological Survey of Finland, P.O. Box 96, FI-02151 Espoo, Finland.
E-mail addresses: johanna.salminen@gtk.fi, johanna.m.salminen@helsinki.fi (J. Salminen), sten-ake.elming@ltu.se (S.-Å. Elming), satu.mertanen@gtk.fi (S. Mertanen), wangchong@mail.iggcas.ac.cn (C. Wang), bjarne.almqvist@geo.uu.se (B. Almqvist), m_oveisy@razi.ac.ir (M.O. Moakhar).

https://doi.org/10.1016/j.precamres.2021.106406
Received 15 December 2020; Received in revised form 6 September 2021; Accepted 8 September 2021
Available online 27 September 2021

that because of the "thermal blanket" caused by a stationary supercontinent, a convective mantle superswell developed beneath it giving rise to ~1640–1400 Ma bimodal massif-type anorthosite magmatism. This was further elaborated by Vigneresse (2005). Though, according to Ashwal and Bybee (2017) consensus on the tectonic environment for Proterozoic massif-type anorthosites has gradually shifted towards convergent margin settings (Corrigan and Hanmer, 1997; Scoates and Chamberlain, 1997; Ashwal, 2010). They suggest a tectonic model with an Andean-type continental arc setting, where magmatism is initiated during active convergent margin processes, to be most consistent with the overall observations made so far for massif-type anorthosites and related rocks. This would account for the ~80–100 m.y. duration of mantle-derived massif-type anorthosite magmatism (Bybee et al., 2014), the emplacement into deep continental crust of variable age, and the common spatial arrangement of different massif-type anorthosites in linear belts that may exceed 1500 km in length (Ashwal and Bybee, 2017). Furthermore, Kukkonen and Lauri (2009) have proposed a link between ~1850 and 1780 Ma Svecofennian late orogenic thermal evolution and the rapakivi granite magmatism in Finland caused by thickened crust. In their collisional model the middle-lower crust and the upper mantle continued warming 200 m.y. after the collision, until Mesoproterozoic times.

Paleomagnetism provides a tool to test some of these hypotheses (e.g. Hoffman, 1989) by generating data for paleogeographical reconstructions, particularly to determine paleolatitudes and relative configuration of cratons, and to calculate minimum plate velocities. According to Ashwal and Bybee (2017) continental rifting environments are mostly unable to explain massif-type anorthosite occurrences, like the Grenville/Nain Provinces of eastern North America, which were emplaced over time spans of at least 500 m.y. in belts, without invoking an idea of multiple rift systems. However, in the eastern Canadian Shield multiple collisional events have juxtaposed once distant terranes (Gower and Krogh, 2002) and associations between magmatic and metamorphic events await detailed reconstructions of continental fragments (Ashwal, 2010). Instead, a plume, with a single stationary hotspot, should produce magmas in a spatial distribution with an expected age progression if cratons were drifting over this hotspot. Same age progression should be obtained if the hotspots were in motion (Tarduno et al., 2009). This age progression should be visible in paleogeographical reconstructions of cratons during the time of magmatism. If on the other hand, enhanced Proterozoic anorogenic magmas are produced by a stationary supercontinent relative to the underlying mantle (Hoffman, 1989) superswells should stabilize equatorially (Goldreich and Toomre, 1969). Hoffman (1989) proposed that paleolatitude variations for Laurentia are consistent with the theoretical predictions (Pollack et al., 1981), where rapid plate motions should precede supercontinental aggregation and magmatism is enhanced on a stationary low-latitude position. However, if Proterozoic magmatism during the Nuna supercontinent assembly was initiated by active convergent margin processes (e.g. Ashwal and Bybee, 2017), it is likely that the spatial arrangement of linear belts of massif-type anorthosites continue from one craton to the other in a supercontinental reconstruction and can be visualized in paleogeographical reconstructions. We will use new data from the intrusions related to the Mesoproterozoic Obbnäs, Ragunda Strömsbro, Rödö and Noran rapakivi complexes in Baltica together with existing high-quality paleomagnetic data (Elming et al., 2021; Evans et al., 2021) for testing these hypotheses.

2. Geological setting

The work of late Svetlana Bogdanova in southern-southeastern Fennoscandia forms a fundamental contribution to our knowledge of the geological setting of the East European Craton. The East European Craton (Bogdanova, 1993; Gorbatschev and Bogdanova, 1993; Bogdanova et al., 2005), from now on called Baltica (Bogdanova et al., 2008), comprises three different cratonic units; Fennoscandia, Volgo-Uralia and Sarmatia (Fig. 1). These cratons experienced distinct tectonic and metamorphic evolution since the Archean before their final amalgamation to form the Baltica at about 1800–1700 Ma (Bogdanova, 1993; Elming et al., 2010; Bogdanova et al., 2015; Salminen et al., 2021).

The majority of the Paleoproterozoic crustal growth of Fennoscandia occurred during the Svecofennian (a.k.a. Svecokarelian) orogen (Lahtinen et al., 2008). According to Lahtinen et al. (2008) the Svecofennian orogen is a collage of 2100–2000 Ma microcontinents and 2020–1820 Ma island arcs accreted with the Karelian craton at 1920–1790 Ma in an oblique collision. This accretion of island arcs and microcontinents extended down to the Trans-European suture zone southwest of Fennoscandia (Bogdanova et al., 2015; Nironen, 2017). Nearly simultaneously with the accretion Fennoscandia collided in the east with Volgo-Sarmatia at 1840–1790 Ma (Svecobaltic orogeny) and after an orogenic collapse at 1790–1770 Ma the crust stabilized (Bogdanova et al., 2015) and Sarmatia rotated and amalgamated with Fennoscandia into its present relative position at ca. 1700 Ma (Elming et al., 2010). In the southwestern part of Baltica the Svecofennian orogeny was followed by a formation of 1730–1480 Ma westward younging crustal belts during the Gothian orogeny (Bogdanova et al., 2008). Bogdanova et al. (2008) suggested that the formation of these belts was because of collision between Baltica and another terrane (Bogdanova et al., 2008), but others have suggested that it was because of the episodic accretionary growths of the crust (e.g. Bingen et al., 2008; Nironen, 2017). Semi-simultaneously with the Gothian orogen, substantial bimodal igneous activity took place in the stabilized interior of Baltica. This is emphasized by the emplacement of rapakivi massifs and associated dyke swarms that form four distinct age groups of 1640–1620 Ma, 1590–1560 Ma, 1550–1520 Ma and 1530–1440 Ma (Rämö and Haapala, 1995; Bogdanova et al., 2008; Rämö and Mänttäri, 2015; Ripa and Stephens, 2020) (Fig. 1). A sequence of intracratonic orogenic events, the Danopolonian orogeny, has been suggested to have taken place in the western part of Baltica partly simultaneously with the emplacement of rapakivi complexes in Sweden at 1500–1400 Ma (Bogdanova et al., 2008). Ca. 1470 Ma old NW-SE trending dolerite dyke swarms in central Sweden, thick sills of olivine dolerite in western Russia (Lake Ladoga) together with 1470–1420 Ma magmatism on the Danish island of Bornholm, in Lithuania and northern Poland may also be related with this orogeny (Bogdanova et al., 2008). These magmatic units have been traditionally called Subjotnian (ca. 1670–1450 Ga) based on their age relation to the rift-fillig ("Jotnian") sandstones (Gaál and Gorbatschev, 1987). Therefore, also the magmatic units younger that sandstones are referred as Post Jotnian. Below we describe briefly the geology of the sampled Kopparnäs dyke swarm related to Obbnäs rapakivi granite in southeastern Finland and the Ragunda, Strömsbro, Rödö and Noran rapakivi complexes and associated dyke swarms in central Sweden.

2.1. The Kopparnäs dyke swarm

The E-W trending ~0.05–2 m wide Kopparnäs diabase dykes outcrop in a very limited area in southeastern Finland extending about two kilometers in length and about half a kilometer in width (Figs. 1 and 2). The widest dykes are located in the eastern part of the swarm close to the Obbnäs rapakivi pluton (Fig. 1), and they gradually decrease in width towards the west further away from the rapakivi pluton. The Kopparnäs dykes are vertical or subvertical cutting sharply the Svecofennian host rock, some of them showing *en echelon* structures. The dykes are visibly undeformed, but show low-grade metamorphism, which is believed to be related to the late stages of dyke emplacement caused by circulation of fluids from the Svecofennian host rocks shortly after the emplacement (Luttinen and Kosunen, 2006). On the basis of field observations, it is suggested that the rapakivi magmatism of the Obbnäs pluton, a satellite intrusion of the 1650–1620 Ma Wiborg rapakivi complex (e.g. Heinonen et al., 2010; Rämö et al., 2014), originates from the same source as the Kopparnäs dykes (Kosunen, 2004). This is further supported by the high Ti-content observed in both the Kopparnäs dykes and the Obbnäs

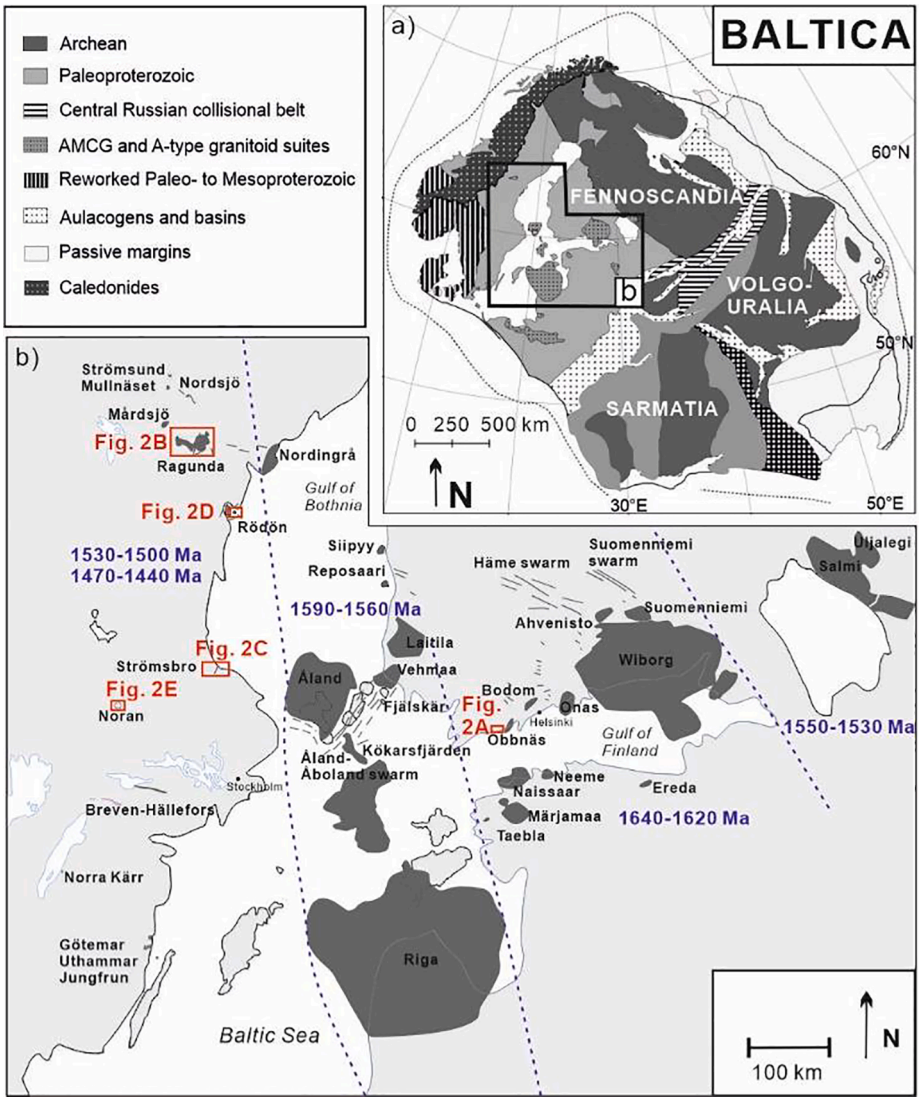

Fig. 1. (a) General geology of Baltica (modified from Bogdanova et al., 2008). (b) Distribution of 1670–1440 Ma rapakivi granites and associated dykes across Fennoscandia (modified from Ripa and Stephens, 2020). The studied locations are shown as squares and shown in detailed in Fig. 2. Blue dashed lines indicate four NNW rapakivi zones. (For interpretation of the references to color in this figure legend, the reader is referred to the web version of this article.)

rapakivi magma (Kosunen, 2004). Additionally, at recent geochemical study of several diabase dykes from the ~1640 ma and ~1570 Ma swarms of southern Finland shows that the Kopparnäs dyke magma resembles the Nb/Y and Zr/Y ratios of ~1640 Ma magmas of the Häme and Suomenniemi swarms while being distinctly different from ~1540 Ma magmas of the Åland and Satakunta diabase swarms (Luttinen et al., submitted). This further support an association to 1650–1620 Ma magma pulses in the southeastern Finland. The dykes have not been found to cut the Obbnäs rapakivi pluton and therefore they are regarded as of similar age or slightly older than the granite. Other small satellite intrusions of Wiborg rapakivi (e.g. Heinonen et al., 2010; Rämö et al., 2014) in the vicinity of the Obbnäs pluton are the Onas and Bodom plutons. Vaasjoki (1977) provided a combined U-Pb (zircon) upper intercept age of 1645 ± 5 Ma for these three plutons. Later the Obbnäs granite was dated at 1640 ± 14 Ma (U-Pb, zircon) (Kosunen unpublished data in Heinonen et al., 2010), the Onas rapakivi granite at 1630 ± 10 Ma (Laitala, 1984) and the Bodom rapakivi granite at 1638 ± 2 Ma (Kosunen unpublished data in Heinonen et al., 2010). In addition, the U-Pb (zircon) age of the quartz porphyry dykes related to the Onas intrusion is 1633 Ma (Törnroos, 1984).

The host rocks of the Kopparnäs dykes belong to the Southern Finland Granitoid Zone mainly composed of Svecofennian gabbros and granodiorite-tonalites dated at 1880–1820 Ma (Hopgood et al., 1983; Väisänen and Mänttäri, 2002; Pajunen et al., 2008). The unbaked Svecofennian gabbro studied in this work is unaltered or only slightly altered. Instead, the gabbroic host rock baked by the Subjotnian Kopparnäs dykes shows strong alteration and shearing with strongly seritized plagioclase. The shearing has probably taken place during the emplacement of the dykes into the already cooled environment. In addition, strongly deformed Svecofennian diabase dykes with an U-Pb age of 1831 ± 3 Ma (Pajunen et al., 2008) are also present in the Kopparnäs area.

2.2. *The Ragunda, Rödö, Strömbro and Noran rapakivi complexes in Sweden*

The intrusive rapakivi complexes in central Sweden were formed by repeated magma injections of pulses of variable composition that spread out laterally (Lundqvist et al., 1990; Persson, 1999). They have predominantly granitic or bimodal granitic and gabbroic composition with associated acid and basic dykes. *In situ* melting and mixing has been obtained at the contact of gabbro and hybrid rocks in several of these rapakivi plutons (e.g. Laitakari, 1969; Lundqvist et al., 1990; Lindberg et al., 1991; Rämö, 1991; Persson, 1999). The Ragunda, Rödö,

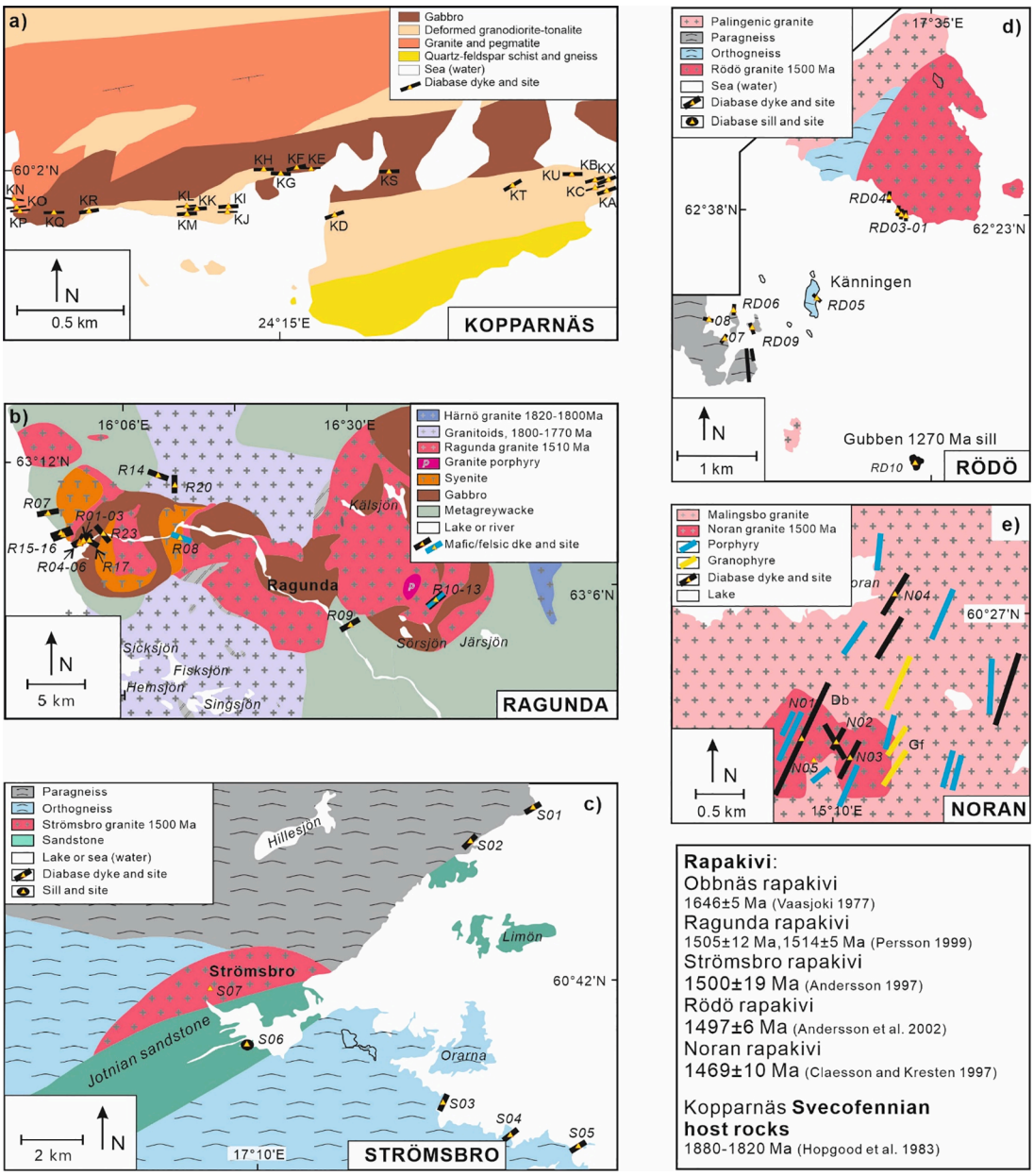

Fig. 2. Geological maps of the study areas with the location of sampling sites (a) Kopparnäs dyke swarm, (b) Ragunda rapakivi massif, (c) Strömsbro rapakivi massif, (d) Rödö rapakivi massif, (e) Noran pluton.

Strömsbro and Noran rapakivi complexes form part of a system of 1530–1440 Ma anorogenic intrusions distributed in one of a broad WNW trending zones running from Lithuania in the south, west of Åland (Finland) towards central Sweden (Fig. 1) (e.g. Persson, 1999; Andersson et al., 2001; Ripa and Stephens, 2020). The basic components of these rapakivi complexes have been compared with continental flood basalts (e.g. Ripa and Stephens, 2020) and earlier this zone has been interpreted as an aborted intracontinental rift (e.g. Emslie, 1985; Haapala and Rämö, 1992; Korja et al., 2001). Three other linear zones of early Mesoproterozoic magmatic provinces of Fennoscandia are located eastward from central Sweden where the westernmost of these three includes plutons in Nordingrå in Sweden, Åland, and Lithuania with ages ranging 1590–1560 Ma (e.g. Ripa and Stephens, 2020). Two other zones include rapakivi complexes of southeastern Finland and westernmost Russia with ages ranging 1640–1620 Ma and 1550–1530 Ma, respectively (Fig. 1).

2.2.1. *The Ragunda rapakivi complex*

The bimodal Ragunda rapakivi complex, intruding Svecofennian igneous and metamorphic rocks in central Sweden, is formed by three massifs altogether ca. 550 km^2 in size (Figs. 1 and 2b). These massifs produce clear aeromagnetic anomalies being consistent with existing large amount of basic rocks (Persson, 1999) distinguishing it from the classic Finnish rapakivi complexes (Haapala and Rämö, 1992). The overall crystallization order in the Ragunda rapakivi complex is anorthositic gabbro, gabbro, syenite, hornblende granite, porphyritic granite, biotite granite and acid and basic dykes. Magma mingling structures are observed in contact zones between granite and gabbro throughout the complex (Persson, 1999; Ripa and Stephens, 2020) indicating that the gabbro was only partly crystallized during the emplacement of granite. The U-Pb (zircon) upper intercept age of the granite of the western massif is 1514 ± 5 Ma and granite of the central massif is 1505 ± 12 Ma (Persson, 1999). The abundant silicic and basic dykes are considered as the youngest parts of the Ragunda rapakivi

complex (Persson, 1999). These dykes trend between E-W and NW-SE and cut both the Ragunda pluton and surrounding Svecofennian host rock and most of them have sharp, chilled margin, contacts with the rapakivi complex. However, a few silicic (quartz-feldspar) dykes in the western massif show sinuous contact with the gabbro, indicating that gabbro was only partly crystallized during the emplacement of dykes and therefore implies no significant age difference between dykes and gabbro. In addition, wider composite dykes with silicic interior and basic margins are found cutting both the western and the central massif and at the silicic-basic contacts there are zones of mingled rocks indicating that there is no significant age difference between silicic and basic magmas either (Persson, 1999).

2.2.2. The Strömsbro rapakivi complex

The Strömsbro rapakivi complex, intruding Svecofennian gneisses in central Sweden, is ca 12 km^2 in size (Andersson, 1997b) (Figs. 1 and 2c). All the exposed outcrops are granitic, but the number and size of outcrops is small (Andersson, 1997b). The complex consists of coarse grained biotite granite with ovoidal K-feldspar phenocrysts and it has a geochemical composition similar to pyterlitic and porphyritic rapakivi granites in the southern Finland (Vorma, 1976; Rämö and Haapala, 1995; Andersson, 1997b). The U-Pb (zircon) upper intercept age of granite is 1500 ± 19 Ma (Andersson, 1997b). The granite intrusion is truncated in the south by a graben filled with Jotnian sedimentary rocks, which in turn have been intruded by 1270–1260 Ma dykes and sills (e.g. Gorbatschev et al., 1979) (Fig. 2c). A few NE trending ca. 1.0 m wide basic dykes have been suggested to be related to the Strömsbro complex on the basis of their similarity with other rapakivi related dykes elsewhere, i.e. fine grained, non-ophitic texture and sometimes plagioclase porphyritic, in contrast to 1270 Ma larger intrusions with ophitic texture (Andersson, 1997b; Andersson, 1997a).

2.2.3. The Rödö rapakivi complex

The round shaped Rödö rapakivi complex (Andersson, 1997a) covers an area of ca 20 km^2 (Figs. 1 and 2d). It consists of granite, syenite or monzonite plutons accompanied by silicic and basic dykes. The Rödö granite is a coarse porphyritic hornblende granite with ovoidal K-feldspars mantled by plagioclase (Andersson, 1997a) typical for wiborgite rapakivi granite (e.g. Vorma, 1976; Haapala and Rämö, 1992). The U-Pb (zircon) upper intercept age of the selected zircon fractions of hornblend granite is 1497 ± 6 Ma (Andersson et al., 2001) being significantly lower than the earlier U-Pb (zircon) upper intercept age of 1513 ± 5 Ma (Welin, 1994). Because of a possible small amount of Archean zircons in the dated zircon fractions in the analyses of Welin (1994), Andersson et al. (2001) argue for a lower Archean influence for the 1497 Ma age, which they regard to be more reliable. A large number of silicic, basic, and mixed silicic and basic dykes with varying proportions and stages of fractionation (Andersson, 1997a; Andersson et al., 2001) associated with the complex are cutting both the rapakivi complex and surrounding Svecofennian host rock. The width of the dykes vary from ca 1 to 10 m and the intrusion pattern is often sinuous indicating that the rapakivi granite was only partly crystallized during the emplacement of dykes. Basic and mixed dykes are often found mingled with rapakivi granite indicating no significant age difference between these dykes and rapakivi complex. In addition, dykes are cone-sheet intrusions, i.e. the dykes follow the outer shape of the western part of the rapakivi granite complex (Andersson, 1997a) and dip towards the center of the massif.

2.2.4. The Noran rapakivi complex

The small Noran rapakivi complex intruded Svecofennian Malingsbro granite in central Sweden and covers an area of ca. 1.5 km^2 (Figs. 1 and 2e). The Noran complex consists of granite and syenite plutons, with a chemical composition similar to rapakivi granitesin Finland (e.g. Vorma, 1976; Haapala and Rämö, 1992; Rämö and Haapala, 1995; Claesson and Kresten, 1997). The granite is medium grained alkali feldspar granite with K-feldspar lamellae. The U-Pb (zircon) upper intercept age for granite is 1469 ± 10 Ma (Claesson and Kresten, 1997) and it is amongst the youngest rapakivi intrusion so far recognized in Sweden (e.g. Brander and Söderlund, 2009). Both the Noran intrusion and Malingsbro host granite are cut by a number of NE–trending 2–5 m wide basic dykes that are suggested to be related with the rapakivi granite intrusion (Claesson and Kresten, 1997; Lundström et al., 2002). A bimodal relationship between the spatially associated Noran intrusion and Tuna dolerites is apparent (Claesson and Kresten, 1997). There are also silicic dykes and composite varieties of both basic and silicic dykes cutting both host Malingsbro granite and the Noran rapakivi granite intrusions (Fig. 2e) (Claesson and Kresten, 1997).

3. Sampling and methods

Standard oriented drill core samples were collected with a portable field drill during the paleomagnetic field campaign in the Kopparnäs dykes, Ragunda, Strömsbro, Rödö, and Noran rapakivi complexes. Cored samples were oriented using both sun and magnetic compasses. In the laboratory the cores were cut into specimens. Altogether 225 oriented standard drill core samples from 22 sites were taken from the Koppärnäs dykes and their baked and unbaked host rocks (Fig. 2a, Table 1). From the Ragunda complex altogether 13 basic, one silicic and one composite dykes associated with the rapakivi complex were sampled. In addition, the gabbroic part of the rapakivi complex was sampled in six sites from the baked zone of the intruding dykes and at five sites at a distance from the dykes aiming to sample the unbaked zone (Fig. 2b). Altogether 141 samples were collected from the Ragunda rapakivi complex. From the Strömsbro complex four basic dykes associated with the rapakivi granite, a sill and a 1260 Ma dyke were sampled and in addition the rapakivi granite was sampled in one site (Fig. 2c). Altogether 54 samples were collected from the Strömsbro rapakivi complex. Four basic dykes intruding the Rödö rapakivi granite and five presumably coeval basic dykes intruding the Svecofennian gneiss were sampled (Fig. 2d). Baked and unbaked rapakivi granite was sampled from three dyke sites and additionally unbaked rapakivi granite was sampled at far distance from the dykes in the four sites in the Rödö island. Furthermore a 1270 Ma sill was sampled in the Gubben island. Altogether 75 samples were collected. Four basic dykes associated with the Noran granite complex have been sampled, three of them are cutting the intrusion and one is located ca 1 km north of the complex (Fig. 2e). Baked granite was sampled in three sites and unbaked granite and gneiss were samples at ca 10–25 m from the basic dykes in the three sites. A total of 47 samples were collected from the Noran rapakivi complex.

3.1. Measurements and analyses

The rock magnetic and paleomagnetic measurements for this study have been conducted in the laboratory at Geological Survey of Finland (GTK) (Kopparnäs), at Luleå University of Technology (LTU) (Strömsbro, Rödö, Noran) and in the Solid Earth Geophysics Laboratory of the University of Helsinki (UH) (Ragunda).

Magnetic susceptibility was measured on each specimen from the Kopparnäs dykes using GTK designed kappabridge with an applied field intensity of 130 A/m.

Magnetic mineralogy of the samples of the Kopparnäs dykes, Ragunda and Rödö rapakivi massifs was investigated by thermomagnetic analysis of selected powdered whole-rock samples. Temperature dependence of low-field magnetic susceptibility was measured from −192 °C to 700 °C (in argon gas) followed by cooling back to room temperature using an AGICO CS3-KLY-3S Kappabridge system with an applied field intensity of 300 A/m (UH, GTK). Curie temperatures were determined using the maximum in the second derivatives of the thermomagnetic curves (e.g. Tauxe et al., 2018) using the Cureval 8.0 program (http://www.agico.com). Anisotropy of magnetic susceptibility (AMS) for Rödö and Strömsbro samples was measured with a KLY-3 (AGICO) instrument. Three axes isothermal remanent magnetization

(IRM) (Lowrie, 1990) and acquisition of IRM curves were carried out with a Molspin pulse magnetizer (GTK) for Kopparnäs samples. In addition, Scanning Electron Microscope (SEM; Jeol JSM-5900LV) analyses and thin section studies were performed for these samples to verify the nature of the magnetic carriers (GTK). For determination of domain states of the magnetic carriers (Ragunda) hysteresis properties of powdered whole rock samples were measured using a Princeton Measurement Corporation's (now Lake Shore cryotronics) MicroMagTM3900 model Vibrating Sample Magnetometer (VSM) (UH).

Stepwise alternating field (AF) demagnetizations for samples from the Swedish rapakivi massifs were done using a three-axis demagnetizer with a maximum field of up to 160 mT, coupled with a cryogenic 2G DC SQUID magnetometer (UH, LTU) and for the Kopparnäs dykes with a RF SQUID magnetometer (GTK) to isolate a characteristic remanent magnetization (ChRM). Sister specimens were thermally demagnetized using an argon-atmosphere ASC Scientific model TD-48SC furnace (UH), a Schonstedt model TSD-1 (LTU) and home built furnace (GTK). Remanent magnetizations were measured with 2G DC and RF SQUID magnetometers.

For each of the cases vector components were visually identified using stereographic and orthogonal projections (Zijderveld, 1967) and the directions were calculated by a least squares method (Kirschvink, 1980). We employed the standard convention of assigning "normal" polarity to north-directed ChRM vectors from Proterozoic rocks in Baltica; relating this arbitrary definition to the absolute sense of Mesoproterozoic geomagnetic polarity is uncertain due to the lack of continuity in the apparent polar wander path (APWP) of Baltica through Neoproterozoic ages. Mean remanence directions for the different components of magnetization were calculated according to Fisher (1953), giving a unit weight to each sample (each specimen has a unit weight within a sample) to calculate site mean directions and corresponding virtual geomagnetic poles (Irving, 1964). We used the site dependent paleosecular variation (PSV) test of Deenen et al. (2011) to explore if the virtual geomagnetic poles average the secular variation. For dual polarity data, we conducted reversals test on the normal and reversed polarity groups (McFadden and McElhinny, 1990) using paleomagnetism.org 2.2.0 (Koymans et al., 2016) and super-IAPD (Torsvik et al., 2000) program (Tables 1, 2 and 6). In case of indeterminate results, we tested with the bootstrap statistics described in Tauxe et al. (1991), Tauxe et al. (2018) if the normal and reversed polarity sites share a common true mean direction at 95% confidence level (see Supplementary 1). The result of this shows bootstrapped (x, y, z) coordinates for both normal and reversed polarity data as a cumulative distribution function. If the confidence intervals for each co-ordinate overlap, the associated directions are statistically indistinguishable and the sites share a common true mean direction at 95% confidence level (Tauxe et al., 1991). The paleogeographical reconstructions and pole plots were done with the GPlates program (Müller et al., 2019).

4. Results and discussion of rock magnetism and paleomagnetism

Below we describe and discuss the results of magnetic mineralogy and paleomagnetism from the Kopparnäs diabase dykes, the Ragunda, Strömsbro, Rödö and Noran complexes. The results are shown in Figs. 3–10 and paleomagnetic results are tabulated in Tables 1–5.

4.1. The Kopparnäs dykes

The Kopparnäs dykes are relatively weakly magnetized, however magnetic susceptibility and remanence intensity varies (Fig. 3a). Detailed rock magnetic tests show that the intensity of the Isothermal Remanent Magnetization (IRM) increases exponentially up to 0.3 T and is not saturated by 1.5 T, indicating the presence of magnetite and a hard coercivity mineral, such as pyrrhotite (Dekkers, 1988), respectively (Fig. 3b). Furthermore, the Lowrie test (Lowrie, 1990) shows the presence of titanomagnetite with variable Ti-content as exemplified with the drop of remanence intensity of the soft and medium coercivity components at varying temperatures between 550℃ and 580℃. In addition, some samples indicate the presence of pyrrhotite as the intensity of the hard coercivity component drops at 320 ℃ (Fig. 3c-e). Thermomagnetic curves of basic dyke samples are mainly irreversible demonstrating mineralogical alteration upon heating (e.g. Özdemir, 1987). Some samples show the presence of Hopkinson's peak close to 580 °C during heating indicating the presence of single-domain magnetite (Dunlop, 2014). The host gabbro shows nearly reversible heating and cooling curves with the sharp Hopkinson's peak close to 520 °C, indicative of titanomagnetite (Fig. 3). SEM studies of the dykes show the presence of titanomagnetite, ilmenite, pyrite and occasionally pyrrhotite (Fig. 3).

Paleomagnetic results of the Kopparnäs dykes are listed in Table 1, and representative demagnetization behaviors are illustrated in Fig. 4. The AF demagnetization was more effective than thermal demagnetization in isolating the ChRM, with coercivities varying between 20 and 160 mT and unblocking temperatures between 500 and 560 °C typical for titanomagnetite (Fig. 4). The directions are defined with a Mean Angular Deviation (MAD) typically $<7^{\circ}$, but in some cases a MAD as high as 12° was accepted. A normal polarity northeast both up- and downward pointing shallow ChRM direction was obtained in 14 sites (85 samples) and a reversed polarity southwest downward pointing shallow inclinations ChRM component in three sites (13 samples) (Fig. 4). Samples carrying a ChRM of reversed polarity showed higher coercivities than normal polarity samples, however they were isolated in similar temperatures during demagnetization. For seven dykes both polarities are present in a single specimen, shown as a great circle from normal to reversed polarity. In the transitional samples, the reversed polarity component could typically not be isolated although the normal polarity component was obtained, in addition to typical steep PEF direction (Fig. 4). The samples with transitional polarities were taken from the coarser grained central parts of the wider dykes where also susceptibility and remanence intensity are higher than at the dyke margins. Because the width of these dykes is only two meters at maximum, the cooling time of magma is too short for acquiring a reversal of the magnetic field. Therefore, it is probable that the central parts record varied mineralogical alteration.

Baked contact tests were carried out at six dyke sites. The distances of the baked rocks from the dykes varied from 0.05 to 0.2 m depending on the width of the dyke (Table 1). Typically, the remanence directions at the baked contact zone are rather scattered. However, in the baked contact zones of four dykes (10 samples) a stable northwesterly magnetization direction with an upward pointing inclination was obtained. This direction does not correspond to the ChRM direction of the dykes that show a northeasterly direction with a shallow inclination.

Therefore, a full baked contact test was not obtained. Although the scatter of these directions between sites is quite high ($\alpha_{95} = 18.2^{\circ}$, Table 1), the directions are clearly isolated in Zijderveld diagrams (Fig. 4). The origin of this remanence is not clear. One explanation may be related with the simultaneous shearing of the contact zone. In the gabbroic host rock shearing is also accompanied with alteration, seen as strong preferred orientation of minerals and of sericitization in thin sections. These factors may have caused the peculiar remanence direction of the baked contact zone. The unbaked Svecofennian aged host rocks comprising granites, gneisses and gabbros (Table 1) carry a stable and consistent ChRM with northwest declination and intermediate downwards pointing inclination, typical for Svecofennian age (1900–1800 Ma) formations (Neuvonen et al., 1981). Despite of clear typical Svecofennian direction obtained for the unbaked host rocks, a full positive baked contact test was not obtained. However, since this direction clearly deviates from the dyke direction, we suggest that the remanence of the dykes is primary. Consequently, any pervasive overprinting is ruled out.

The mean dual polarity ChRM for 17 Kopparnäs dyke sites is D: 27°,

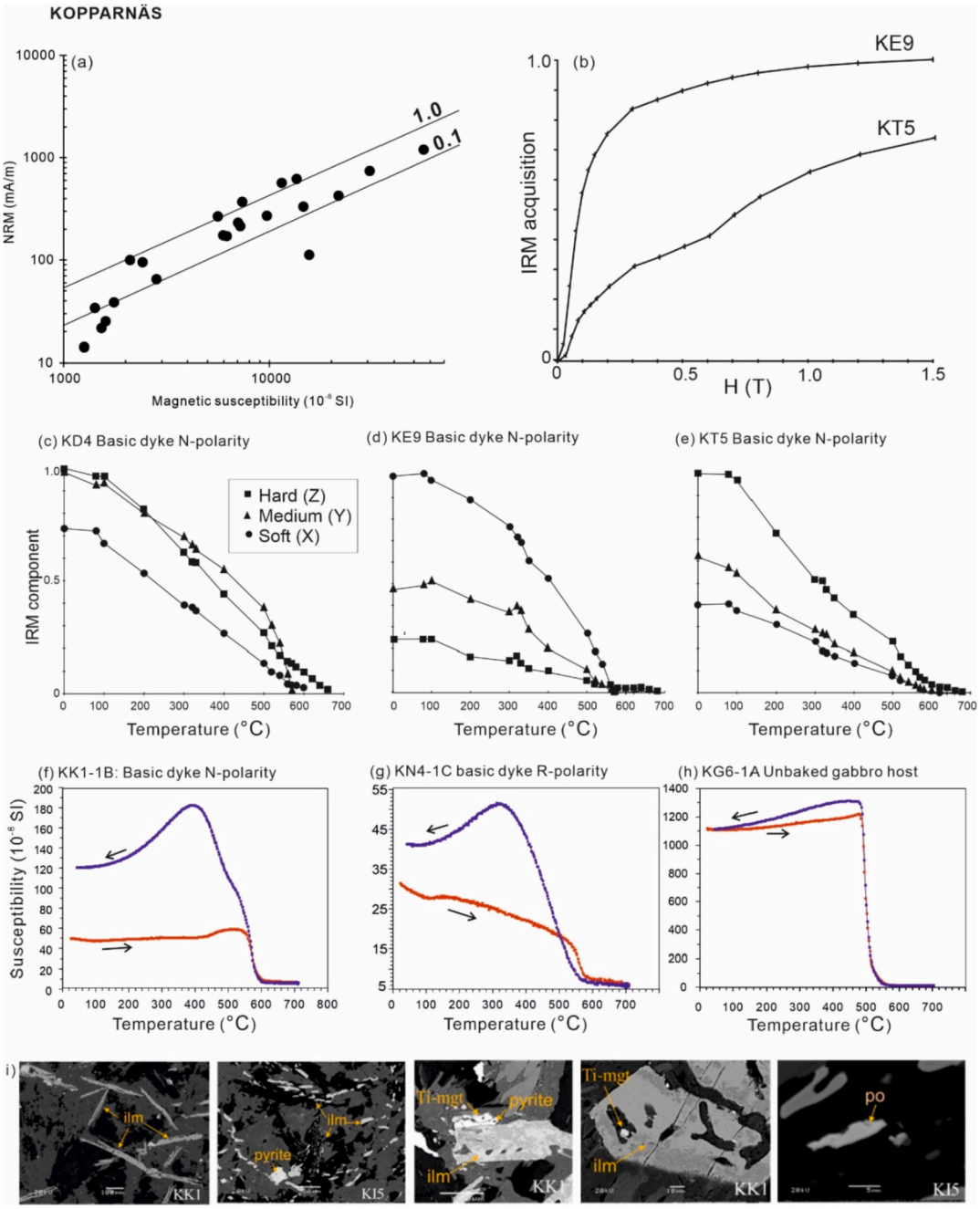

Fig. 3. Kopparnäs petrophysics, rock magnetism and SEM (a) Remanence – magnetic susceptibility plot (logarithmic scales) of the site mean values of the dykes. Koenigsberger's Q ratios (calculated with magnetic field value of 41 A/m) are shown as straight lines. (b) Isothermal Remanent Magnetization acquisition curves. (c-e) 3-axis Lowrie tests (Lowrie, 1990). (f-h) Thermomagnetic curves. (i) Scanning electron microscope (SEM) images of the samples KK1 and KI5. Abbrevations: ilm = ilmenite, Ti-mgt = titanomagnetite, po = pyrrhotite.

I: 1.2° (α_{95}: 7°, k: 27) yielding a paleomagnetic pole at Plat: 27°N, Plong: 173°E (A_{95}: 5°, K: 47, with N: 98, B: 17) (Figs. 5 and 11, Table 1). According to secular variation test of Deenen et al. (2011) this data averages out the secular variation (obtained $A_{95obt.} = 5°$, $A_{95min} = 4°$, $A_{95max=}14°$). The reversal test (McFadden and McElhinny, 1990) for the Kopparnäs data fails because of low number of reversed polarity sites. In addition, based on the bootstrap statistics described in Tauxe et al. (1991); Tauxe et al. (2018) normal and reversed polarity directions for the Kopparnäs data do not share a common true mean (see Supplementary 1). The pole is close to the combined 1633 Ma pole from the Sipoo diabase and quartz porphyry dykes (Mertanen and Pesonen, 1995) and a 1639 Ma pole from the Suomenniemi dyke swarm (Salminen et al., 2019). All these are slightly different from a new ~ 1645 Ma combined pole from the Häme dyke swarm (Salminen et al., 2017) and E-W trending dykes in the Satakunta (Salminen et al., 2014b) (Table 6, Fig. 11). However, on the basis of the overlapping position with 1640–1630 Ma poles, similar geochemical composition with the Häme and Suomenniemi dyke swarms (Luttinen et al., submitted) and association with the ~1640 Ma Obbnäs rapakivi complex, we suggest a ~1640 Ma age for the Kopparnäs pole.

Table 1
Paleomagnetic results of the Kopparnäs dykes and host rocks.

Site	Rock type	SLat (°N)	SLong (°E)	Trend (N°)	Dyke width (m)	Pol.	B/N/n	D (°)	I (°)	α95 (°)	k	Plat (°N)	Plong (°E)	A95 (°)	K
KD	diabase dyke	60.043	24.265	80	0.7	N	*9/20	21.1	5.2	7.8	45.1	30.5	179.7	4.8	
KE	diabase dyke	60.045	24.264	80	0.3	N	*5/8	18.5	2.1	19.6	16.2	29.2	183.0	11.3	
KF	diabase dyke	60.045	24.259	80	1	N	*8/13	43.5	−2.3	7.5	56.0	20.2	157.1	6.6	
KG	diabase dyke	60.045	24.259	90	1	N	*4/8	37.0	3.7	26.9	12.6	25.5	162.6	19.0	
KH	diabase dyke	60.045	24.257	90	0.2–1	N	*2/2	46.1	11.2	x	x	25.5	151.6	x	
KI	diabase dyke	60.044	24.255	85	1	N	*5/11	24.3	−2.4	15.4	25.6	26.0	177.0	11.7	
KJ	diabase dyke	60.043	24.255	85–90	0.3–0.8	N	*4/7	25.9	15.9	11.0	70.4	34.6	172.5	9.9	
KK	diabase dyke	60.043	24.254	85	1	N	*4/6	26.4	−12.5	17.4	28.9	20.4	176.3	14.6	
KL	diabase dyke	60.044	24.253	90	0.4	N	*5/8	29.1	6.4	26.0	9.6	29.2	170.5	16.9	
KM	diabase dyke	60.043	24.253	90	<1	N	*6/9	31.4	6.2	11.2	36.6	30.6	167.3	8.2	
KP	diabase dyke	60.043	24.244	85	0.12	N	*8/16	33.3	24.2	13.7	17.3	37.6	162.0	10.0	
KR	diabase dyke	60.043	24.248	85	0.15–0.7	N	*12/19	36.0	6.4	12.2	13.6	27.1	162.9	9.6	
KS	diabase dyke	60.044	24.264	90	1	N	*5/7	28.8	6.9	24.5	10.7	29.6	170.8	18.6	
KT	diabase dyke	60.044	24.271	80	1	N	*8/17	20.1	−0.7	15.2	14.3	27.5	181.6	8.8	
Mean diabase, N polarity						N	*14/85/151	30.1	5.1	6.0	45.3	28.1	169.7	4.7	73.1
KA		60.040	24.280	70	1	R	*5/7	189.1	11.5	15.2	26.2	23.5	194.5	9.8	
KB		60.040	24.280	70	0.7	R	*4/4	192.1	11.2	35.2	7.8	23.7	191.3	23.6	
KN		60.044	24.243	95–110	0.05	R	*6/11	200.4	27.4	6.9	96.7	13.7	184.1	6.9	
Mean diabase, R polarity						R	*3/13/22	193.7	16.7	16.5	56.7	20.5	189.7	11.8	110.8
Combined mean diabase, N + R polarity[a]						C	*17/98/173	27.3	1.2	7.0	27.0	26.9	173.3	5.0	46.9
Baked host rocks					Distance from the dyke (m)										
KD	baked granite				0.05–0.2	N	*4/7	336.9	−35.1	11.2	68.6	8.3	226.4	11.6	
KE	baked gneiss				0.01	N	*1/1	342.8	−57.5	x	x	−9.1	217.9	x	
KG	baked gabbro				0.01–0.35	N	*2/4	336.8	−22.8	x	x	15.6	228.0	x	
KT	baked granite				0.02	N	*3/6	336.2	−25.7	7.6	267	14	228.2	7.8	
Mean baked rocks						*N*	*4/10/18	337.7	−35.2	18.2	26.3	7.3	225.0	14.1	43.3
KE11-1B	baked gneiss				0.01	R	*1/1	210.3	19.0	x	x	16.2	173.1	x	
KS12-1A	baked granite				0.01	N	*1/1	13.8	14.4	x	x	36.3	187.2	x	
Unbaked host rocks															
KD	granite				6		*2/5	343.1	35.4	x	x	47.8	228.4	x	
KE	gneiss				5.5		*2/4	332.5	42.7	x	x	50.0	244.9	x	
KG	gabbro				0.5–3.5		*2/2	344.0	34.7	x	x	47.5	227.0	x	
KH	granite/px-gneiss				1.5–5 *m*		*2/4	331.9	41.7	x	x	49.0	245.4	x	
KS	granite				4		*2/4	345.6	42.4	x	x	53.1	226.5	x	
KT	granite				8		*2/4	339.6	30.1	x	x	43.7	231.9	x	
Mean unbaked rocks							*6/12/23	339.6	38.0	5.8	136.6	48.8	234	5.44	152.9

Slat/Slong, Latitude/longitude of sampling site. Pol., polarity of the isolated magnetization direction: N/R/C, normal/reversed/combined polarity. Decl., declination. Incl., inclination. a95, the radius of the 95% confidence cone in Fisher (1953) statistics. Plat/Plong, paleolatitude/paleolongitude of the pole. A95, radius of the 95%. *, level of statistics. Reversal test of McFadden and McElhinny (1990), γc, citical angle; γo, observed angle.
Reversal test: γc: 14°; γo: 8.7°. Does not pass.
Based on bootstrap statistics described in Tauxe et al. (1991), Tauxe et al. (2018) normal and reversed polarity directions are not the same (see Supplementary 1).
With $A_{95} = 5°$ passes the PSV test of Deenen et al. (2011), (2014) ($A_{95min} = 4°$, $A_{95max} = 14°$)

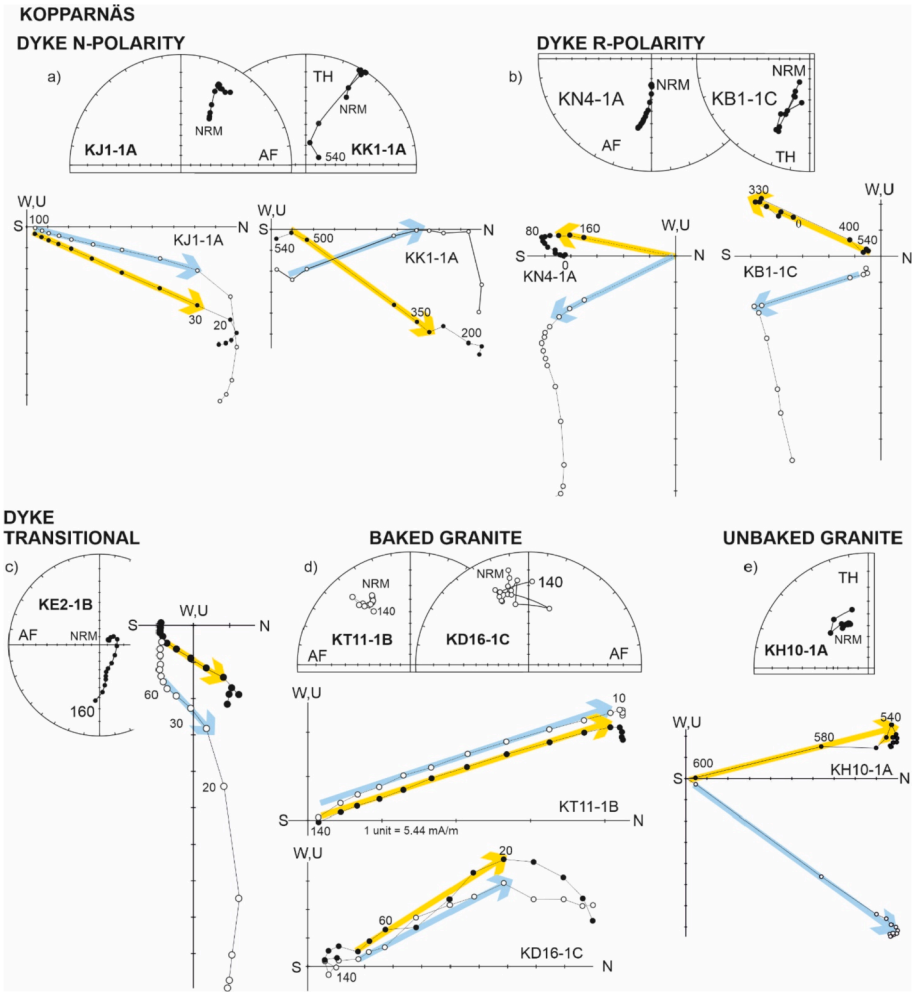

Fig. 4. AF and thermal demagnetization examples from the Kopparnäs dykes. Figures show equal area stereographic and orthogonal projections (units: mA/m) of ChRM directions in geographic coordinates. Closed (open) symbols represent downward (upward) directions. Numbers at the demagnetization steps denote the used AF field (in mT) or temperature (in °C). Yellow (blue) arrows show the direction of declination (inclination) interpreted from the demagnetization data. (For interpretation of the references to color in this figure legend, the reader is referred to the web version of this article.)

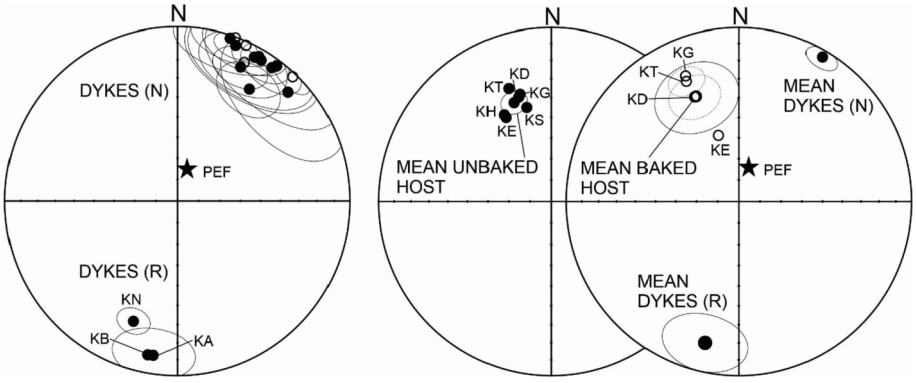

Fig. 5. Kopparnäs site mean ChRM directions with α_{95} error circles for dykes (left); unbaked Svecofennian host (middle); and both baked and mean dykes (right). Directions are shown in geographic coordinates on an equal area stereonet. Closed (open) symbols represent downward (upward) directions, black stars represent Present Earth Field (PEF) direction on the sampling area. R (N) refers to reversed (normal) polarity.

4.2. The Ragunda rapakivi complex

Representative thermomagnetic curves and hysteresis loops for samples from the Ragunda complex are shown in Fig. 6. Thermomagnetic curves of basic dyke and gabbro samples are mainly irreversible indicating mineralogical alteration upon heating. Basic dyke samples show sharp, high to moderate, Hopkinson's peak close to 580 °C during heating indicating the presence of single-domain magnetite (Dunlop, 2014). This peak is smaller or absent in the cooling curves. The heating curve for the basic part of the composite dyke at site R10 is different from the other basic dykes. In addition to the Hopkinson's peak at ~580 °C, it also shows a prominent hump at ~300 °C, which could indicate the presence of pyrrhotite (Dekkers, 1990) transforming to magnetite during the heating (Fig. 6c) or magnetite with higher Ti-content. Heating curves for gabbro samples show Curie point at ~580 °C, but a Hopkinson's peak is absent. Additionally, both unbaked and baked gabbro samples indicate a presence of titanomagnetite by showing a small decline in susceptibility at ~320 °C during the heating

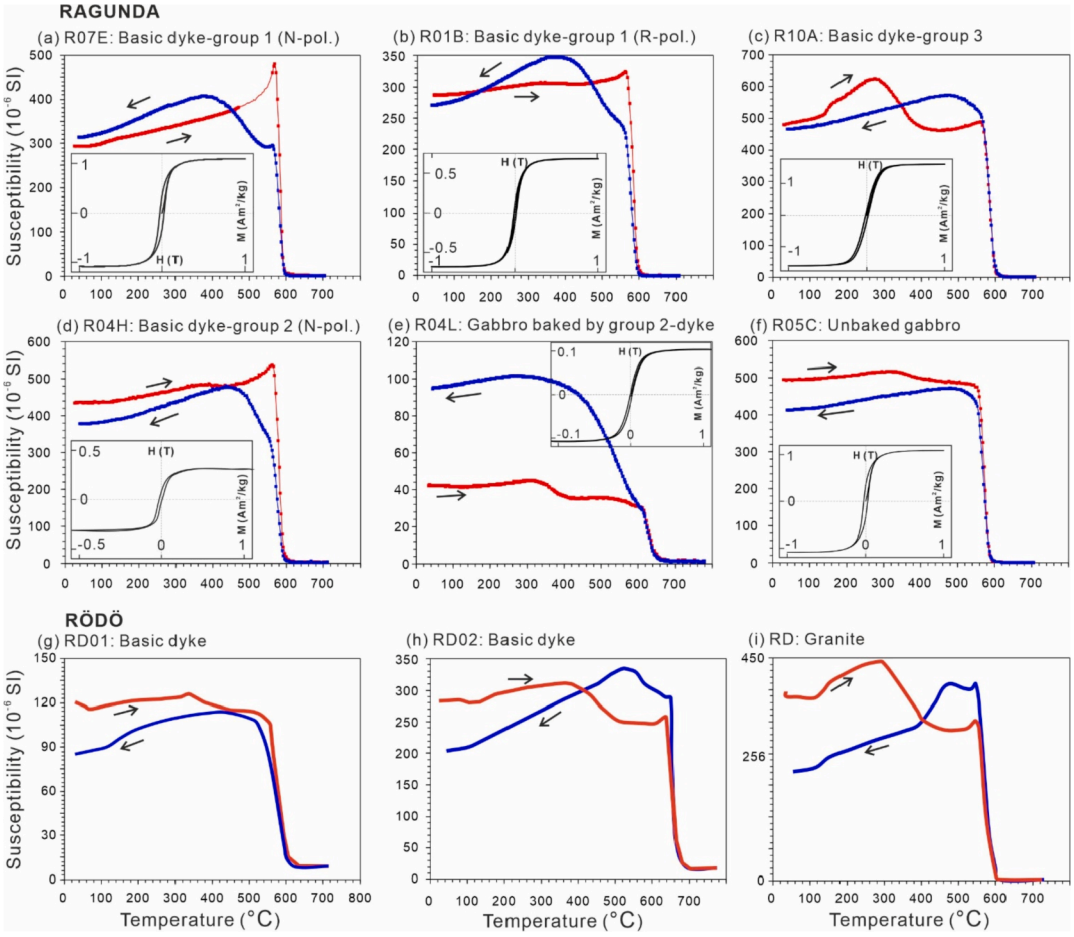

Fig. 6. Thermomagnetic and hysteresis analyses of samples from the Ragunda and Rödö rapakivi complexes.

(Fig. 6ef). The measured hysteresis loops agree with the presence of small grain-sized magnetite in all samples (Fig. 6).

Paleomagnetic results of the Ragunda rapakivi complex are listed in Table 2, and representative demagnetization behaviors are illustrated in Fig. 7. In total, in eight out of fifteen dyke sites and five out of six gabbro sites sampled for this study stable remanent magnetizations directions are isolated (Table 2). Both in AF and thermal demagnetizations a ChRM was defined with coercivities and unblocking temperatures typical for magnetite (Fig. 7), however AF demagnetizations were more efficient in the isolation of a ChRM. The directions are defined with a MAD generally <8°. We divided the dykes into three groups on the basis of the obtained ChRM directions in this study and on the results from a previous study of Piper (1979) (Fig. 8). Group 1 includes samples showing dual polarity, southerly mainly downward and northerly mainly upward pointing magnetization directions with low to intermediate inclination (Figs. 7 and 8). Gabbro samples close to the contact of the reversed polarity dyke R01 of Group 1 show similar ChRM direction to that of the dyke (Fig. 7b). The gabbro samples far away from the same dyke show clearly different southerly ChRM direction with steep upward pointing inclination (Figs. 7h and 8). This indicates a positive baked contact test for the Group 1 dykes. Group 2 includes samples showing mainly northerly magnetization directions with downward pointing intermediate inclinations (Figs. 7 and 8). Gabbro from the contact of the dyke R04 of Group 2 shows different direction than that of the dyke (Fig. 7g) but similar to the reversed polarity ChRM direction of Group 1 (Figs. 7 and 8). Group 3 includes samples obtained from silicic and basic parts of a composite dyke showing easterly ChRM direction with steep downward pointing inclination (Figs. 7 and 8). Both baked and unbaked gabbro intruded by the composite dyke show magnetization directions similar with the dyke (Fig. 8) indicating a pervasive magnetization event of unknown origin. Thermomagnetic analyses point to the presence of pyrrhotite in the basic part of the composite dyke.

We combine our data with the earlier data of Piper (1979) (Table 2, Fig. 8). In case of duplicate sampling we made a note on the Table 2. Data of (Piper, 1979) was filtered by excluding the sites with $\alpha_{95} > 26°$ and magnetization directions overlapping with the Present Earth Field (PEF) direction at the sampling site (D: 7°, I: 75°). Fig. 8 shows the selected data. In total, we include twelve dyke sites into the Group 1, with five dykes carrying a reversed and seven a normal polarity magnetization. While the reversal test of McFadden and McElhinny (1990) for the Group 1data yields an indeterminate class (a critical angle 25°, and an obtained angle18°), the normal and reversed polarity data share the common mean based on bootstrap statistics described in (Tauxe et al., 1991; Tauxe et al., 2018) (see Supplementary 1).

The mean magnetization direction of Group 1 is D: 3°, I: -24° (α_{95}: 19°, k: 6) (Figs. 8, 11) yielding a paleomagnetic pole at Plat: 13°N, Plong: 194°E (A_{95}: 15°, K: 10, with N: 63, B: 12) (Fig. 11). According to secular variation test of Deenen et al. (2011) this data averages out the secular variation (obtained $A_{95obt.} = 14.9°$, $A_{95min} = 4°$, $A_{95max=}17°$).

Four normal and one reversed polarity dyke sites are included into the Group 2. The mean direction of dyke Group 2 is D: 28°, I: 54° (α_{95}: 20°, k: 16) (Figs. 8, 11) yielding a paleomagnetic pole at Plat: 58°N, Plong: 150°E (A_{95}: 23°, K: 12, with N: 31, B: 5) (Fig. 11). Additionally, unbaked gabbro sampled in total eight sites show directions similar with the Group 2, with both reversed and normal polarity magnetizations. In addition, granite sampled in seven sites show similar directions, with normal directions in six sites and a reversed polarity in one site. Samples from sites #13 and #14 (Piper, 1979) carrying reversed and normal

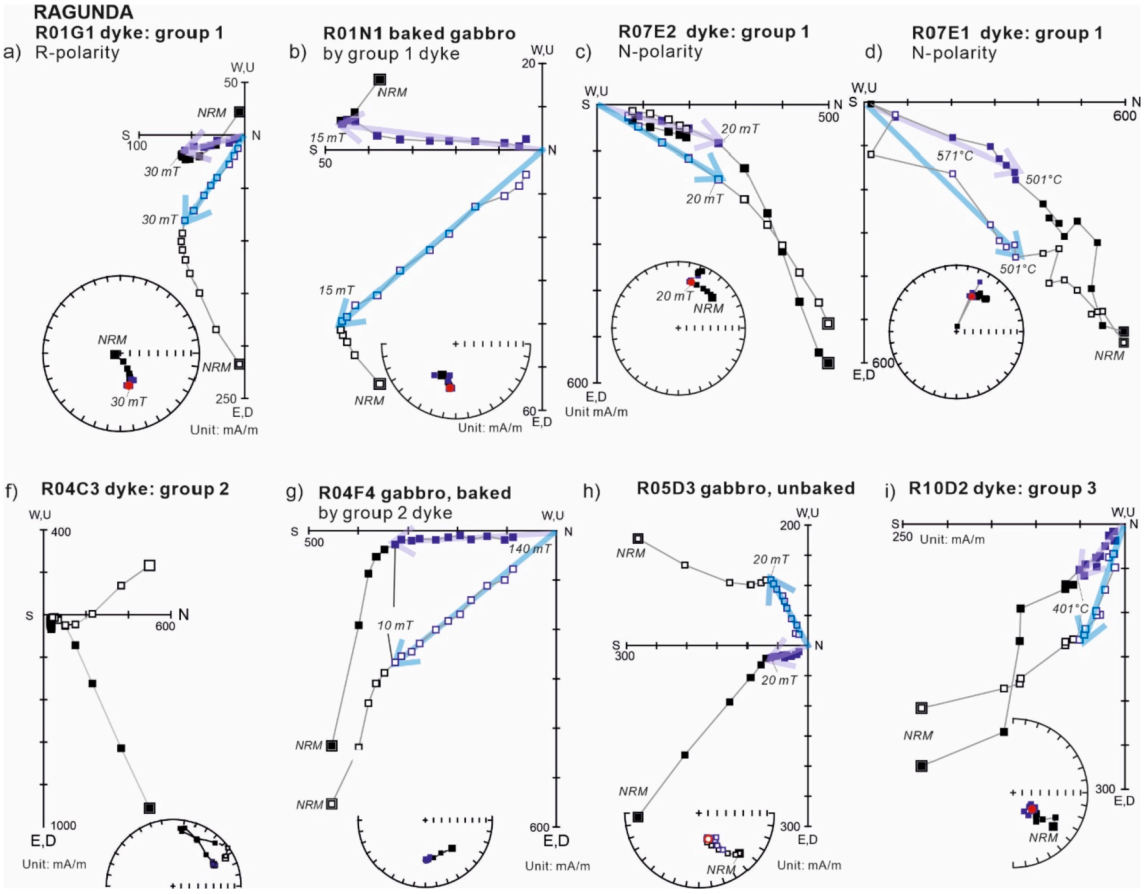

Fig. 7. Examples of AF and thermal demagnetization of the samples from the Ragunda rapakivi complex including cutting dykes and rapakivi gabbro. Figures show equal area stereographic and orthogonal projections (units: mA/m) of ChRM directions in geographic coordinates. Closed (open) symbols represent downward (upward) directions. R (N) refers to reversed (normal) polarity. Numbers by the demagentization step denotes the used AF field (in mT) or temperature (in °C).

polarity magnetizations, respectively, are taken from the central massif dated at 1505 ± 12 Ma (Persson, 1999). Samples from other granite sites of the 1514 ± 5 Ma (Persson, 1999) western massif show only normal polarity (Fig. 8d). The gabbro crystallized before the granite, but magma mingling of silicic and basic magmas is observed (Persson, 1999) indicating no significant age difference between the two. Additionally, magnetization directions from unbaked gabbro and granite sites are statistically the same. A combined mean direction for six reversed polarity and fourteen normal polarity sites of the rapakivi complex is at D: 20°, I: 49° (α_{95}: 11°, k: 10) (Fig. 9, 17) yielding a paleomagnetic pole at Plat: 56°N, Plong: 163°E (A_{95}: 11°, K: 10, with N: 122; B: 20) (Fig. 11). According to secular variation test of Deenen et al. (2011) this data averages out the secular variation (obtained $A_{95obt.} = 11.1°$, $A_{95min} = 4°$, $A_{95max=}12°$). The data for Group 2 yields an indeterminate class (a critical angle 23°, an obtained angle 9°) for the reversal test (McFadden and McElhinny, 1990). Based on the bootstrap statistics described in Tauxe et al. (1991) normal and reversed polarity directions are not the same for the Ragunda Group 2 data (see Supplementary 1).

Apart from Group 3 magnetization direction, which is interpreted as an overprint, two groups of directions are obtained at the Ragunda rapakivi complex and dykes. Assigning the age for magnetization is complicated. The group 1 directions are obtained from undated basic dykes and only from baked gabbro sites. As discussed above a positive baked contact test for the dykes with reference to the gabbro indicates that this direction is primary and is inherently younger than the granite (1505 ± 12 Ma, 1514 ± 5 Ma; Persson, 1999) and gabbro. Group 2 type magnetization directions are obtained from basic dykes. Furthermore, similar directions are also isolated in samples from the granite and the gabbro without known dykes in the vicinity. All these three rock types carry magnetizations of both polarities and the obtained mean directions are the same within the error limits (Fig. 8). The error circle of the Group 2 mean dyke direction overlaps slightly with the PEF direction of the sampling site (Fig. 8). Additionally, both dyke and rapakivi directions of Group 2 are close to the known secondary magnetization direction obtained widely in Fennoscandia (e.g. Mertanen et al., 2008; Preeden et al., 2009; Salminen et al., 2014b) (Fig. 8). Based solely on comparison of mean directions one would lean on interpreting Group 2 direction as an overprint, but the obtained inverse baked contact test with reference to the dykes of Group 1 would indicate the primary nature for the magnetization. In addition, the reversed polarity directions argue against an overprint, since reversed polarity overprints have not been obtained in Fennoscandian studies Furthermore, the rocks in the sites carrying Group 1 and Group 2 directions are not clustering geographically and we did not obtain differences in magnetic mineralogy between these groups. This also argue against a remagnetization of the rocks. If the magnetization of Group 2 is primary an age of granite 1505 ± 12 Ma, 1514 ± 5 Ma (Persson, 1999) can be assigned for it.

Table 2
Paleomagnetic results of the Ragunda rapakivi complex.

Site	Rock type	SLat (N°)	SLong (E°)	Trend (N°)/dip(°)	Dyke width (m)	Pol.	(B)/N	Decl. (°)	Incl. (°)	α95 (°)	k	Plat. (N°)	Plon. (E°)	A95 (°)	K	Notes/Ref
Group 1																
R01	diabase dyke	63.14	16.03	240/90	1.2	R	4	146.2	52.9	22.6	17.5	12.2	45.0	28.6		
R02	diabase dyke	63.14	16.03	240/90	0.6	N	4	59.1	−12.8	11.8	61.4	7.4	136.7	8.9		Site 36 of Piper (1979)
R07	diabase dyke	63.16	15.96	260/90	0.2	N	7	20.1	21.1	28.2	5.5	36.3	170.0	18.2		
R15	diabase dyke	63.15	15.99	250/80	5	N	4	3.4	−26.0	26.0	13.4	12.3	192.1	19.3		Site 28 of Piper (1979)
R17	diabase dyke	63.14	16.04	300/90	0.3	N	4	352.6	−3.3	18.9	24.5	24.9	204.2	10.9		
Mean Group 1 dykes	diabase dykes, group 1					C	5*/23	11.2	−16.7	43.6	4.0	16.4	186.7	37.9	5.0	This work only
R01	gabbro, baked	63.14	16.03			R	5	193.0	39.1	14.3	29.6	3.6	184.7	15.0		Close to sites 5–8 of Piper (1979)
Group 2																
R04	diabase dyke	63.14	16.03	240/90	3.5	N	7	40.5	29.0	21.0	9.2	35.6	146.1	19.1		Site 31 of Piper (1979)
R05 + R06	gabbro, unbaked	63.14	16.03			R	7	161.7	−63.3	6.5	87.2	−69.7	55.6	9.1		For sites R01-R04, R17 and 9 of Piper (1979)
Group 3 (one composite dyke)																
R10	felsic part	63.09	16.68	230/80	5.5		8	113.4	68.7	8.2	46.7	37.8	60.3	12.7		
R11	mafic, west part	63.09	16.68		0.5		7	108.2	68.8	13.5	21.1	38.5	63.7	21.4		
R12	mafic, east part	63.09	16.68		0.6		5	28.3	80.6	13.8	31.9	76.9	51.9	24.6		
R13	gabbro, baked	63.09	16.68				8	125.7	72.4	7.7	52.5	38.7	50.1	13.3		
R13	gabbro, unbaked	63.09	16.68				3	120.4	67.4	17.6	50.2	34.0	57.8	25.1		
Excluded from the means																
R03	diabase dyke	63.14	16.03	240/90	1.3	N	5	299.6	−3.2	24.9	10.4	11.3	258.6	23.1		Site 37 of Piper(1979)
R04	gabbro, baked	63.14	16.03			R	5	179.5	45.0	7.6	101.3	0.0	196.2	7.7		Close to sites 5–8 of Piper (1979)
Previous data of Piper 1979 for Group 1**																
25	diabase dyke	63.14	16.00			N	5	4.5	−46.6	11.9	42.0	−1.1	192.1	x		Piper 1979
28	diabase dyke	63.14	16.00			N	6	8.3	−13.0	12.4	30.0	20.0	187.3	x		Piper 1979
30	diabase dyke	63.14	16.00			N	6	349.2	−36.0	10.5	42.0	6.5	206.3	x		Piper 1979
19	diabase dyke	63.14	16.00			R	6	185.1	−14.4	10.3	43.0	34.1	189.9	x		Piper 1979
21	diabase dyke	63.14	16.00			R	4	178.3	6.1	9.9	87.0	23.8	197.9	x		Piper 1979
22	diabase dyke	63.14	16.00			R	6	168.0	47.2	22.3	10.0	−2.0	206.6	x		Piper 1979
24	diabase dyke	63.14	16.00			R	7	164.4	54.3	9.2	44.0	−8.8	208.9	x		Piper 1979
Grand mean group 1 (dykes) R-polarity						R	5*/27	351.1	−30.5	34.1	5.9	7.4	206.1	23.2		
Grand mean group 1 (dykes) N-polarity						N	7*/36	6.4	−18.3	22.8	6.9	16.7	189.7	19.3		
Grand mean group 1[a]	diabase dykes					C	12*/63	3.3	−23.5	18.7	6.3	12.8	194.1	14.9	9.5	
Previous data of Piper 1979 for Group 2**																
31	diabase dyke	63.10	16.00			N	6	58.3	63.5	6.9	96.0	53.1	107.1			Piper 1979
33	diabase dyke	63.10	16.00			N	6	37.5	56.1	10.5	42.0	55.1	137.4			Piper 1979
34	diabase dyke	63.10	16.00			N	6	357.2	48.0	5.7	141.0	55.9	200.4			Piper 1979
37	diabase dyke	63.10	16.00			R	6	181.7	−63.9	9.2	54.0	72.0	179.3			Piper 1979
Group 2 mean	diabase dykes					C	5*/31	28.2	54.2	19.9	15.8	58.3	150.0	23.2	11.8	
1	rapakivi massif	63.10	16.00			N	7	7.0	33.4	5.1	143.0	44.9	187.1			Piper 1979
2	rapakivi massif	63.10	16.00			N	6	13.6	35.2	26.6	7.0	45.3	176.1			Piper 1979
7	rapakivi massif	63.10	16.00			N	6	26.4	58.7	4.2	262.0	61.6	150.3			Piper 1979
8	rapakivi massif	63.10	16.00			N	4	42.0	51.2	10.8	73.0	49.2	136.2			Piper 1979
10	rapakivi massif	63.10	16.00			N	4	28.7	41.6	14.9	39.0	46.4	157.0			Piper 1979

(*continued on next page*)

Table 2 (*continued*)

Site	Rock type	SLat (N°)	SLong (E°)	Trend (N°)/dip(°)	Dyke width (m)	Pol.	(B)/N	Decl. (°)	Incl. (°)	α95 (°)	k	Plat. (N°)	Plon. (E°)	A95 (°)	K	Notes/Ref
11	rapakivi massif	63.10	16.00			N	6	30.3	59.3	8.4	65.0	60.9	144.1			Piper 1979
13	rapakivi massif	63.10	16.00			N	7	201.4	−26.7	4.4	186.0	50.3	184.6			Piper 1979
14	rapakivi massif	63.10	16.00			N	7	8.3	41.4	16.2	15.0	50.3	184.6			Piper 1979
15	rapakivi massif	63.10	16.00			N	8	27.1	38.6	7.9	50.0	44.8	159.9			Piper 1979
16	rapakivi massif	63.10	16.00			N	4	27.6	23.0	11.7	63.0	35.3	162.8			Piper 1979
17	rapakivi massif	63.10	16.00			N	6	349.9	52.9	13.6	25.0	59.7	213.4			Piper 1979
3	rapakivi massif	63.10	16.00			R	6	196.8	−55.6	2.4	811.0	61.1	167.5			Piper 1979
4	rapakivi massif	63.10	16.00			R	6	193.7	−56.1	4.1	274.0	62.3	172.5			Piper 1979
9	rapakivi massif	63.10	16.00			R	7	213.9	−53.2	2.9	439.0	53.9	144.6			Piper 1979
Host rapakivi massif	granite, gabbro					C	15*/91	19.8	47.9	13.3	9.2	54.9	166.2	13.6	8.9	Includes R05, R06 of this study 1505 ± 12 and 1514 ± 5 Ma from Persson (1999).
Grand mean group 2 (dykes + rapakivi massif) R-polarity						R	5*/32	11.6	59.6	10.4	54.8	66.7	175.1	15.0	27.0	
Grand mean group 2 (dykes + rapakivi massif) N-polarity						N	15*/90	24.2	45.8	13.7	8.7	52.0	159.8	14.1	8.3	
Grand mean group 2 (dykes + rapakivi massif)[b]						C	20*/122	20.4	49.4	10.7	10.3	56.0	163.0	11.1	9.6	1505 ± 12 and 1514 ± 5 Ma from Persson (1999).

Slat/Slong, Latitude/longitude of sampling site. Pol., polarity of the isolated magnetization direction: N/R/C, normal/reversed/combined polarity. Decl., declination. Incl., inclination. a95, the radius of the 95% confidence cone in Fisher (1953) statistics. Plat/Plong, paleolatitude/paleolongitude of the pole. A95, radius of the 95%.*, level of statistics. **α^{95} calculated here based on k and N. Pole calculated here based on direction and sampling site.

Reversal test of McFadden and McElhinny (1990), γc, citical angle; γo, observed angle.

[a] Reversal tes: γc: 25°; γo: 18°, indeterminate. Based on bootstrap statistics described in Tauxe et al. (1991), Tauxe et al. (2018) normal and reversed polarity directions are statistically indistinguishable (see Supplementary 1). With $A_{95} = 14.9°$ passes the PSV test of Deenen et al. 2011, 2014 ($A_{95min} = 4°$, $A_{95maz} = 17°$)

[b] Reversal test: γc: 23.4°; γo: 8.7°, indeterminate. Based on bootstrap statistics described in Tauxe et al. (1991), Tauxe et al. (2018) normal and reversed polarity directions are not the same (see Supplementary 1). With $A_{95} = 11.1°$ passes the PSV test of Deenen et al. (2011), (2014) ($A_{95max} = 12°$, $A_{95min} = 4°$)

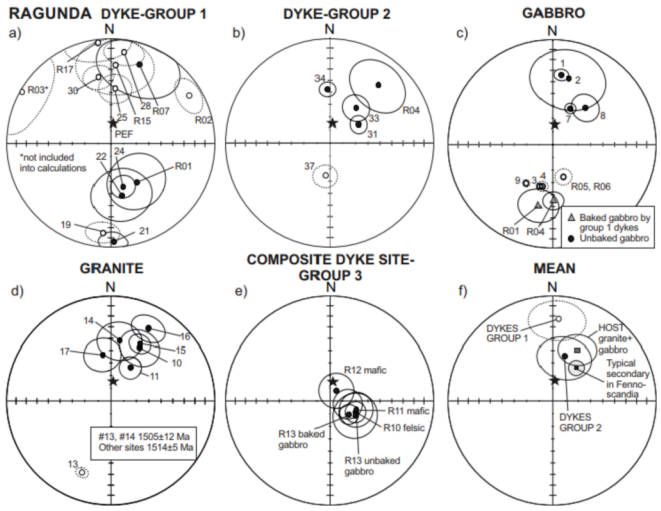

Fig. 8. Site mean ChRM directions with α_{95} error circles for the Ragunda rapakivi complex from this study combined with selected sites from the previous study of Piper (1979). (a) Dykes included in to Group 1. (b) Dykes included in to Group 2. (c) Rapakivi gabbro. (d) Rapakivi granite. (e) Composite dyke and rapakivi gabbro at the same site. (Means of different groups is shown in (f). Directions are shown in geographic coordinates on an equal area stereonet. Closed (open) symbols represent downward (upward) directions, black stars represent Present Earth Field (PEF) direction on the sampling area. Codes R01 (this study), 1 (Piper, 1979).

4.3. The Strömsbro rapakivi complex

Paleomagnetic results of the Strömbro rapakivi complex are listed in Table 3, and representative demagnetization behaviors are illustrated in Fig. 9. For the basic dykes both AF and thermal demagnetization were separating the ChRM with coercivities and unblocking temperatures typical for magnetite (Fig. 9), but AF was more efficient for isolating a ChRM. The directions are defined with a MAD $< 8°$. Four dyke and one sill sites show northeasterly magnetization directions with upward pointing low to intermediate inclination (Fig. 10). An exception is the dyke at the site S04, which shows distinctly steeper inclination. This dyke has been dated at 1258.4 ± 6.3 Ma (Furuvik; Söderlund et al., 2006) and is thus not related with the rapakivi complex. At site S06 samples from a basaltic sill were collected. The sill is located in the graben together with Jotnian sediments, which are partly assimilated to the sill, indicating a Post Jotnian age for the sill. The dyke S04 and sill data are not included in any mean calculations for the rapakivi complex.

The mean for the Strömsbro rapakivi complex is calculated from rapakivi related dykes at four sites (Table 3) at D: 13°, I: –22° (α_{95}: 16°, k: 35) (Fig. 10) yielding a paleomagnetic pole at Plat: 18°N, Plong: 184°E (A95: 15°, K: 38, with N: 35, B: 4) (Fig. 11, Table 3). A ChRM in the 1500 ± 19 Ma (Andersson, 1997b) rapakivi granite is best defined from AF demagnetizations and in the coercivity range 40–160 mT (Fig. 9), and traced during thermal demagnetizations in unblocking temperatures from 200 to ~ 560 °C typical for small grain (single domain) (titano)magnetite. Thermal demagnetization of the granite indicates a high unblocking temperature antipodal component (>500C°) carried by <ca 10% of the NRM (Fig. 9). However, the intensity of remanence is irregularly varying and no remanence vector could be defined. The ChRM directions are defined with a MAD generally $< 8°$. A poorly defined mean remanence direction for five granite samples is obtained at D: 17°, I: -49° (α_{95}: 17°, k: 21) yielding a virtual paleomagnetic pole at Plat: -1°N, Plong: 182°E (A_{95}: 18°) (Figs. 10 and 11, Table 3).

The main difference between the ChRM directions related with the Strömbro rapakivi granite and those of the 1260 Ma intrusions is in the inclination. The Post Jotnian intrusion in site S04 carries a direction close to the typical 1270 Ma northeasterly upward pointing intermediate inclination (e.g. Elming and Mattsson, 2001). Within the error limits the mean direction of the granite is the same as for the rapakivi related dykes, however with a steeper inclination (Figs. 10 and 11, Table 3). This invites a speculation of a possible 1270 Ma remagnetization of the granite. Yet, we consider this unlikely since the sill is located beyond the baking zone from the granite (ca 2.0 km, Andersson, 1997b) and the 2.0–4.7 % of the degree of AMS for the granite indicates a primary magnetic fabric with a steeply dipping foliation plane (Hrouda, 1982).

The poorly defined ChRM mean direction of the 1500 ± 19 Ma (Andersson, 1997b) Strömsbro granite (D: 17°, I: - 48.7°, α_9:17°) is very different from that previously presented by Piper (1980) (D: 26°, I: 17°, α_{95}: 17°), which is a typical secondary remanence direction obtained widely in Fennoscandia (e.g. Mertanen et al., 2008; Preeden et al., 2009; Salminen et al., 2014a) (Fig. 8f) and discussed also in the case of the Ragunda complex. Moreover, a similar low coercivity remanence direction is also observed in some of the Strömsbro complex samples (Fig. 9). We suggest that used modern demagnetizing techniques here are capable to isolate the ChRM, where as in the earlier study of Piper (1980) the ChRM was masked by secondary remanence.

4.4. The Rödö rapakivi complex

Representative thermomagnetic curves for samples from the Rödö complex are shown in Fig. 6. Thermomagnetic curves of basic dyke and rapakivi granite samples are irreversible indicating mineralogical alteration upon heating. Heating curves of dyke samples show Curie points near 580 °C and occasionally Hopkinson's peak indicating magnetite with variable grain size (Dunlop, 2014). Additionally, heating curves also indicate the presence of titanomagnetite by a decrease in susceptibility at 350–400 °C. A granite sample shows a sharp Hopkinson's peak and a Curie point at 580 °C indicating magnetite to be the carrier of magnetization. In addition, a prominent hump in susceptibility during the heating is obtained at 300 °C. For the Ragunda data similar thermomagnetic behavior was interpreted to be because of presence of pyrrhotite (Dekkers, 1990), which alters to magnetite during the heating.

Anisotropy of the magnetic susceptibility (AMS) directions of rapakivi related dykes (sites RD01–07) are generally not well-defined, possibly because of the samples have often been collected from the margins. On the contrary, the 1270 Ma sill site RD10 shows a well-defined horizontal foliation plane indicating a sill intrusion. The AMS of the granite reveal a predominantly magnetic foliation with steeply dipping foliation planes and nearly vertical directions of the axis of maximum susceptibility, possibly reflecting the flow direction of magma.

Paleomagnetic results of the Rödö rapakivi complex are listed in Table 4, and representative demagnetization behaviors are illustrated in Fig. 9. For the basic dykes, thermal demagnetization was more effective than AF demagnetization in isolating the ChRM, with unblocking temperatures typical for magnetite (Fig. 9). In addition, Hopkinson's peak obtained in thermomagnetic analyses indicated the presence of single-domain magnetite. The results from the thermal demagnetizations are therefore chosen for further analysis. The directions are defined with a MAD $< 5°$. Seven dykes show reversed polarity southerly magnetization directions with upward pointing shallow to intermediate inclinations (Fig. 9). The dyke at site RD09 carries a distinctly different northeasterly magnetization direction with downward pointing intermediate inclination and is not included into the mean (Fig. 10). A mean from in total six basic and one hybrid dykes is at D: 178°, I: -27° (α_{95}: 11°, k: 34) (Fig. 10, Table 4) yielding a paleomagnetic pole at Plat: 42°N, Plong: 201°E (A_{95}: 8°, K: 53, with N: 55, B: 7) (Fig. 11, Table 4). The 1270 Ma sill at RD10 shows typical 1270 Ma northeast magnetization direction with upward pointing intermediate inclination (e.g. Elming and Mattsson, 2001) (Table 4, Fig. 10b). The rapakivi granite in the contacts of basic dykes have been sampled in some sites. At two sites (RD02 and RD03) the

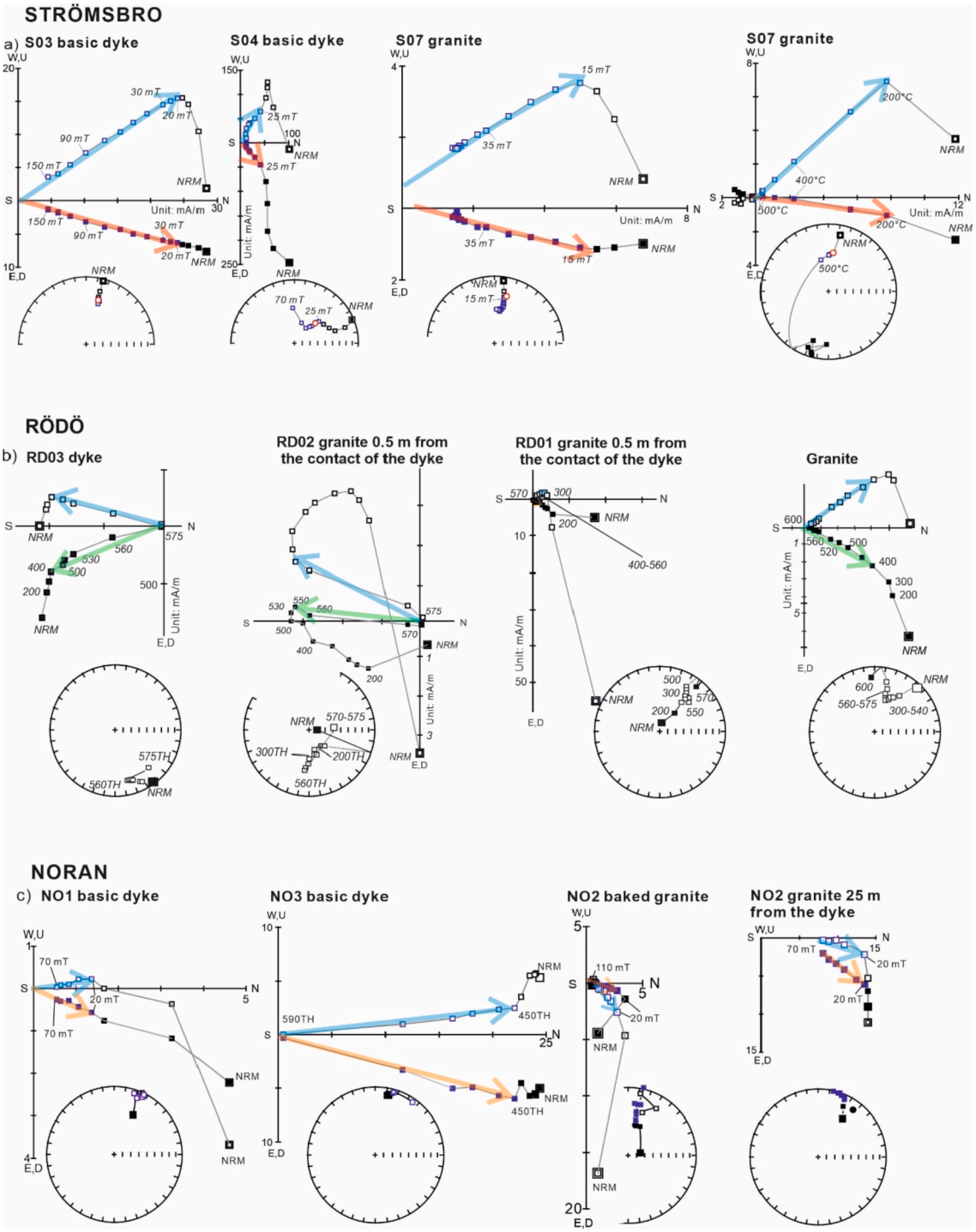

Fig. 9. Examples of AF and thermal demagnetization of the samples from the Strömbro, Rödö, and Noran rapakivi complexes. (a) the Strömsbro massif examples include cutting dykes and rapakivi granite. (b) the Rödö massif including cutting dykes and rapakivi granite. Figures show equal area stereographic and orthogonal projections (units: mA/m) of ChRM directions in geographic coordinates. Closed (open) symbols represent downward (upward) directions. R (N) refers to reversed (normal) polarity. Numbers by the demagnetization step denotes the used AF field (in mT) or temperature (in °C).

Table 3
Paleomagnetic results of the Strömsbro rapakivi complex.

Dyke site	Rock type	SLat (N°)	SLong (E°)	Trend (N°)/ dip(°)	Dyke width (m)	Polarity	(B)/ N	Decl. (°)	Incl. (°)	α95 (°)	k	Plat. (N°)	Plon. (E°)	A95 (°)	K	Notes
Dolerite																
S01	dolerite dyke	60.75	17.36	60		N	8	24.9	−14.1	6.5	75	19.3	171.1	4.7		
S02	dolerite dyke	60.73	17.31	47		N	7	355.2	−19.9	11.2	30	18.9	202.3	8.4		
S03	dolerite dyke	60.67	17.31	25		N	7	18.5	−30.6	5.4	128	11.4	179.2	4.5		
S04[a]	dolerite dyke	60.66	17.35	52		N	8	45.5	−63.6	7.3	59	−22.1	164.5	10.3		1258.4 ± 6.3 Ma (Furuvik) from Söderlund et al., 2006
S05	dolerite dyke	60.65	17.39	58		N	13	11.3	−19.9	4.1	106	18.5	185.7	3.1		
S06[a]	basic sill	60.67	17.18			N	6	15.9	−34.6	11.3	36	9.3	182	9.9		
Mean[b]	dolerite dykes						4*/ 35	12.5	−21.5	15.9	35	17.5	184.4	15.1	38.2	
S07	granite	60.7	17.15			N	1/5	17.2	−48.7	17.2	21	−1.4	182.3	18.4		1500 ± 19 Ma from Andersson, 1997

Slat/Slong, Latitude/longitude of sampling site. Pol., polarity of the isolated magnetization direction: N/R/M, normal/reversed/mixed polarity. (B)/N, number of (sites) samples. Decl., declination. Incl., inclination. a95, the radius of the 95% confidence cone in Fisher (1953) statistics. Plat/Plong, paleolatitude/paleolongitude of the pole. A95, radius of the 95%.*, level of statistics. [a]excluded, [b]With $A_{95} = 15.1°$ pass the PSV test of Deenen et al. (2011), (2014) ($A_{95min} = 7°$, $A_{95max} = 34°$), but the number of sites B < 8..

granite baked by dykes shows directions similar to those of the dykes with southerly magnetization direction and upward pointing shallow inclination (Figs. 9 and 10, Table 4). However, at site RD01 the obtained northeasterly ChRM direction with upward pointing shallow inclination from the presumably baked granite is very different from the dyke direction (Fig. 10). This direction is similar to the ChRM obtained from several granite sites, with no visible intruding dykes. Additionally, similar ChRM direction is obtained in unbaked granite at the sites RD02 and RD03 (Figs. 9 and 10; Table 4). In general, the ChRM of both baked and unbaked granite is best isolated by thermal demagnetization with unblocking temperatures typical for magnetite generally with MAD < 8°. The mean ChRM from 1497 ± 6 Ma (Andersson et al., 2001) granite sites is at D: 24°, I: -35° (α_{95}: 6°, k: 36) yielding a paleomagnetic pole at Plat: 6°N, Plong: 175°E (A_{95}: 5°, K: 47, with N: 20) (Figs. 10 and 11, Table 4).

The mean ChRM direction for the Rödö granite is well off from known 1270 Ma direction (Fig. 10, Table 4). However, the observation, that the error limit of the mean ChRM from four samples on granite at site RD03 overlaps with both the mean granite and the 1270 Ma directions, may argue for a selective 1270 Ma remagnetization of the granite (Table 4, Fig. 10). The origin of such remagnetization may be in different porosities and fluids related with the Post Jotnian dykes might more easily have penetrated the granite, resulting in a chemical remagnetization. The measured porosity of the granite is low (ca 0.9 %) but the porosity of the dykes is even lower (ca 0.3%). There are also cavities in the granite, which may support such a fluid related selective remagnetization, but in case of the Rödö granite we doubt this option. If the remagnetization is not the case, the paleomagnetic pole calculated from the ChRM of the rapakivi related dykes may represents an original 1497 Ma magnetization. The difference in pole positions between the ChRM of the dykes at sites RD01-07 and that of site RD09 may be related to age differences. Andersson (1997a) discusses a possible succession in age between the different types of dykes, a succession that may explain the different pole positions.

Apart from the Rödö rapakivi related dykes the area is intruded by Post Jotnian dykes and ca 1.5 km south of the rapakivi intrusion samples have been collected from a Post Jotnian sill (site RD11). The AMS measurements reveal a magnetic foliation in the sill, with foliation plane that dips a few degrees to north-west, i.e. towards and beneath the present surface of the rapakivi granite. This indicates that a remagnetization of the rocks in the area may be possible.

4.5. The Noran rapakivi complex

Paleomagnetic results of the Noran rapakivi complex are listed in Table 5, and representative demagnetization behaviors are illustrated in Fig. 9. For the basic dykes both AF and thermal demagnetization were isolating a ChRM with coercivities and unblocking temperatures typical for magnetite (Fig. 9). Four dykes show normal polarity north-northeasterly ChRM direction with both up- and downward pointing shallow inclinations (Figs. 9 and 10) with MAD < 9°.

The natural remanent magnetization (NRM) of the basic dykes sometimes includes only a soft component, which is reflected in Mean Destructive Fields (MDFs) as low as 7 mT. Harder magnetization components are found in part of the samples with MDFs up to 90 mT. NRM of the samples with a dominant soft component is often close to that of the PEF direction (D: 6°, I: 75°). The mean for four well-defined site means of basic dyke is D: 15°, I: − 1° (α_{95}: 19°, k: 24) yielding a paleomagnetic pole at Plat: 28°N, Plong: 179°E (A_{95}: 11°, K: 72, with N: 31, B: 4) (Figs. 10 and 11, Table 5).

The baked granite contact carries different magnetization directions in the different sites. For the baked granites 50% of the NRM is erased in temperatures < 250 °C and unblocking temperatures are low. The MDFs vary between ca. 15 and 25 mT and the direction of the soft magnetization component is close to PEF direction at the sampling site. The ChRM directions are isolated in demagnetization fields ≥ 30 mT with MAD ≤ 12°. At site NO2 ChRM direction is northerly with shallow downward pointing inclination (D: 359.8°, I: 9.0°) close to ChRM of the dykes (Figs. 9 and 10). Whereas in the sites NO3 and NO4 the ChRM direction is northeasterly with intermediate downward pointing inclinations (Table 5). The ChRM direction of the baked granite in site NO3 and NO4 is probably reflecting an imperfect thermal cleaning from the PEF magnetization. The granite far away from the intruding dykes carries a NRM, which sometimes is characterized by a large portion of low coercivity remanence, with a direction close to that of the PEF at the sampling site. However, the coercivity varies, reflected in the MDF which are between 7 and 55 mT and the ChRM direction for the 1469 ± 10 Ma old granite (Claesson and Kresten, 1997) is obtained in both AF

Table 4
Paleomagnetic results of the Rödö rapakivi complex.

Dyke site	Rock type	SLat (N°)	SLong (E°)	Trend (N°)/dip(°)	Dyke width (m)	Pol.	(B)/N	Decl. (°)	Incl. (°)	α95 (°)	k	Plat. (N°)	Plon. (E°)	A95 (°)	K	Notes
RD01	hyb. porphyry dyke	62.37	17.56	360	2	R	7	171.0	−38.3	5.5	119.8	21.5	228.7	5.0		
RD02	dolerite dyke	62.37	17.56	360	5	R	17	179.1	−17.8	4.2	74.0	36.7	198.7	3.1		
RD03	dolerite dyke	62.37	17.56	4	10	R	8	177.9	−11.3	6.1	83.2	33.3	200.1	4.4		
RD04	dolerite dyke	62.37	17.56	4	0.3	R	3	177.3	−17.7	10.3	144.3	36.7	200.9	7.7		
RD05	dolerite dyke	62.37	17.56	342	2	R	11	180.9	−47.4	4.1	126.4	56.2	196.1	4.3		
RD06	dolerite dyke	62.37	17.56	0	3	R	4	177.0	−18.1	23.3	16.6	36.9	201.1	17.5		
RD07	dolerite dyke	62.37	17.56	5	?	R	5	180.4	−36.2	12.3	39.9	47.7	197.0	10.9		
RD09[a]	dolerite dyke?	62.37	17.56		1.2	N	6	38.1	35.9	3.4	515.7	40.1	148.2	3.0		
Mean dykes sitesRD01-07[b]						R	7*/55	177.6	−26.7	10.5	33.9	41.7	200.7	8.4	52.6	
					Distance from the dyke (m)											
RD01 - granite	granite, unbaked?				0.5	N	2	27.8	−18.1			15.2	169.1			
RD02 - granite	granite, baked				0.5–2	R	2	189.5	−12.5			33.5	186.2			
RD02	granite, unbaked				0.7–6.5	N	4	23.5	−40.3	6.3	212.0	2.6	176.0			
RD03 - granite	granite, baked					R	1	182.0	−13.0			34.2	195.2			
RD03	granite, unbaked				2.1–10.5	N	4	23.3	−29.6	21.0	20.1	9.7	174.9			
RD05 - gneiss	gneiss, baked					R	1	166.0	−40.0			49.3	217.5			
Rapakivi granite host - several sites	granite					N	20	23.7	−35.0	5.5	36.2	6.2	175.1	4.8	47.2	1497 ± 6 Ma from Andersson et al., 2002
RD10	1270 Ma sill	10					15	45.9	−44.1	3.1	155.0	−5.5	157.1	3.1		

Slat/Slong, Latitude/longitude of sampling site. Pol., polarity of the isolated magnetization direction: N/R/M, normal/reversed/mixed polarity. (B)/N, number of (sites) samples. Decl., declination. Incl., inclination. a95, the radius of the 95% confidence cone in Fisher (1953) statistics. Plat/Plong, paleolatitude/paleolongitude of the pole. A95, radius of the 95%.*, level of statistics. [a]excluded. [b]With A95=8.4° pass the PSV test of Deenen et al.,(2011), (2014) (A95min=7°, A95max=34°), but the number of sites B<8.

Table 5
Paleomagnetic results of the Noran rapakivi complex.

Dyke site	Rock type	SLat (N°)	SLong (E°)	Trend (N°)	Dyke width (m)	Pol.	(B)/N	Decl. (°)	Incl. (°)	α95 (°)	k	Plat. (N°)	Plon. (E°)	A95 (°)	K	Notes
NO1	diabase dyke	60.43	15.16			N	8	9.3	−5	10.5	27	26.6	184.8	7.7		
NO2	diabase dyke	60.43	15.16			N	8	19.6	16	12.9	19	35.7	171	9.5		
NO3	diabase dyke	60.43	15.16	24		N	8	12.2	−20.6	10.2	31	18.3	182.5	7.7		
NO4	diabase dyke	60.46	15.18	7		N	7	18.3	8.3	9.6	40	32	173.5	6.9		
Mean[a]	diabase dykes					N	4*/31	14.8	−0.3	19.4	24	28.3	178.7	10.9	71.8	
NO2	granite, baked	60.43	15.16			N	3	359.8	9	36.5	13	34.1	195.4			
NO5	granite, unbaked	60.43	15.16			N	7	24.2	−0.5	10.9	32	26.5	167.9	7.7		1469 ± 10 Ma from Claesson and Kresten (1997)

Slat/Slong, Latitude/longitude of sampling site. Pol., polarity of the isolated magnetization direction: N/R/M, normal/reversed/mixed polarity. (B)/N, number of (sites) samples. Decl., declination. Incl., inclination. a95, the radius of the 95% confidence cone in Fisher (1953) statistics. Plat/Plong, paleolatitude/paleolongitude of the pole. A95, radius of the 95%.*, level of statistics.

[a] With $A_{95} = 10.9°$ pass the PSV test of Deenen et al. 2011, 2014 ($A_{95min} = 7°$, $A_{95max} = 34°$), but the number of sites B < 8.

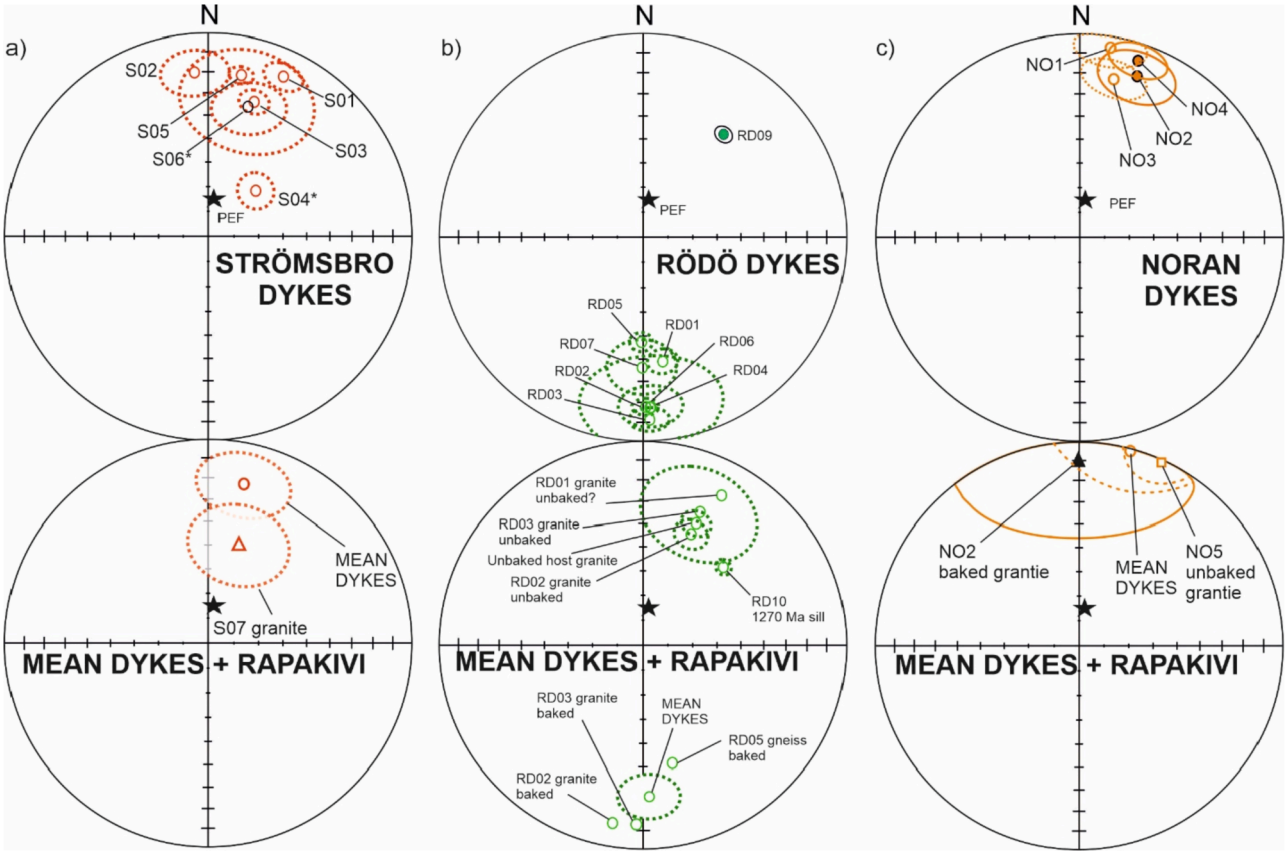

Fig. 10. Site mean ChRM directions with α_{95} error cirles for the Strömsbro, Rödö and Noran rapakivi complexes. (a) Strömsbro dykes and one sill (S06) (upper), and means of selected dykes and rapakivi granite (lower). (b) Rödö dykes (upper) and means of selected dykes, 1270 Ma sill, and rapakivi granite (lower). (c) Noran dykes (upper) and means of dykes and rapakivi granite (lower). Directions are shown in geographic coordinates on an equal area stereonet. Closed (open) symbols represent downward (upward) directions, black stars represent Present Earth Field (PEF) direction on the sampling area. * indicate site excluded from the mean.

and thermal demagnetization with coercivities and unblocking temperatures typical for magnetite (Fig. 9) with MAD ≤ 8°. The mean ChRM from seven samples is at D: 24°, I: − 1° (α_{95}: 11°, k: 32) yielding a pole at Plat: 27°N, Plong: 168°E (A_{95}: 8°) (Figs. 10 and 11, Table 5).

The site means from basic dykes and the Noran rapakivi granite are the same within the error limits (Figs. 10, 11 and Table 5) and may represent a 1469 Ma magnetization for the Fennoscandian shield. A primary magnetization of the granite and basic dykes is suggested because the intrusions of the granite and associated dykes post dates all significant tectonismanyhow in the region (Claesson and Kresten, 1997). Moreover the poles are located close to the 1452 Ma Lake Ladoga pole (Lubnina et al., 2010) and the mean 1469 Ma pole from Swedish dyke swarms (Table 6; Fig. 11).

5. Origin of the magnetization in the studied intrusions and the quality of the data

The mean magnetizations directions of the Kopparnäs dykes, the Ragunda, the Strömsbro, the Rödö and the Noran rapakivi complexes together with the obtained poles and paleolatitudinal position for Baltica are shown in Fig. 11 (Table 6). To discuss the magnetization ages we compare the poles of this study with the high-quality paleomagnetic

data of Baltica tabulated in to the Table 6, where the quality of the data is expressed on basis of the grading scheme by Van der Voo (1990) and on reliability Grade-A and Grade-B established in the Nordic Paleomagnetic Workshops (NPW) (Pesonen et al., 1991; Evans et al., 2021). For data of this work and the recent poles, not yet graded in the NPWs, we show revised quality R-criteria of Meert et al. (2020).

The granites from the rapakivi complexes studied here are previously dated, but geochronology for dykes does not exist. The vertical to subvertical Kopparnäs dykes in southern Finland are considered to be temporally close with the Obbnäs rapakivi granite dated at 1645 ± 5 Ma (Vaasjoki, 1977) and 1640 ± 14 Ma (Kosunen unpublished data in Heinonen et al., 2010). Moreover, the Kopparnäs dykes do not cut the Obbnäs rapakivi granite and are regarded slightly older than the granite. The granites from the Ragunda complex have ages of 1505 ± 5 Ma and 1514 ± 5 Ma (Persson, 1999), granite from the Strömsbro complex yields an age 1500 ± 19 Ma (Andersson, 1997b), the Rödö complex is dated to 1497 ± 6 Ma (Andersson et al., 2001), and the age for the Noran granite is 1469 ± 10 Ma (Claesson and Kresten, 1997). The sampled vertical to subvertical dykes associated with these Swedish rapakivi complexes cut the rapakivis. In addition, field relations (see the section 2.2) point out that during the intrusion of some of these dykes the rapakivi was only partly crystallized, indicating very close temporal relation between rapakivi and dykes. Additionally, there might be several temporally close generations of the dykes intruding rapakivi such as the ones in the Ragunda complex (see section 2.2.2). Since the studied dykes are vertical to subvertical the blocks they intruded have not been tilted after the emplacement of the dykes. In addition, the sampled dykes and rapakivi complexes are all regarded younger than the last tectonic deformation (Svecokarelian) in the area (Stephens, 2020).

The undated Kopparnäs dykes carry dual polarity ChRM, yet these directions do not share a common mean. In addition, a full positive baked contact test was not obtained (Fig. 11; Tables 1 and 6). Since the unbaked Svecofennian host rocks carry a ChRM consistent with a known Svecofennian direction (Neuvonen et al., 1981), which clearly deviates from the dyke direction, it is speculated that the remanence of the dykes is primary. Consequently, any pervasive overprinting for the Kopparnäs dykes is ruled out. The dykes of the Ragunda Group 1 carry ChRMs with dual polarity and a positive baked contact test is demonstrated for a dykes intruding a gabbroic part of the rapakivi complex (Fig. 11; Tables 2 and 6). This argues for a primary magnetization of the Ragunda Group 1 undated dykes. For the Ragunda Group 2 dual polarity ChRM directions are obtained from basic dykes, and from both the dated

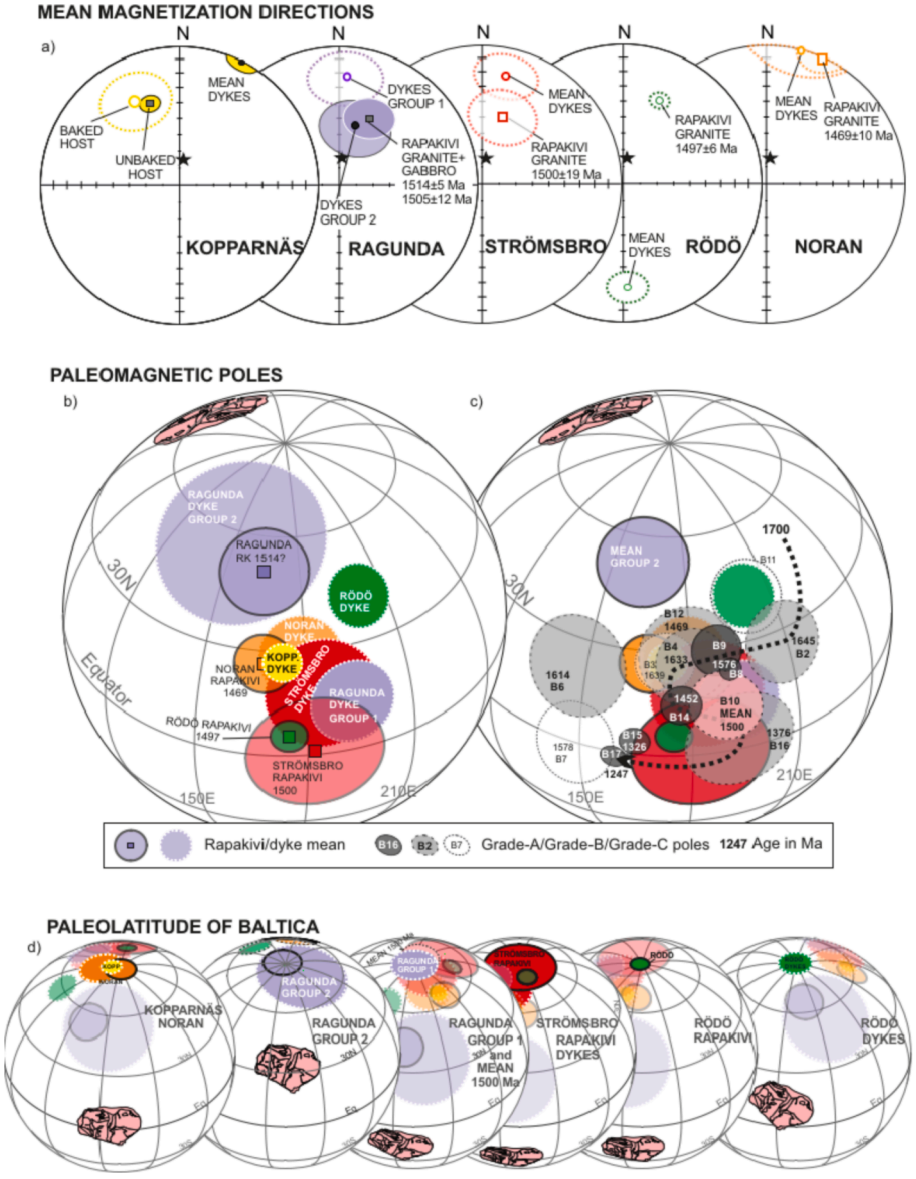

Fig. 11. Mean paleomagnetic data from this study. (a) Mean magnetization directions of all the study areas (geographic coordinates on an equal area stereonet). Closed (open) symbols represent downward (upward) directions, black stars represent Present Earth Field (PEF) direction on the sampling area. (b) The poles of this study. (c) The poles of this study with the 1650–1250 Ma high quality paleomagnetic poles for Baltica (Table 6). (d) Paleolatitude of Baltica based on data of this study. Note: the grand mean 1500 Ma is shown together with the Ragunda Group 1. Closed (open) symbols represent downward (upward) directions, black stars represent Present Earth Field (PEF) direction on the sampling area. Color coding of poles matches between the figures.

Table 6
Selected paleomagnetic data for Baltica.

Code	Rockname	Slat (°N)	Slon (°E)	Age (Ma)	Met	Age references	NominalAge (Ma)	Pol	B	N	D (°)	I (°)	α_{95} (°)	k	Plat (°N)	Plon (°E)	A_{95} (°)	Q/R1234567 SUM	Key	Pole references/ Notes
B1	Turinge gabbro-diabase	63	15	1703 ± 6, 1687 ± 13, 1622 ± 5, 1700 ± 4	c, g	Elming et al. (2019)	1700	N	6	56	343	44	5	199	52	220	4.8	Q1 1 1 1 1 0 1 6 R1 0 0 1 1 0 1 4	**	Elming et al. (2019)
B2	Häme dyke + Satakunta E-W dykes	61	21–27	1642 ± 2, 1647 ± 14, 1640 ± 6	g	Salminen et al. (2017), Luttinen et al. (submitted)	1645	C	15	75	355	−04	13	10	26	209	10.9	R1 1 1 1 1 1 1 7	**	this work
B3	Suomenniemi dyke swarm	61	27	1635 ± 2, 1643 ± 5, 1638 ± 32	g	Siivola (1987), Vaasjoki et al. (1991), Siivola (1987)	1639	N	9	32	031	07	11	22	28	172	7.6	R1 1 1 0 1 1 1 6	**	Salminen et al. (2019)
B4	Sipoo quartz porphyry dyke swarm	60	25	1633 ± 10	g	Törnroos (1984)	1633	N	5	34	022	−02	13	34	26	180	9.4	Q1 1 1 0 1 0 1 5 R1 0 1 0 1 0 1 4	B	Mertanen and Pesonen (1995)
B5	Sipoo diabase dyke swarm	60	25				1633	C	5	21	198	−07	28	8	32	185	20.2	Q0 0 1 0 1 1 1 4 R0 0 1 0 1 1 1 4	***	Mertanen and Pesonen (1995)
B6	Hoting basic dykes	64	16	1614 ± 24	c	Elming et al. (2009)	1614	N	4	41	045	09	19	24	22	147	13.7	Q1 0 1 1 1 0 1 5 R0 0 1 1 1 0 1 4	B	Elming et al. (2004), Elming et al. (2009)
B7	Nordingrå granite	63	19	1578 ± 19	g	Welin and Lundqvist (1984)	1578	C	28	28	221	−25	13	5	03	149	10.5	Q1 0 1 0 0 1 0 3 R0 0 1 0 0 1 0 2	***	Piper (1980)
B8	Åland intrusives	60	20	1575.9 ± 3, 1569 ± 3, 1577 ± 12	g	Salminen et al. (2016a), Salminen et al. (2016b)	1576	C	96	366	009	−11	4	14	24	191	2.9	Q1 1 1 1 1 1 1 7 R 1 1 1 1 1 1 1 7	A	Salminen et al. (2016a), Salminen et al. (2016b)
B9	Satakunta dyke swarm	62	22	1565 ± 35, 1575.9 ± 3	g	Lehtonen et al. (2003), Salminen et al. (2014b)	1576	C	20	104	012	03	3	16	29	188	6.6	Q1 1 1 1 1 1 1 7 R1 1 1 1 1 1 1 7	A	Salminen et al. (2014b)
	Kopparnäs dykes	60	20	1645 ± 5; 1640 ± 14	g	Vaasjoki (1977), Kosunen (2004)	1640	C	17	98	027	01	7	27	27	173	5	R0 1 1 0 1 0 1 4	**	this work, , see Table 2 age from Obnäss rapakivi granite
	Ragunda-dykes group 2 + host	63	16	1505 ± 12, 1514 ± 5	g	Persson (1999)	1514	C	20	122	020	49	11	10	56	163	11	R1 1 1 1 1 0 1 6	**	this work, see Table 2
	Ragunda-dykes group 1*	63	16					C	12	63	003	−24	19	6	13	194	14.9	R0 1 1 1 1 1 1 5	**	this work
	Strömsbro rapakivi*	61	17	1500 ± 19	g	Andersson (1997b)	1500	N	1	5	017	−49	17	21	−01	182	18.4	R0 0 1 0 1 0 0 2	**	this work
	Strömsbro dykes*	61	17		g	Andersson (1997b)	1500	N	4	35	013	−22	16	35	18	184	15.1	R0 0 0 0 1 0 1 2	**	this work
	Rödö rapakivi*	62	18	1497 ± 6	g	Andersson et al. (2001)	1497	N	1	20	024	−35	6	36	06	175	4.8	R1 0 1 1 1 0 1 5	**	this work
	Rödö dykes	62	18			Andersson et al. (2001)	1497	R	7	55	178	−27	11	34	42	201	8.4	R0 0 1 1 1 0 1 4	**	this work
	Noran	60	15	1469 ± 10	g	Claesson and Kresten (1997)	1469	N	4	31	015	00	19	24	28	179	10.9	R1 0 1 0 1 0 1 4	**	this work
	*R-polarity Mean 1500 (Ragunda-dykes group 1, R-polarity)	62	17					R	5	27	351	−31	34	6	07	206	23		**	this work
	*N-polarity Mean 1500 (Ragunda-dykes group 1 N-polarity, Strömsbro, Rödö rapakivi)	62	17					N	13	96	014	−30	11	11	11	184	8.6		**	this work

(*continued on next page*)

Table 6 (*continued*)

Code	Rockname	Slat (°N)	Slon (°E)	Age (Ma)	Met	Age references	NominalAge (Ma)	Pol	B	N	D (°)	I (°)	α_{95} (°)	k	Plat (°N)	Plon (°E)	A_{95} (°)	Q/R1234567 SUM	Key	Pole references/ Notes
B10	*Mean 1500[a] (Ragunda-dykes group 1, Strömsbro, Rödö)	62	17	1497 ± 6, 1500 ± 19, 1505 ± 12, 1514 ± 5	g	Persson (1999), Andersson (1997b), Andersson et al. (2001)	1500	C	18	123	007	−25	13	8	13	190	10	R1 1 1 1 1 1 1 7	**	
B11	Rödö basic dykes	62	18	1497 ± 6	g	Andersson et al. (2001)	1497	R	6	53	177	−27	12	33	42	202	9.5	Q1 1 1 1 1 0 0 5 R1 0 1 0 1 0 0 3	B	Moakhar and Elming (2000)
B12	MEAN Turinge/Bunkris/ Glysjon/Oje	62	14	1461.2 ± 1.2, 1474 ± 4	g	Lundström et al. (2002), Söderlund et al. (2005)	1469	N	4	65	011	00	0	24	28	180	13.2	Q1 1 1 0 1 0 1 5 R 1 1 1 0 1 0 1 5	B	LULEÅ WORKSHOP in Evans et al. (2021)
B13	Valaam sill	61	31	1457 ± 2	g	Rämö et al. (2001)	1457	N	9	36	043	−14	3	239	14	166	2.4	Q1 1 1 0 1 0 1 5 R 1 1 1 0 1 0 1 5	B	Salminen and Pesonen (2007)
B14	Lake Ladoga basalt, sill, dykes	62	31	1452 ± 12	g	Lubnina et al. (2010)	1452	M	13	278	033	−17	7	169	15	177	5.3	Q1 1 1 1 1 1 1 7 R1 1 1 1 1 1 1 7	A	Lubnina et al. (2010)
B15	Bornholm Group I dykes	55	15	1326 ± 10	g	Holm et al. (2005)	1326	C	32	232	032	−41	6	22	06	165	5.6	R1 1 1 1 1 1 1 7	**	Luoto et al. this issue
B16	Mashak suite: Combined South Urals intrusions	54	57	1366 ± 6, 1384 ± 3	g	Ernst et al. (2006)	1376	M	4	55	051	−39	16	34	02	193	14.8	Q1 0 0 1 1 1 1 5 R1 0 0 1 1 1 1 5	B	Lubnina (2009)
B17	Mean Post Jotnian (Luleå)	62	18	1247.4 ± 2.2	g	Söderlund et al. (2006)	1247	N	53	938	043	−40	6	143	−02	159	3.4	Q1 1 1 1 1 0 1 6 R 1 0 1 1 1 0 1 5	A	Elming and Mattsson (2001), α 95 and k calculated in this work

Code, code used in Fig. 11. Rockname, name of the rock unit. Slat/Slong, Latitude/longitude of sampling site. Age, isotope age results. Method: c, 39Ar-40Ar; g, U-Pb. Nominal age, Mean of several age determinations or the one favored by pole authors. Pol, polarity of the isolated magnetization direction. N/R/C/M, normal/reversed/combined/mixed polarity. B/N, number of sites/samples. D, declination. I, inclination. alpha95, the radius of the 95% confidence cone in Fisher (1953) statistics. Plat/Plong, paleolatitude/paleolongitude of the pole. A95, radius of the 95% confidence cone of the pole. Key, Grade of the pole (Pesonen et al., 1991; Evans et al., 2021).

*included in to 1500 Ma mean pole for Baltica.

** in key-column indicates that the pole has not been graded yet in the Nordic Paleomagnetic Workshop. Q, van der Voo (1990) criteria. R, updated van der voo criteria (Meert et al. 2020). Reversal test of McFadden and McElhinny (1990), γc, citical angle; γo, observed angle.

***in key-column indicates that the pole has been graded in the NPW, the grade is lower than B.

[a] this work (site weighted mean); K: 14. Reversal test: γc: 45°; γo: 21°, indeterminate. Based on bootstrap statistics described in Tauxe et al. (1991, Tauxe et al. (2018) normal and reversed polarity directions are statistically indistinguishable (see Supplementary 1). With $A_{95} = 10°$ pass the PSV test of Deenen et al. (2011), (2014) ($A_{95max} = 12°$, $A_{95min} = 4°$).

~1510 Ma granite and the gabbro at a far distance from any observed dyke, however these directions do not share a common true mean. An inverse baked contact test with Ragunda Group 1 dykes against the Group 2 gabbro (Fig. 11) suggests a primary magnetization also for the Ragunda Group 2 ChRM with an age of ~1510 Ma (see also section 4.2). In addition, the Ragunda Group 1 dykes must be younger than the Ragunda Group 2 dykes. Moreover, based on paleosecular variation test of Deenen et al. (2011) the secular variation is averaged out. The distance of ca. 60° between the 1510 Ma Ragunda Group 2 and undated Group 1 poles (Fig. 11) may be explained in two ways. Either the Group 1 pole is substantially younger than the Group 2 or if their ages are nearly coeval, Baltica experienced an apparent rapid drift (ca. 40 cm/yr) between the magnetization of the Group 2 and Group 1 intrusions. Based on the close proximity of the Ragunda Group 1 pole with other ca. 1500 Ma poles of this study we favor the latter, in this case the true polar wander (Evans, 2003) event offers a possible explanation for the apparent rapid drift.

For the ~1497 Ma Rödö granite a primary origin of the ChRM cannot be proved, even if a positive inverse baked contact test may be demonstrated in some cases. The magnetization of the baked Rödö granite is complex since sometimes the granites are baked by the dykes and sometimes not, which may relate to differences in magnetic mineralogy. For both the ~1500 Ma Strömsbro and ~1469 Ma Noran granite and associated dykes there are no field tests to demonstrate the primary origin of ChRM. The ChRM of the Noran rapakivi agrees with that of the Noran dykes indicating a coeval magnetization age and the same applies to the ChRMs of the Strömsbro granite and Strömsbro dykes. In contrast, the magnetization of the Rödö rapakivi and the dykes are distinctly different (Fig. 11). The R-scoring (Meert et al., 2020) of the paleomagnetic data from this work is shown in the Table 6. In case of dual polarity, we conducted reversals test on the normal and reversed polarity groups (McFadden and McElhinny, 1990) using paleomagnetism.org 2.2.0 (Koymans et al., 2016) and super-IAPD (Torsvik et al., 2000) program (Tables 1, 2 and 6). In case of indeterminate results, we tested with the bootstrap statistics described in Tauxe et al. (1991); Tauxe et al. (2018) if the normal and reversed polarity sites share a common true mean direction at 95% confidence level (see Supplementary 1). The quality of data varies from poor quality Strömsbro data (R-score: 2) to high-quality Ragunda Group 2 (R-score: 6) data. We calculated a new high-quality ~1500 Ma mean pole including the data of the Strömsbro dykes and rapakivi granite, the Rödö rapakivi granite and the Ragunda Group 1 at Plat: 13°N and Plong: 190°E (with A95: 11°, K: 14) fulfilling all the R-criteria (R-score: 7). The data for the mean 1500 Ma pole yields an indeterminate class (a critical angle 45°, an obtained angle 21°) for thea reversal test (McFadden and McElhinny, 1990). However, based on the bootstrap statistics described in Tauxe et al. (1991), Tauxe et al. (2018) normal and reversed polarity data share the common mean for the mean 1500 Ma data (see Supplementary 1).

Most of the poles of this work define a somewhat spread cluster located at equatorial to low latitudes so that A_{95} confidence cones of poles partly overlap (Fig. 11). The cluster includes poles of the Kopparnäs dykes, the Ragunda dykes (Group 1), the ~1497 Ma Rödö granite, both the ~1500 Ma Strömsbro granite and the dykes, and both the ~1469 Ma Noran granite and the dykes (Table 6). The cluster overlaps with the 1645 Ma, 1633 Ma, 1576 Ma, 1450 Ma, 1376 Ma and 1326 Ma high-quality poles of Baltica. Furthermore, the Kopparnäs pole overlaps with the 1633 Ma Sipoo and 1639 Ma Suomenniemi poles and also with the 1469 Ma Noran poles and the 1469 Ma mean pole from Swedish dykes, but ca. 30° west from the new well-defined 1645 Ma combined Häme and Satakunta E-W-dykes pole (Table 6). The 1650–1610 Ma poles show a wide spread on the latitude of ca. 25° (Table 6, Fig. 11) this controversy is previously noted and discussed in Salminen et al. (2019).

The new ~1500 Ma mean pole plots on a younger part of the of 1650–1380 Ma apparent polar wander path defined by high-quality poles of Baltica (Fig. 11). This comparison with the high-quality data indicates that Baltica did not experience marked plate movement during the time period at about 1650–1380 Ma and Baltica was located on equatorial to southerly latitudes (Fig. 11).

Outliers to the cluster are the poles from the Ragunda Group 2 dykes, the ~1510 Ma Ragunda rapakivi (Group 2), and the <1497 Ma Rödö dykes located on intermediate latitudes (Fig. 11; Table 6). A possibility for Post Jotnian remagnetization for the Rödö dykes pole was discussed in section 4.4, but for the Ragunda Group 2 it is unlikely because of positive baked contact test and we doubt it also for the Rödö dyke pole because of partially baked host rock. The existence of nearly coeval high and low latitude poles indicate rapid oscillations from ~1510 Ma high latitude pole (Ragunda Group 2) to ~1500 Ma low latitude pole (Ragunda Group 1) and back to high latitude by ≤1497 Ma (Rödö dykes). This rapid oscillation resembles the known Ediacaran rapid shifts between high and low latitude pole positions (e.g. Abrajevitch and Van der Voo, 2010; Meert, 2014; Klein et al., 2015). Abrajevitch and Van der Voo (2010) argue that the shifts in pole positions during Ediacaran are the result of the geomagnetic field switching between a dominant axial dipole field and an equatorial dipole field. Unfortunately, coeval paleomagnetic data is lacking from other cratons than Baltica (PALEOMAGIA database, Veikkolainen et al., 2017), so testing this hypotheses waits for new paleomagnetic data. Same applies to testing other hypotheses proposed for apparent rapid shifts in pole positions, such as rapid plate motions (Meert et al., 1993) or true polar wander (Evans, 1998).

6. Origin of massif-type anorthosites in light of paleomagnetic data

6.1. Rifting as the origin of massif-type anorthosite magmatism

Proterozoic massif-type anorthosite batholiths and related crustal magmatic rocks (Ashwal and Bybee, 2017) are widely distributed throughout the cratonic regions of majority of the continents (Fig. 12). One of the theories explaining the origin of the Proterozoic massif-type anorthosite magmatism include a rift environment (e.g. Emslie, 1978; Sharkov, 2010). Shallow and undulating Moho is often associated with the Fennoscandian rapakivi granite occurrences (e.g. Korja et al., 1993; Vigneresse, 2005). Korja et al. (2001) interpreted these Moho undulations as crustal thinning to 42 km during extension because of an aborted intracontinental listric fault zones in connection with the rapakivi magmatism. Since the present day Moho depth in the Fennoscandia is suggested to coincide with that formed either during the Proterozoic orogenies or during the rapakivi magmatism (Korja et al., 1993) we have explored global massif-type anorthosites (Table 7) against the Moho depth using a 1-degree grid CRUST1.0-model (Laske et al., 2013) and for the Europe using the Moho model of Grad et al. (2009) (Fig. 12). The present day crust with Late Paleo- to Mesoproterozoic massif-type anorthosites is thickest in Baltica. The crustal thickness undulates from ~55 km beneath the 1640–1620 Ma rapakivi intrusions in Finland, through ~47 km beneath the 1580–1560 Ma rapakivi intrusions in Finland, Latvia and Estonia to ~ 42 km beneath the 1470–1440 Ma group of rapakivi batholiths in Sweden. Whereas, in Laurentia the coeval 1630 Ma and slightly younger ~1470–1410 Ma rapakivi complexes are found in the ~38 km thick crust. Similar crustal thickness of ~41–39 km is obtained under the1560–1540 Ma massif-type anorthosite complexes in Amazonia. It is evident, that there is no correlation of present-day Moho thickness with the global massif-type anorthosites and related crustal magmatic rocks. This observation does not support or negate the rifting hypotheses. However, continental rifting environment hypotheses is challenged by the fact that alluvial and lacustrine sedimentation is present only locally and no thick contemporaneous sedimentary cover associated to lithospheric stretching is found in Laurentia (e.g. Hoffman, 1989) or in Fennoscandia (e.g. Ripa and Stephens, 2020). In addition, as Ashwal and Bybee (2017) summarize, rifting environments fail to account for anorthosite

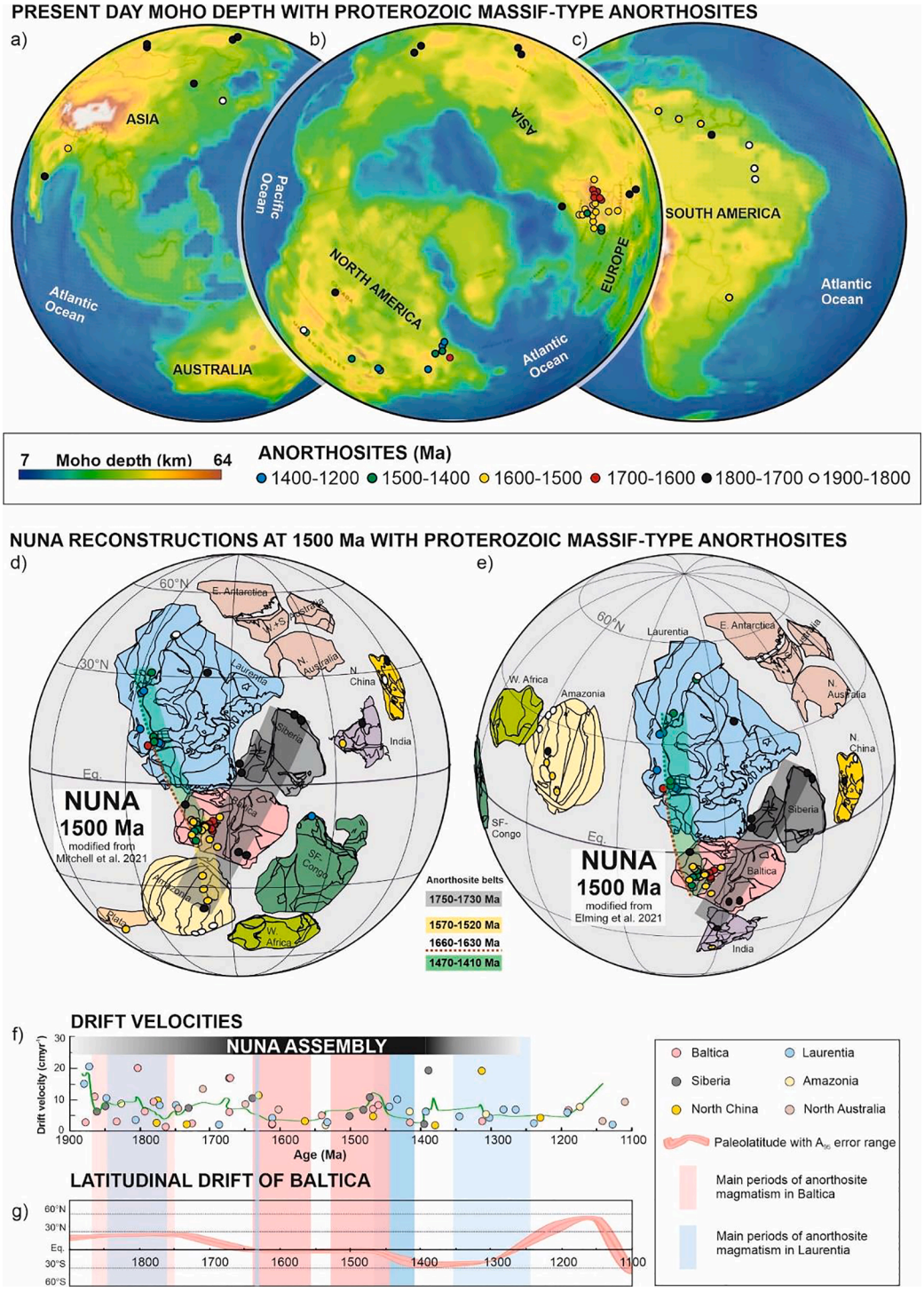

Fig. 12. Global distribution of Proterozoic (1900–1200 Ma) AMCG complexes (Table 7) and Moho depth (km) (Laske et al., 2013) in present day continental configuration of (a) Australia and Asia, (b) North America, Europe and Asia, (c) South America. Global distribution of Proterozoic massif-type anorthosite complexes in two different recent reconstruction of Nuna models at 1500 Ma (d) Reconstruction modified from Elming et al., 2021, (e) Reconstruction modified from Mitchell et al. 2021 (see Euler data in the Table 8). (f) Drift velocities as measured by paleomagnetic data from six individual cratons (data from Elming et al., 2021; see Euler data in the Table 8).). The colored dots are velocities for individual plates with the green line representing a moving-average. (g) Latitudinal drift history as measured by paleomagnetic data of Baltica indicating the drift history of the core of Nuna (modified from Salminen et al., 2021). Note that latitudes extend up to 30°N and 60°S. Pink and blue rectangles highlight the main period of massif-type anorthosite (i.e. rapakivi magmatism) magmatism in Baltica and Laurentia, respectively. Intensity of the color indicates the frequency. Moho depth was plotted using 3D-map function accompanied with Bing Maps in Excel-program. Moho depth was restricted to 7–64 km for clarity, therefore grey areas indicate Moho depth > 64 km. (For interpretation of the references to color in this figure legend, the reader is referred to the web version of this article.)

occurrences that were emplaced over time spans of at least 500 m.y. in belts such as the Grenville/Nain Provinces of eastern North America, without having initiated major continental break-up. Furthermore Kukkonen and Lauri (2009) point out that this type of lithospheric-scale excessive extension is not supported by the present-day thick crust in Fennoscandia, and needed excessive whole lithosphere scale thinning is not obtained in Finland

6.2. Plume –hotspot as the origin of massif-type anorthosite magmatism

Another hypotheses related to extensional environment suggest that the massif-type anorthosite are plume-related (e.g. Sharkov, 2010). A plume, with single stationary or a moving hotspot, should produce magmas in a spatial distribution with an obvious age progression if cratons were drifting over this hotspot. Present day spatial distribution of massif-type anorthosites do not show obvious age progression of coeval batholiths of any scale, not extending from one continent to the other and not within one continent (Fig. 12) (Ashwal and Bybee, 2017). According to Ashwal and Bybee (2017) this challenges the analogy with hotspot or plume related magmatism. In addition, on the basis of paleomagnetic data at the time Moakhar and Elming (2000) proposed that the latitude of Baltica was temporally changing during the interval

Table 7
Global ~ 1800–1250 Ma massif-type anorthosites.

Name	Lat (°N)	Long (°E)	Age (Ma)	Craton	Reference
Mucajaí	2	300	1526 ± 2	Amazonia	Heinonen et al. (2012)
Parguaza granite	6	292	1545 ± 20	Amazonia	Gaudette et al. (1978), DallÍAgnoll et al. (1994)
Surucucus granites	4	296	1551 ± 5	Amazonia	Gaudette et al. 1978, DallÍAgnoll et al. (1994)
Serra do Acari granites	0	302	1730 ± 30	Amazonia	DallÍAgnoll et al. (1994), Dall'Agnol et al. (1999).
Pitinga granites	−2	309	1834 ± 6	Amazonia	DallÍAgnoll et al. (1994), Costi et al. (2000)
Cigano, Carajás, Pojunca granites	−6	310	1880 ± 2	Amazonia	DallÍAgnoll et al. (1994), Dall'Agnol et al. (2005)
Seringa, Musa, Jamon, Velho Guilerme and Marajoara granites	−8	310	1883 ± 5	Amazonia	DallÍAgnoll et al. (1994), Dall'Agnol et al. (2005)
Capivarita	−30	306	1573 ± 21	Rio de La Plata	Chemale et al. (2011)
Jönköping	58	14	1455 ± 6	Baltica	Brander and Söderlund (2009)
Mårdsjö	60	15	1524 ± 3	Baltica	Persson (1999), Andersson et al. (2001)
Mullnäset	64	16	1526 ± 3	Baltica	Persson (1999), Andersson et al. (2001)
Nordsjö	60	13	1520 ± 3	Baltica	Persson (1999), Andersson et al. (2001)
Noran	60	15	1469 ± 10	Baltica	Persson (1999), Claesson and Kresten (1997)
Strömsbro	61	17	1500 ± 19	Baltica	Persson 1999, Andersson et al. (2001)
Rödö	62	18	1497 ± 6	Baltica	Persson (1999), Andersson et al. (2001)
Nordingrå	63	18	1578 ± 17	Baltica	Persson (1999)
Suwalki/Mazury	54	23	1559 ± 39	Baltica	Stein et al. (1998), Wiszniewska et al. (2002)
Ragunda	63	16	1514 ± 5	Baltica	Persson (1999)
Laitila	61	22	1573 ± 5	Baltica	Vaasjoki (1977), Vaasjoki (1996)
Salmi	61	32	1543 ± 8	Baltica	Neymark et al. (1994)
Kolinummi (SE from Laitila)	61	22	1576 ± 3	Baltica	Heinonen et al. (2010)
Eurajoki	61	22	1571 ± 3	Baltica	Heinonen et al. (2010)
Åland	60	19	1575 ± 11	Baltica	Heinonen et al. (2010)
Riga	57	21	1584 ± 7	Baltica	Rämö et al. 1996
Wiborg	60	27	1627 ± 3	Baltica	Heinonen et al. (2010)
Suomenniemi	61	27	1644 ± 4	Baltica	Rämö and Mänttäri (2015)
Ahvenisto	61	24	1633 ± 6	Baltica	Heinonen et al. (2010)
Märjamaa	59	24	1629 ± 7	Baltica	Rämö et al. (1996)
Naissaar	60	25	1624 ± 10	Baltica	Rämö et al. (1996)
Geransky			1736 ± 6	Siberia, Aldan	Ashwal (2010)
Korsun-Novomyrgorod	48	32	1750	Baltica, Ukrainan shield	Ponomarenko et al. (2013)
Korosten	50	30	1760	Baltica, Ukrainan shield	Ponomarenko et al. (2013)
Lofoten, charnokite	68	15	1795 ± 1	Baltica	Corfu (2004)
Lofoten, granite	68	15	1795 ± 5	Baltica	Corfu (2004)
Salno Tundra			1870	Baltica	Ashwal (1993)
Kunene	−19	14	1385 ± 25	Congo	Bybee et al. (2019)
Bengal	23	87	1550 ± 12	India	Chatterjee et al. (2007)
Pangidi	17	81	1739 ± 220	India	Rao et al. (2004)
West Bay Batholith	46	280	1240	Laurentia	Prevec (2004)
St. Charles-Mercer	46	280	1245 ± 48	Laurentia	Prevec (2004)
Kiglapait, Labrador	57	299	1321	Laurentia	Morse (1996)
Nain	57	298	1320.5 ± 1.5	Laurentia	Myers et al. (2008)
Whitestone	46	280	1350 ± 50	Laurentia	van Breemen et al. (1986)
Rivière-Pentecôte	50	294	1354 ± 3	Laurentia	Martignole et al. (1993)
Flowers River	55	298	1411 ± 48	Laurentia	Hill (1988)
Laramie	41	254	1434 ± 3	Laurentia	Scoatese and Chamberline (1995)
Harp Lake	55	298	1448	Laurentia	Krogh and Davis (1973), see also Gower and Krogh (2002)
Wolf River	45	271	1468 ± 4	Laurentia	van Schmus et al. (1975), Dewane and van Schmus (2007)
Michikamau	55	296	1469 ± 1	Laurentia	Emslie (1965), (updated age from Kerr and McNicoll (2010)
Mealy Mountains	53	301	1632 ± 2	Laurentia	Gower et al. (2008), summary of ages in Hegner et al. (2010)
Horse Creek	41	255	1761.5 ± 2	Laurentia	Scoatese and Chamberline (1996)
Clearwater	57	255	1846	Laurentia	Crocker et al. (1993)
Sancheong-Hadong	35	128	1862 ± 2	North China	Lee et al. (2014)
Damiao	40	120	1725 ± 13	North China	Teng and Santosh (2015)
Hodgulingolsky			1710	North China	Ashwal (2010)
Olonkhundksky			1680	North China	Ashwal (2010)
Uchur (Ulkan- Dzhugdzhur)	60	138	1727 ± 6	Siberia, Aldan	Larin (2014)
Geran (Ulkan- Dzhugdzhur)	58	135	1736	Siberia, Aldan	Larin (2014)
Kuzeevo	57	95	1730	Siberia Anabar	Larin (2014)
Tarak	57	95	1750	Siberia Angara	Larin (2014)
Podporozhye	55	98	1750	Siberia Anabar	Larin (2014)

of Late-Paleo – to Mesoproterozoic rapakivi magmatism, and further negated the single stationary hotspot. This can be further tested here with updated high-quality paleomagnetic data.

We explore two recent supercontinent Nuna models at 1500 Ma with the occurrence of massif-type anorthosites (Fig. 12; Table 7; Table 8). In both of the models Baltica – Laurentia – Siberia are shown in typical Nuna configuration forming the core of Nuna (summarized in Elming et al., 2021). The difference between these two models are in the position of Amazonia, Congo-São Francisco, India and North China. In the model by Mitchell et al. (2021) the SAMBA type (modified from Johansson, 2009) connection of Baltica and Amazonia is shown, whereas in the model of Elming et al. (2021) an Atlantica-type (e.g. Rogers, 1996; Rapalini et al., 2015) configuration for Amazonia-Congo-São Francisco is explored. For reasoning behind these reconstructions we guide the reader to an extensive review on the Nuna supercontinent by Elming et al. (2021). In both of the models the ~1470–1440 Ma massif-type anorthosites and associated crustal derived rocks (i.e. rapakivi granites complexes) from Baltica seem to form a NNW trending

Table 8
Euler rotation parameters for Nuna used in Fig. 12.

Continent/craton	Reference frame	Lat (N)	Long (E)	Angle ()	References
Mitchell et al (2021)					
Amazonia	Laurentia	−47	33	280	Modified from Johansson (2009)
Baltica	Laurentia	48	2	49	Evans and Pisarevsky (2008)
Congo	Laurentia	–23	226	−208	Salminen et al. (2016a), Salminen et al. (2016b)
India	Laurentia	56	75	123	Zhang et al. (2012)
Laurentia	absolute	10	−77	281	Nain anorthosite pole Murthy (1978)
North Australia	Laurentia	38	90	103	Kirscher et al. (2019)
North China	Laurentia	46	331	33	Zhang et al. (2012)
Río de La Plata	Laurentia	−47	33	280	Pehrsson et al. (2016)
Siberia	Laurentia	77	98	137	Evans et al. (2016)
West Africa	Amazonia	34	−28	−74	Chardon et al. (2020)
Elming et al. (2021)					
Amazonia	Rotation axis	16	0	−172	Elming et al. (2021)
Baltica	Laurentia	48	2	49	Evans and Pisarevsky (2008)
Congo	Rotation axis	−9	149	301	Elming et al. (2021)
India	Baltica	31	54	175	Pisarevsky et al. (2013)
Kalahari	Rotation axis	4	−91	−91	Elming et al. (2021)
Laurentia	Rotation axis	−36	5	−145	Elming et al. (2021)
North Australia	Laurentia	40	100	102	Payne et al. (2009) Evans and Mitchell (2011)
West Australia	North Australia	−20	135	40	Li and Evans (2010)
South Australia	North Australia	−20	135	40	Following Pehrsson et al. (2016), Evans and Mitchell (2011)
North China	Siberia	−59	−69	127	Modified from Pisarevsky et al. (2013)
São Francisco	Congo	47	−30	56	McElhinny et al. (2003)
Siberia	Laurentia	77	98	137	Evans et al. (2016)
West Africa	Amazonia	−35	146	72	Following SAMBA geology of Johansson (2009). Euler rotation from Zhang et al. (2012)

~3000 km linear belt with coeval and slightly younger ~1470–1410 Ma batholiths in Laurentia, already noted earlier (e.g. Gower and Tucker, 1994; Åhäll and Connelly, 1998; Karlstrom et al., 2001). A striking difference between the models is that in the Nuna of Mitchell et al. (2021) ~1570–1520 Ma massif-type anorthosites form a 2500 km N-S linear belt extending from Amazonia to Baltica (Fig. 12d). Neither of the obtained two belts show spatial age progression (Table 7). Paleoproterozoic ~1880–1840 Ma massif-type anorthosites exist in Amazonia, Laurentia and North China, but amalgamation of these cratons was still ongoing at that time and the Nuna reconstruction cannot be used to study spatial distribution of these intrusions. Instead, ~1790–1720 Ma massif-type anorthosites exist in Amazonia, Baltica, Siberia, India and North China. In the Nuna model of Mitchell et al. (2021) these batholiths extend from Amazonia through Baltica to Siberia along a ~5000 km linear belt with spatial age progression from ~1750 Ma in Amazonia and Baltica to ~1730 Ma in Siberia (Fig. 12). These observations further argue against single hotspot source for ~1640–1620 Ma, ~1590–1520 Ma, and 1470–1410 Ma anorthosites, but invites further examination for the interval of ~1750–1730 Ma.

6.3. *Large-scale mantle upwelling below the supercontinent as the origin of massif-type anorthosite magmatism*

Hoffman (1989) proposed that only during the Late Paleo- to Mesoproterozoic crustal mass was sufficient enough to produce supercontinents large enough to effectively insulate the mantle and promote the low-latitude superswells enhancing massif-type anorthosite

magmatism. Because of secular cooling of the mantle the Nuna supercontinent engendered more pronounced anorogenic magmatism than subsequent supercontinents (Hoffman, 1989). Modelling indicates that it takes about 200 Ma for the focused heat to develop under the insulating supercontinent (Trubitsyn et al., 2003). In theory, rapid plate motions should precede supercontinental aggregation and stationary low latitude position of amalgamated supercontinent is required for the formation of the large-scale mantle upwelling (Pollack et al., 1981; Hoffman, 1989). Rapid paleolatitude variations of Laurentia at ~1900–1600 Ma and stable low-latitude position at ~1500–1200 Ma (e.g. Hoffman, 1989; Swanson-Hysell, 2021) are consistent with the theory. To further elaborate we explored minimum drift velocities as measured by high-quality paleomagnetic data from six individual cratons (data from Elming et al., 2021) (Fig. 12). A striking feature is that at before and after the enhanced massif-type anorthosite magmatism velocities are bimodal, whereas during the pronounced massif-type anorthosite period at 1650–1410 Ma they are unimodal pointing to a distinctly different geodynamics during the anorthosite magmatism. In general, higher average velocity of ~10 cm/yr is obtained during the Nuna amalgamation period (see Elming et al., 2021) with the peak of ~20 cm/yr at the onset of Nuna amalgamation at ~1880 Ma. The amalgamation period includes a lower velocity episode at 1770–1730 Ma coincide temporally with massif-type anorthosite magmatism in Baltica (i.e. rapakivi granite magmatism), Siberia, North China and India. Similar lower velocities of ~5 cm/yr are obtained at 1640–1500 Ma and 1450–1410 Ma during the enhanced massif-type anorthosite magmatism. Furthermore, it is evident from the paleolatidue of Baltica that the core of the Nuna supercontinent occupied low- to equatorial latitudes at 1650–1450 Ma (Fig. 12). Post-1470 Ma the core of Nuna drifts towards southerly latitudes so that Baltica drifts towards higher southerly latitudes and therefore the 1470–1410 Ma anorthosites locations (Table 7) in Laurentia can be reconstructed on equatorial latitudes during their emplacement period. The observed paleomagnetic data of the core Nuna continents support the theoretical hyphothesis of a large-scale superswell under a low-latitude position of supercontinent Nuna during the Late Paleo- to Mesoproterozoic triggering massif-type anorthosite magmatism.

6.4. *Active convergent margin processes – Continental arc setting as the origin of massif-type anorthosite magmatism*

Proterozoic massif-type anorthosites are widely distributed throughout the cratonic regions of all continents (Ashwal and Bybee, 2017), but Late- to Paleo Mesoproterozoic massif-type anorthosites exists mainly in Baltica and Laurentia, with a few in Amazonia (Fig. 12). Magmatism involving granites and associated anorthosites form distinctive magmatic suites on Baltica and Laurentia and some of them can be correlated across Atlantic (Gower and Tucker, 1994; Åhäll and Connelly, 1998), but do not form linear belts in present day configuration (Fig. 12). In the continental arc hypotheses, the onset of broadly simultaneous and bimodal massif-type anorthosite magmatism (i.e.

rapakivi magmatism) at some distance from the margins of both Baltica and northeastern Laurentia is thought to support a continental back-arc processes controlling the morphology of the margin and providing the thermal energy required to produce magmas (Ashwal, 1993; Karlstrom et al., 2001; Ashwal, 2010; Ashwal and Bybee, 2017). If the massif-type anorthosite magmatism was initiated by active convergent margin processes, it is likely that the spatial arrangement of linear belts of coeval batholits continue from one craton to the other and can be visualized in paleogeographical reconstructions. We explored the global massif-type anorthosite occurrences in two recent Nuna models and noted a spatial arrangement of ~1750–1730 Ma (Amazonia, Baltica, Siberia), ~1570–1520 Ma (Amazonia, Baltica) and ~1470–1410 Ma (Baltica, Laurentia) batholiths forming linear belts extending from one craton to the other (Fig. 12de).

According to (Bybee et al., 2014; Bybee et al., 2019) careful geochronological studies on massif-type anorthosites from the 1650–1630 Ma Mealy Mountains Intrusive Suite and the 1363–1298 Ma Nain Plutonic Suite suggest that magmatism in individual massifs may have occurred over long time-scales of up to 100 m.y. A tens of millions years' time-scale is obtained also for emplacement of the Vehmaa batholith in southwest Finland, where Shebanov et al. (2000) showed that the core of the K-feldspar ovoids has a U-Pb (zircon) age of 1630 Ma, while the matrix gives a U-Pb (zircon) age of 1573 Ma. Such a long emplacement time-scales implicate tectonic environments that supplied basaltic magmas to the base of the crust over lengthy time periods, as well as crust-magma rheology that promoted slow ascent of viscous mushes (Ashwal and Bybee, 2017). According to Ashwal and Bybee (2017) this is a proof of convergent margin setting. We note here that also the proposed large-scale mantle superswell produce magmas of similar long emplacement time-scales. Furthermore, Kukkonen and Lauri (2009) have proposed a causal link between ~1850 and 1780 Ma Svecofennian late orogenic thermal evolution and the rapakivi magmatism in Finland because of thickened crust. In their collisional model the middle-lower crust and the upper mantle continued warming 200 m.y. after the collision, until the Mesoproterozoic times.

7. Summary and conclusions

A majority of the new ~1640–1497 Ma paleomagnetic poles presented in this study are clustering on equatorial to low latitudinal positions and most of them have issues hindering their quality. R-score is worst for the ~1500 Ma Strömsbro data (R-score: 2) and best for the Ragunda data (Group 1 R-score: 5; Group 2 R-score: 6). However, by combining data from ~1.5 Ga intrusions a new high-quality pole for Baltica, which fulfils all the refined R-criteria (R-score: 7), can be defined. The new data combined with previous high-quality data supports the view that the Baltica experienced stable low latitude to equatorial locations during the 1640–1470 Ma time range, temporally coinciding with the globally pronounced rapakivi granite-anorthosite magmatism.

The poles off from the low latitude cluster plot on intermediate latitudes and these poles from the ~1510 Ma Ragunda Group 2 and ≤1497 Ma Rödö dykes invited a speculation of the reasons for rapid oscillation between nearly coeval high and low latitude poles. This resembles the known Ediacaran rapid shifts between high and low latitude pole positions, which is thought to be because of behavior of the geomagnetic field. However, owing to lack of coeval paleomagnetic data from the other cratons this remains to be tested in the future. In addition, other suggested reasons for the Ediacaran rapid shifts are fast plate motions or true polar wander, but testing requires paleomagnetic data that is currently lacking.

In addition, we used paleomagnetic data to determine paleolatitudes, relative configuration of cratons, and to calculate minimum plate velocities to further study the origin of the global Proterozoic anorthosite intrusions. Our study argue against single hotspot source for ~1640–1620 Ma, ~1590–1520 Ma, and 1470–1410 Ma rapakivi-anorthosites, but invites further examination for the interval of ~1750–1730 Ma. The observed paleomagnetic data of the core Nuna continents support the theoretical hyphothesis of a large-scale superswell under a low-latitude position of supercontinent Nuna during the Late Paleo- to Mesoproterozoic triggering massif-type anorthosite magmatism. However, ~1750–1730 Ma (Amazonia, Baltica, Siberia), ~1570–1520 Ma (Amazonia, Baltica) and ~1470–1410 Ma (Baltica, Laurentia) massif-type anorthosites forming linear belts extending from one craton to the other does not exclude the possibility for convergent tectonism as the origin of rapakivi-anorthosites. A striking feature is that at before and after the enhanced rapakivi-anorthosite magmatism minimum plate drift velocities are bimodal, whereas during the anorthosite period at 1650–1400 Ma they are unimodal pointing to distinctly different geodynamics during the pronounced massif-type anorthosite magmatism.

CRediT authorship contribution statement

JS, SÅE, SM conceived and designed the analysis; JS, SÅE, SM, BA, MOM collected the data; JS, SÅE, SM, BA, CW contributed data or analysis tools; JS, SÅE, SM performed the analysis; JS, SÅE, SM wrote the paper.

Declaration of Competing Interest

The authors declare that they have no known competing financial interests or personal relationships that could have appeared to influence the work reported in this paper.

Acknowledgements

We are grateful for the efforts and inspiring work of late Svetlana Bogdanova. Her work will form the basis for future research for a long time ahead. We thank guest editors, prof. Lubnina and Dr. S. Pisarevsky and reviewers, Dr. Pivarunas and an anonymous, for their constructive comments, which improved the manuscript. Fredrik Karell and Arto Luttinen are acknowledged for sampling and for overall research of the of the Kopparnäs dyke swarm. Kaiu Piipponen is thanked for help during the Ragunda field work and Ulf Andersson for guidance in the Strömsbro area. This publication contributes to IGCP648 Supercontinent Cycles & Global Geodynamics. JS was funded by Academy of Finland, grant #319277. SÅE was funded by the Swedish Research Council.

Appendix A. Supplementary data

Supplementary data to this article can be found online at https://doi.org/10.1016/j.precamres.2021.106406.

References

Abrajevitch, A., Van der Voo, R., 2010. Incompatible Ediacaran paleomagnetic directions suggest an equatorial geomagnetic dipole hypothesis. Earth and Planetary Science Letters 293, 164–170. https://doi.org/10.1016/j.epsl.2010.02.038.

Alviola, R., Johanson, B.S., Rämö, O.T., Vaasjoki, M., 1999. The Proterozoic Ahvenisto rapakivi granite–massif-type anorthosite complex, southeastern Finland; petrography and U-Pb chronology. Precambrian Research 95, 89–107. https://doi.org/10.1016/S0301-9268(98)00128-4.

Anderson, J., 1983. Proterozoic anorogenic granite plutonism of North America. In: Medaris, L.G.J., Byers, C.W., Mickelson, D.M., Shanks, W.C. (Eds.), Proterozoic geology: Selected papers from an International roterozoic Symposium: Geological Society of America Memoir, pp. 133-154.

Andersson, U.B., 1997a. Petrogenesis of Some Proterozoic Granitoid Suites and Associated Basic Rocks in Sweden:(Geochemistry and Isotope Geology). Sveriges geologiska undersökning (SGU).

Andersson, U.B., 1997. The sub-Jotnian strömsbro granite complex at gävle, Sweden. Geologiska Föreningen i Stockholm Förhandlingar 119, 159–167. https://doi.org/10.1080/11035899709546473.

Andersson, U.B., Neymark, L.A., Billström, K., 2001. Petrogenesis of Mesoproterozoic (Subjotnian) rapakivi complexes of central Sweden: implications from U-Pb zircon ages, Nd, Sr and Pb isotopes. Transactions of the Royal Society of Edinburgh: Earth Sciences 92, 201–228. https://doi.org/10.1017/S0263593300000237.

Ashwal, L.D., 1993. Anorthosites. Springer-Verlag, Berlin Heidelberg.
Ashwal, L.D., 2010. The temporaility of anorthosites. The Canadian Mineralogist 48, 711–728.
Ashwal, L.D., Bybee, G.M., 2017. Crustal evolution and the temporality of anorthosites. Earth-Science Reviews 173, 307–330. https://doi.org/10.1016/j.earscirev.2017.09.002.
Bingen, B., Nordgulen, Ø., Viola, G., 2008. A four-phase model for the Sveconorwegian orogeny, SW Scandinavia. Norwegian Journl of Geology 88, 43–72.
Bogdanova, S., 1993. Segments of the East European Craton. Publ. Inst. Geophys. A, 33–38.
Bogdanova, S., Gorbatschev, R., Skridlaite, G., Soesoo, A., Taran, L., Kurlovich, D., 2015. Trans-Baltic Palaeoproterozoic correlations towards the reconstruction of supercontinent Columbia/Nuna. Precambrian Research 259, 5–33. https://doi.org/10.1016/j.precamres.2014.11.023.
Bogdanova, S.V., Gorbatschev, R., Garetsky, R.G., 2005. EUROPE | East European Craton. In: Selley, R.C., Cocks, L.R.M., Plimer, I.R. (Eds.), Encyclopedia of Geology. Elsevier, Oxford, pp. 34–49.
Bogdanova, S.V., Bingen, B., Gorbatschev, R., Kheraskova, T.N., Kozlov, V.I., Puchkov, V. N., Volozh, Y.A., 2008. The East European Craton (Baltica) before and during the assembly of Rodinia. Precambrian Research 160, 23–45. https://doi.org/10.1016/j.precamres.2007.04.024.
Bonin, B., 2007. A-type granites and related rocks: Evolution of a concept, problems and prospects. Lithos 97, 1–29. https://doi.org/10.1016/j.lithos.2006.12.007.
Brander, L., Söderlund, U., 2009. Mesoproterozoic (1.47–1.44 Ga) orogenic magmatism in Fennoscandia; Baddeleyite U-Pb dating of a suite of massif-type anorthosite in S. Sweden. International Journal of Earth Sciences 98, 499–516. https://doi.org/10.1007/s00531-007-0281-0.
Bybee, G.M., Ashwal, L.D., Shirey, S.B., Horan, M., Mock, T., Andersen, T.B., 2014. Pyroxene megacrysts in Proterozoic anorthosites: Implications for tectonic setting, magma source and magmatic processes at the Moho. Earth and Planetary Science Letters 389, 74–85. https://doi.org/10.1016/j.epsl.2013.12.015.
Bybee, G.M., Hayes, B., Owen-Smith, T.M., Lehmann, J., Ashwal, L.D., Brower, A.M., Hill, C.M., Corfu, F., Manga, M., 2019. Proterozoic massif-type anorthosites as the archetypes of long-lived (≥100 Myr) magmatic systems—New evidence from the Kunene Anorthosite Complex (Angola). Precambrian Research 332, 105393. https://doi.org/10.1016/j.precamres.2019.105393.
Chardon, D., Bamba, O., Traoré, K., 2020. Eburnean deformation pattern of Burkina Faso and the tectonic significance of shear zones in the West African craton. BSGF - Earth Sciences Bulletin 191. https://doi.org/10.1051/bsgf/2020001.
Chatterjee, N., Mazumdar, A.C., Bhattacharya, A., Saikia, R.R., 2007. Mesoproterozoic granulites of the Shillong-Meghalaya Plateau: Evidence of westward continuation of the Prydz Bay Pan-African suture into Northeastern India. Precambrian Research 152, 1–26. https://doi.org/10.1016/j.precamres.2006.08.011.
Chemale, F., Philipp, R.P., Dussin, I.A., Formoso, M.L.L., Kawashita, K., Berttotti, A.L., 2011. Lu–Hf and U-Pb age determination of Capivarita Anorthosite in the Dom Feliciano Belt, Brazil. Precambrian Research 186, 117–126. https://doi.org/10.1016/j.precamres.2011.01.005.
Claesson, S., Kresten, P., 1997. The anorogenic Noran intrusion - a Mesoproterozoic rapakivi massif in south-central Sweden. Geologiska Föreningen i Stockholm Förhandlingar 119, 115–122. https://doi.org/10.1080/11035899709546466.
Corfu, F., 2004. U-Pb Age, Setting and Tectonic Significance of the Anorthosite–Mangerite–Charnockite–Granite Suite, Lofoten-Vesterålen, Norway. Journal of Petrology 45, 1799–1819. https://doi.org/10.1093/petrology/egh034.
Corrigan, D., Hanmer, S., 1997. Anorthosites and related granitoids in the Grenville orogen: A product of convective thinning of the lithosphere? Geology 25, 61–64. https://doi.org/10.1130/0091-7613.
Costi, H.T., Dall'agnol, R., Moura, C.A.V., 2000. Geology and Pb-Pb Geochronology of Paleoproterozoic Volcanic and Granitic Rocks of Pitinga Province, Amazonian Craton, Northern Brazil. International Geology Review 42, 832–849. https://doi.org/10.1080/00206810009465114.
Crocker, C.H., Collerson, K.D., Lewry, J.F., Bickford, M.E., 1993. Sm-Nd, U-Pb, and Rb-Sr geochronology and lithostructural relationships in the southwestern Rae province: constraints on crustal assembly in the western Canadian shield. Precambrian Research 61, 27–50. https://doi.org/10.1016/0301-9268(93)90056-8.
Dall'Agnol, R., Costi, H.T., da S. Leite, A.A., de Magalhães, M.S., Teixeira, N.P.,, 1999. Rapakivi granites from Brazil and adjacent areas. Precambrian Research 95, 9–39. https://doi.org/10.1016/S0301-9268(98)00125-9.
Dall'Agnol, R., Teixeira, N.P., Rämö, O.T., Moura, C.A.V., Macambira, M.J.B., de Oliveira, D.C., 2005. Petrogenesis of the Paleoproterozoic rapakivi A-type granites of the Archean Carajás metallogenic province, Brazil. Lithos 80, 101–129. https://doi.org/10.1016/j.lithos.2004.03.058.
Dall'Agnol, R., Frost, C.D., Rämö, O.T., 2012. IGCP Project 510 "A-type Granites and Related Rocks through Time": Project vita, results, and contribution to granite research. Lithos 151, 1–16. https://doi.org/10.1016/j.lithos.2012.08.003.
Dall'Agnol, R., Lafon, J.-M., Macambira, M.J.B.,, 1994. Proterozoic Anorogenic Magmatism in the Central Amazonian Province, Amazonian Craton: Geochronological, Petrological and Geochemical Aspects. Mineralogy and Petrology 50, 113–138.
Deenen, M.H.L., Langereis, C.G., van Hinsbergen, D.J.J., Biggin, A.J., 2011. Geomagnetic secular variation and the statistics of palaeomagnetic directions. Geophysical Journal International 186, 509–520. https://doi.org/10.1111/j.1365-246X.2011.05050.x.
Dekkers, M.J., 1988. Magnetic properties of natural pyrrhotite Part I: Behaviour of initial susceptibility and saturation-magnetization-related rock-magnetic parameters in a grain-size dependent framework. Physics of the Earth and Planetary Interiors 52, 376–393.
Dekkers, M.J., 1990. Magnetic monitoring of pyrhhotite alteration during thermal demagentization. Geophysical Research Letters 17, 779–782.
Dewane, T.J., Van Schmus, W.R., 2007. U-Pb geochronology of the Wolf River batholith, north-central Wisconsin: Evidence for successive magmatism between 1484Ma and 1468Ma. Precambrian Research 157, 215–234. https://doi.org/10.1016/j.precamres.2007.02.018.
Dunlop, D.J., 2014. High-temperature susceptibility of magnetite: a new pseudo-single-domain effect. Geophysical Journal International 199, 707–716. https://doi.org/10.1093/gji/ggu247.
Elming, S.-Å., Mattsson, H., 2001. Post Jotnian basic Intrusions in the Fennoscandian Shield, and the break up of Baltica from Laurentia: a palaeomagnetic and AMS study. Precambrian Research 108, 215–236. https://doi.org/10.1016/S0301-9268(01)00131-0.
Elming, S.-Å., Moakhar, M.O., Martinsson, O.O., 2004. A palaeomagnetic and geochemical study of basic intrusions in northern Sweden. Geologiska Föreningen i Stockholm Förhandlingar 126, 243–252. https://doi.org/10.1080/11035890401262243.
Elming, S.-Å., Shumlyanskyy, L., Kravchenko, S., Layer, P., Söderlund, U., 2010. Proterozoic Basic dykes in the Ukrainian Shield: A palaeomagnetic, geochronologic and geochemical study—The accretion of the Ukrainian Shield to Fennoscandia. Precambrian Research 178, 119–135. https://doi.org/10.1016/j.precamres.2010.02.001.
Elming, S.-Å., Layer, P., Söderlund, U., 2019. Cooling history and age of magnetization of a deep intrusion: A new 1.7 Ga key pole and Svecofennian-post Svecofennian APWP for Baltica. Precambrian Research 329, 182–194. https://doi.org/10.1016/j.precamres.2018.05.022.
Elming, S.-Å., Salminen, J., Pesonen, L., 2021. Chapter 16: Paleo-Mesoproterozoic Nuna supercycle. In: Pesonen, L.J., Salminen, J., Evans, D.A.D., Elming, S.-Å., Veikkolainen, T. (Eds.), Ancient Supercontinents and the Paleogeography of the Earth. Elsevier.
Elming, S.Å., Moakhar, M.O., Layer, P., Donadini, F., 2009. Uplift deduced from remanent magnetization of a proterozoic basic dyke and the baked country rock in the Hoting area, Central Sweden: a palaeomagnetic and40Ar/39Ar study. Geophysical Journal International 179, 59–78. https://doi.org/10.1111/j.1365-246X.2009.04265.x.
Emslie, R.F., 1965. The Michikamau anorthositic intrusion, Labrador. Canadian Journal of Earth Sciences 2, 385–399. https://doi.org/10.1139/e65-030.
Emslie, R.F., 1978. Anorthosite massifs, rapakivi granites, and late proterozoic rifting of north America. Precambrian Research 7, 61–98. https://doi.org/10.1016/0301-9268(78)90005-0.
Emslie, R.F., 1985. Proterozoic Anorthosite Massifs. In: Tobi, A.C., Touret, J.L.R. (Eds.), The Deep Proterozoic Crust in the North Atlantic Provinces. Springer, pp. 39–60.
Ernst, R., Pease, V., Puchkov, V.N., Kozlov, V.I., Sergeeva, N.D., Hamilton, M., 2006. Geochemical Characterization of Precambrian Magmatic Suites of the Southeastern Margin of the East European Craton, Southern Urals, Russia. Geologicheskiy Sbornik 5, 119–161.
Evans, D.A., 1998. True polar wander, a supercontinental legacy. Earth and Planetary Science Letters 157, 1–8. https://doi.org/10.1016/S0012-821X(98)00031-4.
Evans, D.A.D., 2003. True polar wander and supercontinents. Tectonophysics 362, 303–320. https://doi.org/10.1016/S0040-1951(02)000642-X.
Evans, D.A.D., Pisarevsky, S.A., 2008. Plate tectonics on early Earth? Weighing the paleomagnetic evidence. Special Paper 440: When Did Plate Tectonics Begin on Planet Earth?, pp. 249-263.
Evans, D.A.D., Mitchell, R.N., 2011. Assembly and breakup of the core of Paleoproterozoic-Mesoproterozoic supercontinent Nuna. Geology 39, 443–446. https://doi.org/10.1130/g31654.1.
Evans, D.A.D., Veselovsky, R.V., Petrov, P.Y., Shatsillo, A.V., Pavlov, V.E., 2016. Paleomagnetism of Mesoproterozoic margins of the Anabar Shield: A hypothesized billion-year partnership of Siberia and northern Laurentia. Precambrian Research 281, 639–655. https://doi.org/10.1016/j.precamres.2016.06.017.
Evans, D.A.D., Pesonen, L.J., Eglington, B.M., Elming, S.-Å., Gong, Z., Li, Z.-X., McCausland, P.J., Meert, J.G., Mertanen, S., Pisarevsky, S.A., Pivarunas, A.F., Salminen, J.M., Swanson-Hysell, N., Torsvik, T.H., Trindade, R.I.F., Veikkolainen, T., Zhang, S., 2021. Chapter 19. An expanding list of reliable paleomagnetic poles for Precambrian tectonic reconstructions. In: Pesonen, L.J., Salminen, J., Evans, D.A.D., Elming, S.-Å., Veikkolainen, T. (Eds.), Ancient Supercontinents and the Paleogeography of the Earth. Elsevier.
Fisher, R., 1953. Dispersion of a sphere. Proceedings of the Royal Society of London 217, 295–305.
Gaál, G., Gorbatschev, R., 1987. An Outline of the precambrian evolution of the baltic shield. Precambrian Research 35, 15–52. https://doi.org/10.1016/0301-9268(87)90044-1.
Gaudette, H.E., Mendoza, V., Hurley, P.N., Fairbairn, H.W., 1978. Geology and age of the Paraguaza rapakivi granite, Venzeuela. Geological Society of America Bulletin 89, 1335–1440.
Goldreich, P., Toomre, A., 1969. Some remarks on polar wandering. Journal of Geophysical Research 74, 2555–2567. https://doi.org/10.1029/JB074i010p02555.
Gorbatschev, R., Solyom, Z., Johansson, I., 1979. The Central Scandinavian Dolerite Group in Jämtland, central Sweden. Geologiska Föreningen i Stockholm Förhandlingar 101, 177–190. https://doi.org/10.1080/11035897909448572.
Gorbatschev, R., Bogdanova, S., 1993. Frontiers in the Baltic Shield. Precambrian Research 64, 3–21. https://doi.org/10.1016/0301-9268(93)90066-B.
Gower, C.F., Tucker, R.D., 1994. Distribution of pre-1400 Ma crust in the Grenville province: Implications for rifting in Laurentia-Baltica during geon 14. Geology 22, 827–830. https://doi.org/10.1130/0091-7613(1994)022<0827:DOPMCI>2.3.CO;2.

Gower, C.F., Krogh, T.E., 2002. A U-Pb geochronological review of the Proterozoic history of the eastern Grenville Province. Canadian Journal of Earth Sciences 39, 795–829. https://doi.org/10.1139/e01-090.
Gower, C.F., Kamo, S.L., Kwok, K., Krogh, T.E., 2008. Proterozoic southward accretion and Grenvillian orogenesis in the interior Grenville Province in eastern Labrador: Evidence from U-Pb geochronological investigations. Precambrian Research 165, 61–95. https://doi.org/10.1016/j.precamres.2008.06.007.
Grad, M., Tiira, T., Group, E.S.C.W., 2009. The Moho depth map of the European Plate. Geophysical Journal International 176, 279–292. https://doi.org/10.1111/j.1365-246X.2008.03919.x.
Haapala, I., Rämö, O.T., Stein, H.J., Hannah, J.L., 1990. Petrogenesis of the Proterozoic rapakivi granites of Finland. Petrogenesis and Mineralizing Processes. Geological Society of America, Ore-bearing Granite Systems.
Haapala, I., Rämö, O.T., 1992. Tectonic setting and origin of the Proterozoic rapakivi granites of southeastern Fennoscandia. Earth and Environmental Science Transactions of the Royal Society of Edinburgh 83, 165–171. https://doi.org/10.1017/S0263593300007859.
Hegner, E., Emslie, R.F., Iaccheri, L.M., Hamilton, M.A., 2010. Sources of the Mealy Mountains and Atikonak River Anorthosite-Granitoid Complexes, Grenville Province, Canada. The Canadian Mineralogist 48, 787–808. https://doi.org/10.3749/canmin.48.4.787.
Heinonen, A.P., Andersen, T., Rämö, O.T., 2010. Re-evaluation of Rapakivi Petrogenesis: Source Constraints from the Hf Isotope Composition of Zircon in the Rapakivi Granites and Associated Mafic Rocks of Southern Finland. Journal of Petrology 51, 1687–1709. https://doi.org/10.1093/petrology/egq035.
Heinonen, A.P., Fraga, L.M., Rämö, O.T., Dall'Agnol, R., Mänttäri, I., Andersen, T., 2012. Petrogenesis of the igneous Mucajaí AMG complex, northern Amazonian craton — Geochemical, U-Pb geochronological, and Nd–Hf–O isotopic constraints. Lithos 151, 17–34. https://doi.org/10.1016/j.lithos.2011.07.016.
Hill, J.D., 1988. Alkalic to transitional ferrogabbro magma associated with paleohelikian anorthositic plutons in the Flowers River area, southeastern Nain igneous complex, Labrador. Contributions to Mineralogy and Petrology 99, 113–125. https://doi.org/10.1007/BF00399371.
Hoffman, P.F., 1989. Speculations on Laurentia's first gigayear (2.0 to 1.0 Ga). Geology 17, 135–138. https://doi.org/10.1130/0091-7613.
Holm, P.M., Heaman, L.M., Pedersen, L.E., 2005. First direct age determination for the Kelseaa Dolerite Dyke, Bornholm, Denmark. Bulletin of the Geological Society of Denmark 52, 1–6.
Hopgood, A., Bowes, D., Kouvo, O., Halliday, A., 1983. U-Pb and Rb-Sr isotopic study of polyphase deformed migmatites in the Svecokarelides, southern Finland. In: Atherton, M., Gribble, C. (Eds.), Migmatites, melting and metamorphism. Shiva, Nantwich, pp. 80–92.
Hrouda, F., 1982. Magnetic anisotropy of rocks and its application in geology and geophysics. Geophysical surveys 5, 37–82. https://doi.org/10.1007/BF01450244.
Irving, E., 1964. Paleomagnetism and its Application to Geological and Geophysical Problems. John Wiley, New York.
Johansson, Å., 2009. Baltica, Amazonia and the SAMBA connection—1000 million years of neighbourhood during the Proterozoic? Precambrian Research 175, 221–234. https://doi.org/10.1016/j.precamres.2009.09.011.
Karlstrom, K.E., Åhäll, K.-I., Harlan, S.S., Williams, M.L., McLelland, J., Geissman, J.W., 2001. Long-lived (1.8–1.0 Ga) convergent orogen in southern Laurentia, its extensions to Australia and Baltica, and implications for refining Rodinia. Precambrian Research 111, 5–30. https://doi.org/10.1016/S0301-9268(01)00154-1.
Kerr, A.C., McNicoll, V., 2010. U-Pb ages from mafic rocks assiciated with orthomagmatic Ni-Cu-Co sulphide mineralization in West-Central Labrador. Current Research (2010) Newfoundland and Labrador Department of Natural Resources Geological Survey, Report, pp. 23-39.
Kirscher, U., Liu, Y., Li, Z.X., Mitchell, R.N., Pisarevsky, S.A., Denyszyn, S.W., Nordsvan, A., 2019. Paleomagnetism of the Hart Dolerite (Kimberley, Western Australia) – A two-stage assembly of the supercontinent Nuna? Precambrian Research 329, 170–181. https://doi.org/10.1016/j.precamres.2018.12.026.
Kirschvink, J.L., 1980. The least-squares line and plane and the paleomagnetic data. Geophysical Journal of the Royal Astronomy Society 62, 699–718.
Klein, R., Salminen, J., Mertanen, S., 2015. Baltica during the Ediacaran and Cambrian: A paleomagnetic study of Hailuoto sediments in Finland. Precambrian Research 267, 94–105. https://doi.org/10.1016/j.precamres.2015.06.005.
Korja, A., Korja, T., Luosto, U., Heikkinen, P., 1993. Seismic and geoelectric evidence for collisional and extensional events in the Fennoscandian Shield implications for Precambrian crustal evolution. Tectonophysics 219, 129–152. https://doi.org/10.1016/0040-1951(93)90292-R.
Korja, A., Heikkinen, P., Aaro, S., 2001. Crustal structure of the northern Baltic Sea palaeorift. Tectonophysics 331, 341–358. https://doi.org/10.1016/S0040-1951(00)00290-0.
Kosunen, P., 2004. Petrogenesis of mid-Proterozoic A-type granites: Case studies from Fennoscandia (Finland) and Laurentia (New Mexico). University of Helsinki, Yliopistopaino, Department of Geology, p. 129.
Koymans, M.R., Langereis, C.G., Pastor-Galán, D., van Hinsbergen, D.J.J., 2016. Paleomagnetism.org: An online multi-platform open source environment for paleomagnetic data analysis. Computers & Geosciences 93, 127–137. https://doi.org/10.1016/j.cageo.2016.05.007.
Krogh, T.E., Davis, G.L., 1973. The significance of inherited zircons on the age and origin of igneous rocks -an investigation of the ages of the Labrador adamellites. Carn. Inst. Washington, Yearbook 72, 610–613.
Kukkonen, I., Lauri, L., 2009. Modelling the thermal evolution of a collisional Precambrian orogen: High heat production migmatitic granites of southern Finland. Precambrian Research 168, 233–246. https://doi.org/10.1016/j.precamres.2008.10.004.
Lahtinen, R., Garde, A.A., Melezhik, V.A., 2008. Paleoproterozoic evolution of Fennoscandia and Greenland. Episodes 31, 20–28.
Laitakari, I., 1969. On the set of olivine diabase dikes in Häme, Finland. Bulletin de la Commission Géologique de la Finlande 241, 65.
Laitala, M., 1984. Pellingin ja Porvoon kartta-alueiden kallioperä (Summary: Pre-Quaternary rocks of the Pellinki and Porvoo map-sheet areas). Geological Map of Finland 1:100 000. Geological Survey of Finland, Explanation to the maps of pre-quaternary rocks. sheets 3012 and 3021 (in Finnish with English Summary).
Larin, A.M., 2014. Ulkan-Dzhugdzhur ore-bearing anorthosite-rapakivi granite-peralkaline granite association, Siberian Craton: Age, tectonic setting, sources, and metallogeny. Geology of Ore Deposits 56, 257–280. https://doi.org/10.1134/S1075701514040047.
Laske, G., Masters, G., Ma, Z., Pasyanos, M., 2013. Update on CRUST1.0 - A 1-degree Global Model of Earth's Crust. EGU General Assembly.
Lee, Y., Cho, M., Cheong, W., Yi, K., 2014. A massif-type (~1.86 Ga) anorthosite complex in the Yeongnam Massif, Korea: late-orogenic emplacement associated with the mantle delamination in the North China Craton. Terra Nova 26, 408–416. https://doi.org/10.1111/ter.12115.
Lehtonen, M.I., Kujala, H., Kärkkäinen, N., Lehtonen, A., Mäkitie, H., Mänttäri, I., Virransalo, P., Vuokko, J., 2003. Etelä-Pohjanmaan liuskealueen kallioperä. Summary: Pre-Quaternary rocks of the South Ostrobothnian Schist Belt. Geological Survey of Finland, Report of Investigation 158, 1–125.
Li, Z.X., Evans, D.A.D., 2010. Late Neoproterozoic 40 intraplate rotation within Australia allows for a tighter-fitting and longer-lasting Rodinia. Geology 39, 39–42. https://doi.org/10.1130/g31461.1.
Lindberg, B., Eklund, O., Suominen, V., 1991. Middle Proterozoic, Subjotnian diabases andrelated mafic rocks in the archipelago of southwestern Finland. In: Laitakari, I. (Ed.), IGCP-257 Fennoscandian Meeting and Excursion on Precambrian Dyke Swarms. IGCP-257 Technical Report, pp. 18–30.
Lowrie, W., 1990. Identification of ferromagnetic minerals in a rock by coercivity and unblocking temperature properties. Geophysical Research Letters 17, 159–162.
Lubnina, N.V., 2009. The East European Craton in the Mesoproterozoic: New key paleomagnetic poles. Doklady Earth Sciences 428, 1174–1178. https://doi.org/10.1134/s1028334x09070307.
Lubnina, N.V., Mertanen, S., Söderlund, U., Bogdanova, S., Vasilieva, T.I., Frank-Kamenetsky, D., 2010. A new key pole for the East European Craton at 1452Ma: Palaeomagnetic and geochronological constraints from mafic rocks in the Lake Ladoga region (Russian Karelia). Precambrian Research 183, 442–462. https://doi.org/10.1016/j.precamres.2010.02.014.
Lundqvist, T., Gee, D.G., Kumpulainen, R., Karis, L., Kresten, P., 1990. Beskrivning till berggrundskartan över Västernorrlands län (with English summary). Maps to the scale 1:200000. Sveriges geologiska undersökning Rapporter och meddelanden. Series Ba 31, 1–429.
Lundström, I., Eriksson, G., Strömerg, A., 2002. The Post-tectonic Breccias at Bjursås and Pellesberget as Manifestations of Post-Svecokarelian Volcanism. Sveriges geologiska undersökning Rapporter och meddelanden 109, 16.
Luoto, T., Salminen, J., Karsten, O., this issue. Revisiting mafic dykes of Bornholm – implications for Baltica in supercontinent Nuna at 1.3 Ga. Precambrian Research.
Luttinen, A., Lehtonen, E., Bohm, K., Lindholm, T., Söderlund, U., Salminen, J., submitted. Age and geochemistry of the Mid-Proterozoic Häme mafic dyke swarm, southern Finland. Bulletin of the Geological Society of Finland.
Luttinen, A.V., Kosunen, P., 2006. The Kopparnäs dike swarm in Inkoo, southern Finland: new evidence for Jothnian magmatism in the SE Fennoscandian shield. In: Hanski, E., Mertanen, S., Rämö, T., Vuollo, J. (Eds.), Dike Swarms –Time Markers of Crustal Evolution. Taylor & Francis Group, London, pp. 85–97.
Martignole, J., Machado, N., Nantel, S., 1993. Timing of Intrusion and Deformation of the Rivière-Pentecôte Anorthosite (Grenville Province). The Journal of Geology 101, 652–658. https://doi.org/10.1086/648256.
McElhinny, M.W., Powell, C.M., Pisarevsky, S.A., 2003. Paleozoic terranes of eastern Australia and the drift history of Gondwana. Tectonophysics 362, 41–65. https://doi.org/10.1016/s0040-1951(02)00630-3.
McFadden, P.L., McElhinny, M.W., 1990. Classification of the reversal test in palaeomagnetism. Geophysical Journal International 103, 725–729. https://doi.org/10.1111/j.1365-246X.1990.tb05683.x.
Meert, J.G., Voo, R.V.d., Powell, C.M., Li, Z.-X., McElhinny, M.W., Chen, Z., Symons, D.T.A.,, 1993. A plate-tectonic speed limit? Nature 363, 216–217. https://doi.org/10.1038/363216a0.
Meert, J.G., 2014. Ediacaran-Early Ordovician paleomagnetism of Baltica: A review. Gondwana Research 25, 159–169. https://doi.org/10.1016/j.gr.2013.02.003.
Meert, J.G., Pivarunas, A.F., Evans, D.A.D., Pisarevsky, S.A., Pesonen, L.J., Li, Z.-X., Elming, S.-Å., Miller, S.R., Zhang, S., Salminen, J.M., 2020. The magnificent seven: A proposal for modest revision of the Van der Voo (1990) quality index. Tectonophysics 790, 228549. https://doi.org/10.1016/j.tecto.2020.228549.
Mertanen, S., Pesonen, L.J., 1995. Palaeomagnetic and rock magnetic investigations of the Sipoo Subjotnian quartz porphyry and diabase dykes, southern Fennoscandia. Physics of the Earth and Planetary Interiors 88, 145–175. https://doi.org/10.1016/0031-9201(94)02992-K.
Mertanen, S., Airo, M.L., Elminen, T., Niemelä, R., Pajunen, M., Wasenius, P., Wennerström, M., 2008. Paleomagnetic evidence for Mesoproterozoic–Paleozoic Paleomagnetic evidence for Mesoproterozoic–Paleozoic. In: Pajunen, M. (Ed.), Tectonic Evolution of the Svecofennian Crust in Southern Finland — A Basis for Characterizing Bedrock Technical Properties, Finland, pp. 215-252.

Mitchell, R.N., Zhang, N., Salminen, J., Liu, Y., Spencer, C.J., Steinberger, B., Murphy, J. B., Li, Z.-X., 2021. The supercontinent cycle. Nature Reviews Earth & Environment 2, 358–374. https://doi.org/10.1038/s43017-021-00160-0.

Moakhar, M.O., Elming, S.Å., 2000. A palaeomagnetic analysis of rapakivi intrusions and related dykes in the Fennoscandian Shield. Physics and Chemistry of the Earth, Part A: Solid Earth and Geodesy 25, 489–494. https://doi.org/10.1016/S1464-1895(00)00075-2.

Murthy, G.S., 1978. Paleomagnetic results from the Nain anorthosite and their tectonic implications. 15, 516–525. https://doi.org/10.1139/e78-058.

Myers, J.S., Voordouw, R.J., Tettelaar, T.A., 2008. Proterozoic anorthosite–granite Nain batholith: structure and intrusion processes in an active lithosphere-scale fault zone, northern Labrador. Canadian Journal of Earth Sciences 45, 909–934. https://doi.org/10.1139/E08-041.

Müller, R.D., Zahirovic, S., Williams, S.E., Cannon, J., Seton, M., Bower, D.J., Tetley, M. G., Heine, C., Le Breton, E., Liu, S., Russell, S.H.J., Yang, T., Leonard, J., Gurnis, M., 2019. A Global Plate Model Including Lithospheric Deformation Along Major Rifts and Orogens Since the Triassic. Tectonics 38, 1884–1907. https://doi.org/10.1029/2018tc005462.

Neuvonen, K.J., Korsman, K., Kouvo, O., Paavola, J., 1981. Paleomagnetism and age relations of the rocks in the main sulphide ore belt in central Finland. Bulletin of The Geological Society of Finland 53, 109–133.

Neymark, L.A., Amelin, V., Larin, A.M., 1994. Pb-Nd-Sr Isotopic and Geochemical Constraints on the Origin of the 1.54-1.56 Ga Salmi Rapakivi Granite Anorthosite Batholith (Karelia, Russia). Mineralogy and Petrology 50, 173–193.

Nironen, M., 2017. Guide to geological map of Finland - Bedrock 1:1000000. In: Nironen, M. (Ed.), Bedrock of Finland at the scale 1:1 000 000 - Major strati-graphic units, metamorphism and tectonic evolution., pp. 41-76.

Pajunen, M., Airo, M., Elminen, T., Mänttäri, I., Niemelä, R., 2008. Tectonic evolution of the Svecofennian crust in Southern Finland. In: Pajunen, M. (Ed.), Tectonic evolution of the Svecofennian crust in southern Finland – a basis for characterizing bedrock technical properties, pp. 15-161.

Payne, J.L., Hand, M., Barovich, K.M., Reid, A., Evans, D.A.D., 2009. Correlations and reconstruction models for the 2500–1500 Ma evolution of the Mawson Continent. Geological Society, London, Special Publications 323, 319–355. https://doi.org/10.1144/sp323.16.

Pehrsson, S.J., Eglington, B.M., Evans, D.A.D., Huston, D., Reddy, S.M., 2016. Metallogeny and its link to orogenic style during the Nuna supercontinent cycle. Geological Society, London, Special Publications 424, 83–94. https://doi.org/10.1144/sp424.5.

Persson, A.I., 1999. Absolute (U–Pb) and relative age determinations of intrusive rocks in the Ragunda rapakivi complex, central Sweden. Precambrian Research 95, 109–127. https://doi.org/10.1016/S0301-9268(98)00129-6.

Pesonen, L.J., Bylund, G., Torsvik, T.H., Elming, S.Å., Mertanen, S., 1991. Catalogue of palaeomagnetic directions and poles from Fennoscandia: Archaean to tertiary. Tectonophysics 195, 151–207. https://doi.org/10.1016/0040-1951(91)90210-J.

Piper, J.D.A., 1979. Paleomagneism of the Ragunda instrusion and dolerite dykes, central Sweden. Geologiska Föreningen i Stockholm Förhandlingar 101, 139–148.

Piper, J.D.A., 1980. Palaeomagnetic study of the Swedish rapakivi suite: Proterozoic tectonics of the Baltic Shield. Earth and Planetary Science Letters 46, 443–461.

Pisarevsky, S.A., Biswal, T.K., Wang, X.-C., De Waele, B., Ernst, R., Söderlund, U., Tait, J. A., Ratre, K., Singh, Y.K., Cleve, M., 2013. Palaeomagnetic, geochronological and geochemical study of Mesoproterozoic Lakhna Dykes in the Bastar Craton, India: Implications for the Mesoproterozoic supercontinent. Lithos 174, 125–143. https://doi.org/10.1016/j.lithos.2012.07.015.

Pollack, H.N., Gass, I.G., Thorpe, R.S., Chapman, D.S., 1981. On the vulnerability of lithospheric plates to mid-plate volcanism: Reply to comments by P. R. Vogt. Journal of Geophysical Research: Solid Earth 86, 961–966. https://doi.org/10.1029/JB086iB02p00961.

Ponomarenko, A.N., Kryvdik, S.G., Grinchenko, A.V., 2013. Alkaline rocks of the Ukrainian Shield: Some mineralogical, petrological and geochemical features. Mineralogia 44, 115–124. https://doi.org/10.2478/mipo-2013-0008.

Preeden, U., Mertanen, S., Elminen, T., Plado, J., 2009. Secondary magnetizations in shear and fault zones in southern Finland. Tectonophysics 479, 203–213. https://doi.org/10.1016/j.tecto.2009.08.011.

Prevec, S.A., 2004. Basement tracing using Mid-Proterozoic anorthosites straddling a palaeoterrane boundary, Ontario, Canada. Precambrian Research 129, 169–184. https://doi.org/10.1016/j.precamres.2003.10.009.

Rao, C.V.D., Kumar, T.V., Rao, Y.J.B., 2004. The Pangidi Anorthosite Complex, Eastern Ghats Granulite Belt, India: Mesoproterozoic Sm–Nd isochron age and evidence for significant crustal contamination. Current Science 87, 1614–1618.

Rapalini, A.E., Sánchez Bettucci, L., Badgen, E., Vásquez, C.A., 2015. Paleomagnetic study on mid-Paleoproterozoic rocks from the Rio de la Plata craton: Implications for Atlantica. Gondwana Research 27, 1534–1549. https://doi.org/10.1016/j.gr.2014.01.012.

Ripa, M., Stephens, M.B., 2020. Chapter 10 Magmatism (1.6–1.4 Ga) and Mesoproterozoic sedimentation related to intracratonic rifting coeval with distal accretionary orogenesis. Geological Society, London, Memoirs 50, 269-288. 10.1144/m50-2017-4.

Rogers, J.J.W., 1996. A History of Continents in the past Three Billion Years. 104, 91–107. https://doi.org/10.1086/629803.

Rämö, O.T., 1991. Petrogenesis of the Proterozoic rapakivi granites and related basic rocks of southeastern Fennoscandia: Nd and Pb istopic and general geochemical constraints. Geological Survey of Finland, Bulletin 355, 1–161.

Rämö, O.T., Huhma, H., Kirs, J., 1996. Radiogenic isotopes of the Estonian and Latvian rapakivi granite suites: new data from the concealed Precambrian of the East European Craton. Precambrian Research 79, 209–226. https://doi.org/10.1016/S0301-9268(95)00083-6.

Rämö, O.T., Mänttäri, I., Vaasjoki, M., Upton, B.G.J., Sviridenko, L., 2001. Age and significance of Mesoproterozoic CFB magmatism, Lake Ladoga region, NW Russia., A Geo-Odyssey. Geological Society of America, Boston.

Rämö, O.T., Turkki, V., Mänttäri, I., Heinonen, A.P., Larjamo, K., Lahaye, Y., 2014. Age and isotopic fingerprints of some plutonic rocksin the Wiborg rapakivi granite batholith with specialreference to the dark wiborgite of the Ristisaari Island. Bulletin of the Geological Society of Finland 86, 71–91.

Rämö, O.T., Mänttäri, I., 2015. Geochronology of the Suomenniemi rapakivi granite complex revisited: Implications of point-specific errors on zircon U-Pb and refined λ87 on whole-rock Rb-Sr. Bulletin of the Geological Society of Finland 87, 25–45. https://doi.org/10.1016/j.lithos.2007.06.01610.17741/bgsf/87.1.002.

Rämö, O.T., Haapala, I.J., 1995. One hundred years of Rapakivi Granite. Mineralogy and Petrology 52, 129–185.

Salminen, J., Pesonen, L., 2007. Paleomagnetic and rock magnetic study of the Mesoproterozoic sill, Valaam island, Russian Karelia. Precambrian Research 159, 212–230. https://doi.org/10.1016/j.precamres.2007.06.009.

Salminen, J., Halls, H.C., Mertanen, S., Pesonen, L.J., Vuollo, J., Söderlund, U., 2014a. Paleomagnetic and geochronological studies on Paleoproterozoic diabase dykes of Karelia, East Finland—Key for testing the Superia supercraton. Precambrian Research 244, 87-99. https://doi.org/.1016/j.precamres.2013.07.011.

Salminen, J., Mertanen, S., Evans, D.A.D., Wang, Z., 2014b. Paleomagnetic and geochemical studies of the Mesoproterozoic Satakunta dyke swarms, Finland, with implications for a Northern Europe – North America (NENA) connection within Nuna supercontinent. Precambrian Research 244, 170–191. https://doi.org/10.1016/j.precamres.2013.08.006.

Salminen, J., Klein, R., Mertanen, S., Pesonen, L.J., Fröjdö, S., Mänttäri, I., Eklund, O., 2016a. Palaeomagnetism and U-Pb geochronology ofc.1570 Ma intrusives from Åland archipelago, SW Finland – implications for Nuna. Geological Society, London, Special Publications 424, 95–118. https://doi.org/10.1144/sp424.3.

Salminen, J., Klein, R., Veikkolainen, T., Mertanen, S., Mänttäri, I., 2017. Mesoproterozoic geomagnetic reversal asymmetry in light of new paleomagnetic and geochronological data for the Häme dyke swarm, Finland: Implications for the Nuna supercontinent. Precambrian Research 288, 1–22. https://doi.org/10.1016/j.precamres.2016.11.003.

Salminen, J., Klein, R., Mertanen, S., 2019. New rock magnetic and paleomagnetic results for the 1.64 Ga Suomenniemi dyke swarm. SE Finland. Precambrian Research 329, 195–210. https://doi.org/10.1016/j.precamres.2018.01.001.

Salminen, J., Lehtonen, E., Mertanen, S., Pesonen, L.J., Elming, S.-Å., Luoto, T., 2021. Chapter 5: The Precambrian drift history and paleogeography of Baltica. In: Pesonen, L.J., Salminen, J., Evans, D.A.D., Elming, S.-Å., Veikkolainen, T. (Eds.), Ancient Supercontinents and the Paleogeography of the Earth. Elsevier.

Salminen, J.M., Evans, D.A.D., Trindade, R.I.F., Oliveira, E.P., Piispa, E.J., Smirnov, A.V., 2016b. Paleogeography of the Congo/São Francisco craton at 1.5Ga: Expanding the core of Nuna supercontinent. Precambrian Research 286, 195–212. https://doi.org/10.1016/j.precamres.2016.09.011.

Scoates, J.S., Chamberlain, K.R., 1997. Orogenic to Post-Orogenic Origin For the 1.76 Ga Horse Creek Anorthosite Complex, Wyoming. Usa. The Journal of Geology 105, 331–344. https://doi.org/10.1086/515928.

Sharkov, E.V., 2010. Middle-proterozoic anorthosite–rapakivi granite complexes: An example of within-plate magmatism in abnormally thick crust: Evidence from the East European Craton. Precambrian Research 183, 689–700. https://doi.org/10.1016/j.precamres.2010.08.008.

Shebanov, A., Savatenkov, V., Eklund, O., Andersson, U.B., Annersten, H., Claesson, S., 2000. Regional mineralogical correlation linking post- and anorogenic magmatic events from unusual barian biotites in the Järppilä rapakivi porphyries, Vehmaa batolith (S. Finland). Meeting: Advances on Micas Rome 2–3.11 2000. Universitá degli Studi Roma Tre MURST – Progetto Fillosilicati: aspetti cristallochimici strutturali e petrologici, Roma, pp. 183-186.

Siivola, J., 1987. The mafic intrusion of Lovasjärvi. Geological Survey of Finland, Report of Investigation, pp. 121–128.

Stein, H.J., Sundblad, K., Markey, R.J., Morgan, J.W., Motuza, G., 1998. Re-Os ages for Archean molybdenite and pyrite, Kuittila-Kivisuo, Finland and Proterozoic molybdenite, Kabeliai, Lithuania: testing the chronometer in a metamorphic and metasomatic setting. Mineralium Deposita 33, 329–345. https://doi.org/10.1007/s001260050153.

Stephens, M.B., 2020. Chapter 1 Introduction to the lithotectonic framework of Sweden and organization of this Memoir. Geological Society, London, Memoirs 50, 1. 10.1144/M50-2019-21.

Swanson-Hysell, N., 2021. Chapter 4: The Precambrian drift history and paleogeography of Laurentia. In: Pesonen, L.J., Salminen, J., Evans, D.A.D., Elming, S.-Å., Veikkolainen, T. (Eds.), Ancient Supercontinents and the Paleogeography of the Earth. Elsevier.

Söderlund, U., Isachsen, C.E., Bylund, G., Heaman, L.M., Jonathan Patchett, P., Vervoort, J.D., Andersson, U.B., 2005. U-Pb baddeleyite ages and Hf, Nd isotope chemistry constraining repeated mafic magmatism in the Fennoscandian Shield from 1.6 to 0.9 Ga. Contributions to Mineralogy and Petrology 150, 174–194. https://doi.org/10.1007/s00410-005-0011-1.

Söderlund, U., Elming, S.-Å., Ernst, R.E., Schissel, D., 2006. The Central Scandinavian Dolerite Group—Protracted hotspot activity or back-arc magmatism? Precambrian Research 150, 136–152. https://doi.org/10.1016/j.precamres.2006.07.004.

Tarduno, J., Bunge, H.-P., Sleep, N., Hansen, U., 2009. The Bent Hawaiian-Emperor Hotspot Track: Inheriting the Mantle Wind. Science 324, 50. https://doi.org/10.1126/science.1161256.

Tauxe, L., Kylstra, N., Constable, C., 1991. Bootstrap statistics for paleomagnetic data. Journal of Geophysical Research: Solid Earth 96, 11723–11740. https://doi.org/10.1029/91JB00572.
Tauxe, L., Banerjee, S.K., Butler, R.F., R, v.d.V.,, 2018. Essentials of Paleomagnetism. Fifth Web Edition.
Teng, X., Santosh, M., 2015. A long-lived magma chamber in the Paleoproterozoic North China Craton: Evidence from the Damiao gabbro-anorthosite suite. Precambrian Research 256, 79–101. https://doi.org/10.1016/j.precamres.2014.10.018.
Torsvik, T.H., Briden, J.C., Smethurst, M.A., 2000. Super-IAPD: InteractiveAnalysis of Palaeomagnetic Data.
Törnroos, R., 1984. Petrography, Mineral Chemistry and Petrochemistry of Granite Porphyry Dykes from Sibbo, Southern Finland. Geological Survey of Finland, Bulletin 326, 43.
Vaasjoki, M., 1977. Rapakivi granites and other postorogenic rocks in Finland. Their age and the lead isotopic composition of certain associated galena mineralizations. Geological Survey of Finland, Bulletin 294, 64.
Vaasjoki, M., Rämö, T.O., Sakko, M., 1991. New U-Pb ages from the Wiborg rapakivi area: constraints on the temporal evolution of the rapakivi granite-anorthosite-diabase dyke association of southeastern Finland. Precambrian Research 51, 227–243. https://doi.org/10.1016/0301-9268(91)90102-G.
Vaasjoki, M., 1996. The Laitila rapakivi batholith revisited: new, more precise radiometric ages. In: Haapala, I., Rämö, O.T., Kosunen, P. (Eds.), The Seventh International Symposium on Rapakivi Granites and Related Rocks Wednesday 24 - Friday 26 July 1996. University Press, Helsinki, p. 82.
Van Breemen, O., Davidson, A., Loveridge, W.D., Sullivan, R.W., 1986. U-Pb zircon geochronology of Grenville tectonites, granulites and igneous precursors, Parry Sound, Ontario. In: Moore, J.M., Davidson, A., Baer, A.J. (Eds.), The Grenville Province. Geological Association of Canada, Special Paper, pp. 191–207.
Van der Voo, R., 1990. The reliability of paleomagnetic data. Tectonophysics 184, 1–9. https://doi.org/10.1016/0040-1951(90)90116-P.
Van Schmus, W.R., Medaris Jr, L.G., Banks, P.O., 1975. Geology and Age of the Wolf River Batholith, Wisconsin. Bulletin of the Geological Society of America 86, 907–914. https://doi.org/10.1130/0016-7606(1975)86<907:GAAOTW>2.0.CO;2.
Veikkolainen, T.H., Biggin, A.J., Pesonen, L.J., Evans, D.A., Jarboe, N.A., 2017. Advancing Precambrian palaeomagnetism with the PALEOMAGIA and PINT(QPI) databases. Scientific Data 4, 170068. https://doi.org/10.1038/sdata.2017.68.
Welin, E., Lundqvist, T., 1984. Isotopic investigations of the Nordingrå rapakivi massif, north-central Sweden. Geologiska Föreningen i Stockholm Förhandlingar 106, 41–49. https://doi.org/10.1080/11035898409454604.
Welin, E., 1994. The U-Pb zircon age of the Rödön rapakivi granite, central Sweden. GFF 116, 113–114. https://doi.org/10.1080/11035899409546169.
Vigneresse, J.L., 2005. The specific case of the Mid-Proterozoic rapakivi granites and associated suite within the context of the Columbia supercontinent. Precambrian Research 137, 1–34. https://doi.org/10.1016/j.precamres.2005.01.001.
Windley, B.F., 1993. Proterozoic anorogenic magmatism and its orogenic connections: Fermor Lecture 1991. Journal of the Geological Society 150, 39–50. https://doi.org/10.1144/gsjgs.150.1.0039.
Wiszniewska, J., Petecki, Z., Rosowiecka, O., Krzemińska, E., 2002. Geotectonic setting of the Suwałki Anorthosite Massif (NE-Poland) - constraints for 3D geological modelling. p. 16533.
Vorma, A., 1976. On the petrochemistry of rapakivi granites with special reference to the Laitila massif, southwestern Finland. Geological Survey of Finland, Bulletin - Bulletin de la Commission Géologique de Finlande 285, 98p.
Väisänen, M., Mänttäri, I., 2002. 1.90-1.88 Ga arc and back-arc basin in the Orijärvi area, SW Finland. Bulletin of the Geological Society of Finland 74, 185–214.
Zhang, S., Li, Z.-X., Evans, D.A.D., Wu, H., Li, H., Dong, J., 2012. Pre-Rodinia supercontinent Nuna shaping up: A global synthesis with new paleomagnetic results from North China. Earth and Planetary Science Letters 353–354, 145–155. https://doi.org/10.1016/j.epsl.2012.07.034.
Zijderveld, J.D., 1967. A.C. demagnetization in rocks: analysis of results. In: Collinson, D. W., Creer, K.M., Runcorn, S.K. (Eds.), Methods in Paleomagnetism. Elsevier, pp. 254–286.
Åhäll, K.-I., Connelly, J., 1998. Intermittent 1.53–1.13Ga magmatism in western Baltica; age constraints and correlations within a postulated supercontinent. Precambrian Research 92, 1–20. https://doi.org/10.1016/S0301-9268(98)00064-3.
Özdemir, Ö., 1987. Inversion of titanomaghemites. Physics of the Earth and Planetary Interiors 46, 184–196. https://doi.org/10.1016/0031-9201(87)90181-6.